RESEARCH ON RADIO ENVIRONMENT MAPS FOR MOBILITY MANAGEMENT IN 5G NETWORKS

by
Antonio Cristo Suárez Rodríguez

Dissertation submitted in fulfilment of the requirements
for the degree of

DOCTOR OF PHILOSOPHY

under the supervision of

Prof. Eryk Dutkiewicz

School of Electrical and Data Engineering
University of Technology Sydney
Sydney, Australia

June 2020

ABSTRACT

One main feature of the fifth generation (5G) of cellular mobile communications is the deployment of an ultra-dense cellular network architecture with much more cell towers. This will construct a multi-tier 5G network, and make ubiquitous access difficult if maintaining the same approaches to mobility management as in previous generations. In recent years, we have witnessed remarkable advancements in cognitive radio, which provides radio-environmental awareness. This awareness can be exploited to improve system performance in various aspects. This thesis studies how to incorporate radio environment maps (REM) into 5G networks with a particular emphasis on mobility management.

Our work begins halfway between Long-Term Evolution (LTE) and 5G. We propose a REM-based handover algorithm that reduces the number of unnecessary handovers in multi-tier networks. The designed handover procedure is fully backward compatible with LTE and exploits the incomplete channel states stored in a REM. We evaluate our method under two different scenarios in which we can deliver the same downlink traffic as current approaches in the literature as well as decrease the overall number of handovers by at least 33% without overloading the backhaul.

We also present a geometric model to derive the handover and handover failure regions taking into consideration imperfect location, by finding the optimal prediction time through numerical optimisation. The effect of multiple mobility-management parameters is investigated as well. The proposed scheme achieves a substantial reduction of up to 30% in the number of un-

necessary handovers in multi-tier networks. We then propose to use REMs for network optimisation in a dense cellular network and obtain the coverage probability for REM cell association using stochastic geometry. The optimal prediction distance maximises the average ergodic rate, including the penalty incurred by the handovers. Our strategy increases the average ergodic rate extensively by 65% across high-mobility users when compared to state-of-the-art strategies found in the literature.

In summary, radio-environmental awareness in mobile cellular networks has not been wholly addressed yet. This thesis introduces REMs as an enabling technology that contributes to the mitigation of the number of unnecessary handovers and capacity growth for mobility management in 5G networks and beyond.

CERTIFICATE OF ORIGINAL AUTHORSHIP

I, Antonio Cristo Suárez Rodríguez declare that this thesis, is submitted in fulfilment of the requirements for the award of Doctor of Philosophy, in the School of Electrical and Data Engineering at the University of Technology Sydney.

This thesis is wholly my own work unless otherwise reference or acknowledged. In addition, I certify that all information sources and literature used are indicated in the thesis.

This document has not been submitted for qualifications at any other academic institution.

This research is supported by the Australian Government Research Training Program.

Signature:

Production Note:
Signature removed prior to publication.

Date: 5 June 2020

ACKNOWLEDGMENTS

First and foremost, I would like to acknowledge that this work has been supported by the University of Technology Sydney, Macquarie University, and Centrale-Supélec.

I would like to express my sincerest gratitude to my supervisors Prof. Eryk Dutkiewicz (University of Technology Sydney) and Prof. Carlos Faouzi Bader (Centrale-Supélec). They have been supporting me with precious opportunities to learn, explore, and improve. I would also like to thank Prof. Michael Heimlich (Macquarie University), who took care of me and inspired me with his passion.

I am grateful to my co-supervisors at the University of Technology Sydney, Dr Ying He and Dr Beeshanga Abewardana Jayawickrama, for the endless technical discussions we shared over the years. This thesis would not be the same without their invaluable input.

I would like to thank my colleagues and friends at Macquarie University. I keep a special place in my heart for Dr Aleksei Marianov, Dr Putu Edy, and Dr des. Kay-Dennis Boom. We made it to the other side!

Thanks to the SCEE team at Centrale-Supélec for their warm welcome in the cold Rennes, especially Dr Lilian Besson, Dr Rémi Bonnefoi, Dr Rami Othman, Dr Hussein Chour, and Prof. Marwa Chafii. It is an honour to have shared a little part of my journey with you during these four years. Daniel Carvalho, I will never forget our visits to the Scoubidou nor our evenings together.

I would then like to thank my team at the University of Technology Syd-

ney. We did not just share a corner office, but also meaningful discussions both at technical and personal levels that enriched my degree. My thoughts go to Dr Shubhekshya Basnet, Dr Meriam Bautista, Hasini Viranaga Abeywickrama, and Dr Qin Qin Cheng. Special mention to Dr Noman Haider without whom I would not have known how to navigate the intricacies of stochastic geometry.

I cannot miss two key individuals in my thesis, long-lasting friends, Dr Crisanto Quintana and Dr Víctor Guerra, for bringing me back to light where there were only darkness and radio waves.

I would then like to thank Jackie and her family for accepting me as one of them here in Australia. As an international student, it meant the world to me.

Of course on a more personal level, thanks to my closest friends: Iván and Celia, Ángel and Raquel, Raúl and Mada, Lito, Iván, Néstor, Cristofer, Jafet, and Oliver. You were present during my last supper, and I hope to see you again to celebrate once more. This list would be meaningless without Carlos and Esther for being there regardless of the time difference and the distance.

I would like to thank my family in Australia, Kosta and Elena, for our gatherings around the best imaginable food and their vital support. For their respect of my dietary choices, thanks to Jo and Jamie. Also, thanks to Thomas for starting traditions together that I will forever cherish. For permeating into my life, thanks to Federico with whom I have been living parallel lives for the last year, and he has kept pushing me harder than anyone else to come out of my shell.

Last but not least, my thoughts are strongly dedicated to my family. Absence makes the heart grow fonder. I thank my sisters Silvia and Victoria, who I am most grateful for and make me proud every day even when I do not

say it out loud. These acknowledgements would not be complete without my sincere gratitude to my parents, Eugenia y Antonio, for shaping me and show me infinite love regardless of the circumstances. Very warm thanks then to my grandparents and extended family. I wish I had space for all of you in these lines!

To My Parents

Eugenia

and

Antonio.

"I've always been fascinated by maps and cartography. A map tells you where you've been, where you are, and where you're going — in a sense it's three tenses in one."

Peter Greenaway

(b. 1942)

Contents

List of Figures

List of Tables

List of Publications

Journal publications

- **Cristo Suarez-Rodriguez**, Noman Haider, Ying He and Eryk Dutkiewicz, "Network Optimisation in 5G Networks: A Radio Environment Map Approach", in *IEEE Transactions on Vehicular Technology*, 2019, major revisions (second round of reviews).

- **Cristo Suarez-Rodriguez**, Ying He and Eryk Dutkiewicz, "Theoretical Analysis of REM-Based Handover Algorithm for Heterogeneous Networks", in *IEEE Access*, vol. 7, pp. 96719–96731, July 2019.

- Noman Haider, Ahsan Ali, **Cristo Suarez-Rodriguez** and Eryk Dutkiewicz, "Optimal Mode Selection for Full-Duplex Enabled D2D Cognitive Networks", in *IEEE Access*, vol. 7, pp. 57298–57311, May 2019.

Conference publications

- **Cristo Suarez-Rodriguez**, Ying He, Beeshanga A. Jayawickrama and Eryk Dutkiewicz, "Low-Overhead Handover-Skipping Technique for 5G Networks", in *Proc. of IEEE Wireless Communications and Networking Conference (WCNC)*, pp. 1–6, 2019.

- **Cristo Suarez-Rodriguez**, Beeshanga A. Jayawickrama, Faouzi Bader, Eryk Dutkiewicz and Michael Heimlich, "REM-Based Handover Algorithm for Next-Generation Multi-Tier Cellular Networks", in *Proc. of IEEE Wireless Communications and Networking Conference (WCNC)*, pp. 1–6, 2018.

- **Cristo Suarez-Rodriguez**, Beeshanga A. Jayawickrama, Ying He, Faouzi Bader and Michael Heimlich, "Performance Analysis of REM-Based Handover Algorithm for Multi-Tier Cellular Networks", in *Proc. of IEEE International Symposium on Personal, Indoor and Mobile Radio Communications (PIMRC)*, pp. 1–6, 2017.

Chapter 1

Introduction

As the first fifth generation (5G) network roll-outs will be upon us soon, it is expected that network densification will play a leading role in achieving future traffic demands estimated to be between 100–1000× the capacity of current 4G networks. However, network densification comes associated with challenges such as network deployment, backhauling, and mobility management.

This chapter provides a general view of the driving forces towards 5G networks and the challenges that mobility management will face. Then, the contributions and the organisation of the thesis are also introduced.

1.1 Background

Cooper's Law states that the amount of data transmitted over radio spectrum doubles every 30 months. For example, between 1950 and 2000, a millionfold increase in spectral efficiency was reached thanks to a combination of different technological developments, where the vast majority of the growth, about 2700×, stemmed from spatial spectrum reuse or network densification [5]. This trend did not cease with the new century. Rather, in the third generation (3G) cellular networks, frequency reuse and sector antennas were the driving forces towards network densification. Furthermore, in the fourth generation (4G) cellular networks, heterogeneous networks (HetNets) were introduced to enhance the area spectral efficiency (ASE) where needed.

The current generation of mobile communications is struggling to service data-hungry users as a result of the rapidly growing demands of multimedia data-intensive applications such as video streaming, gaming, and social networking [6]. Among the envisioned trends, it is expected that global mobile traffic will increase sevenfold for the covered period (2017 – 2022). Approximately 54% of all mobile data traffic is being offloaded onto the fixed network through operator-owned Wi-Fi hotspots or small cells, reaching 13.4 exabytes of accumulated monthly traffic. However, the 5G cellular networks are not limited to mobile broadband. The International Mobile Telecommunications-2020 (IMT-2020) specifications are expected to support three main use cases as depicted in Fig. 1.1 [1]:

- Enhanced mobile broadband (eMBB): it encompasses a wide range of cases from wide-area deployments to small cells, where both extreme high throughput and low-latency communications are not mutually exclusive. It represents yet another evolution over 4G, avoiding identified pitfalls, and it improves the quality of experience (QoE) seamlessly.

- Ultra-reliable and low-latency communications (URLLC): the main focus is shifting towards stringent requirements for reliability, latency, and resilience. Among the possible scenarios, we do have vehicle-to-everything (V2X), industrial control applications, intelligent transport systems (ITS), remote medical

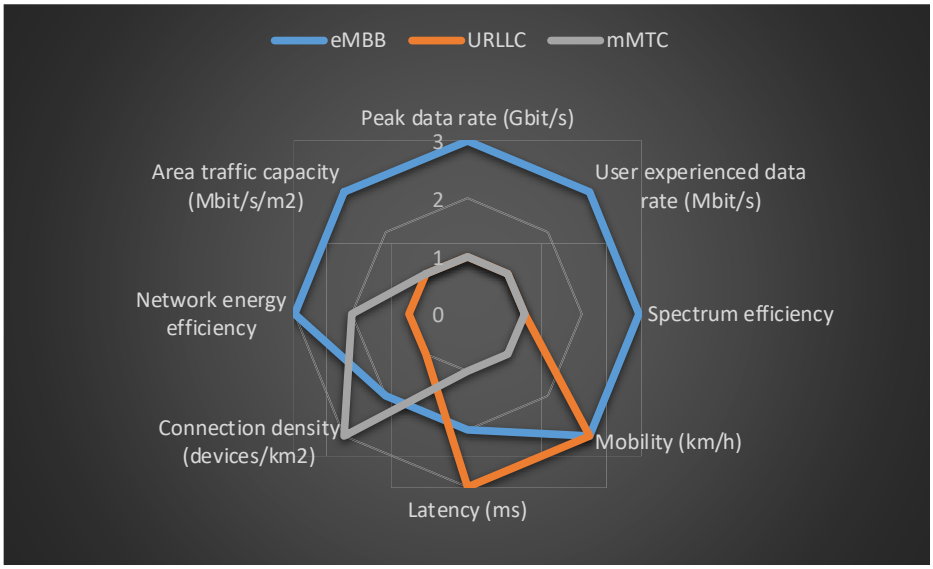

Figure 1.1: The importance of key capabilities in different usage scenarios [1].

surgery, smart grids, and emergency services.

- Massive machine-type communications (mMTC): providing wireless connectivity for an extremely large volume of delay-tolerant, low-powered devices. It provides scalable connectivity for almost dormant devices, whose traffic patterns are not fully characterised, and ensures longer battery life by the use of energy-efficient waveforms.

During the introduction of the 5G cellular networks, the triad of technologies that will make possible a thousandfold increase in capacity are extreme densification along with millimetre wave (mmWave), and massive multiple-input multiple-output (mMIMO) [7].

1. **Extreme densification**: providing a tier of small cells whose footprint does not go beyond tens of meters is a double-edged sword because, while offloading the macro tier, it also increases the interference, especially in co-channel deployments. In this context, advanced interference-mitigation techniques such as joint transmission coordinated multipoint (JT CoMP) can lessen the co-channel interference, and thus achieve higher spectral efficiency and improve

the coverage for cell edge users [8]. However, some concerns have arisen about the fundamental limits of densification [9].

2. **mmWave**: traditionally, cellular network deployments have been carried out in the microwave bands (sub 6 GHz), where they have to coexist with other technologies such as radio and TV stations due to their favourable propagation properties. As a consequence, these bands are under heavy regulations, and it seems implausible that any substantial portion of the spectrum will be auctioned any time soon. Hence, migrating to higher bands like centimetre and millimetre bands (28–60 GHz) becomes appealing to operators, where wide carrier bandwidths are commonly available [10]. Despite the propagation losses, as frequency increases, the physical size of the antennae diminishes, allowing for packing more per unit of area and benefiting multi-antenna signal-processing techniques [11].

3. **mMIMO**: the term mMIMO refers to the large-scale antenna arrays in the order of a few hundred elements (from 256 to 1024) simultaneously transmitting in the same time-frequency resource, hence achieving all the possible spatial multiplexing gain by steering the beam energy into ever smaller surroundings around users. The antennae consist of cross-polarised elements arranged in a variety of configurations: cylindrical, distributed, linear or rectangular [12]. Despite the very high data rates and spectral efficiency, it also uncovers a series of real-world problems such as pilot contamination, reciprocity calibration, non-channel-state-information transmit operation, and low-cost hardware implementations [13].

Besides these leading technologies and their associated signal processing methods, 5G will be based on other essential approaches. In recent years, non-orthogonal multiple access (NOMA) has gained some traction in academia, in which multiple data streams can be multiplexed over a single MIMO beam, and users must perform successive interference cancellation (SIC) in the power domain to decode their streams. Another contender is full-duplex communications, but signal processing is crucial to mitigate self-interference, the dominant issue of this approach. Some as-

pects of cognitive radio are envisaged as a possibility; however, some studies suggest that most of the development should be based more on understanding the trade-off between energy and spectral efficiency in scheduling and interference management rather than on sensing or signal processing [14].

1.2 Challenge and Motivation

The addition of small cells underlying the coverage of macrocells to improve the capacity per unit area in the most crowded urban areas or at cell edges was included in the Long-Term-Evolution (LTE) standard releases. Moreover, ultra-densification has been envisioned to play a vital role in 5G, where network heterogeneity will be a more prominent feature with the new 5G standard along with legacy standards and multi radio-access technologies [7].

The inclusion of small cells helps to offload the loaded macro tier by shrinking its coverage area, although some problems arise. Mobile users face a higher cross-tier handover (HO) rate due to smaller sojourn times, impacting negatively on their quality of service (QoS) as a consequence of the signalling needed. Too many HOs are unnecessary if users are not connected long enough to their serving cell (ping-pong effect, PP), while too few will lead to signal losses (handover failure, HF). The nature of the problem is combinatorial as a result of the existence of multiple handover-related parameters such as the time-to-trigger (TTT) or the handover hysteresis margin (HHM) [4].

The 5G New Radio (5G NR) HO execution time target is 0 ms, a substantial reduction when compared to the current LTE specification of 49.5 ms [15]. This time is heavily dependant of the HO connectivity employed by LTE, i.e. *break-before-make*, where a user equipment (UE) detaches from the network to perform a random access procedure in the target cell. A possible solution is to apply *make-before-break* connectivity, where a UE connects to the target cell without any service interruption, at the cost of increasing the measurement and reporting complexities as well as utilising resources in multiple cells at the same time [16]. Another option is giving UEs a higher degree of autonomy. In this case, UEs release and add various

radio links without network intervention, thus reducing the signalling overhead.

The 5G NR specification has added a feature in this regard called conditional HO (CHO) [17], where the baseline LTE-HO procedure has been split into two separate events. In the LTE-HO procedure, once the conditions for an HO has been met, it automatically follows with an HO execution, i.e. a UE starts a random access procedure in the target cell. In the CHO procedure, once the conditions for an HO have been met, it triggers a CHO preparation without a CHO execution. The execution is left to the UE to decide the optimal time or in case of an imminent radio link failure (RLF) [18]. On the one hand, the CHO preparation can be done in advance, reducing the delay when camping on the new cell, thus virtually reducing potential HFs or RLFs to zero [19]. On the other hand, CHO requires having an updated list of candidate cells where the CHO preparation has been done, even though at most only one potential HO will be executed.

In [20], the authors coined the term *ASE Crawl* to define how transitioning from 4G to 5G will end up plateauing the ASE as densification rises. In the current 4G networks, the density of base stations (BSs) is below 20 BS/km^2, while in the future 5G networks, this density is expected to rise to what is so-called ultra-dense networks, e.g. above 10^3 BS/km^2. Thus, dense cellular networks are considered to be within low tens to high hundreds of BS per square kilometre. What is more, as the density of BSs continues to increase above 10^3 BS/km^2 rapidly, the ASE will plummet to zero, which they referred as the *ASE Crash*. Their proposed solution to overcome this problem was to lower the BS height from current standards to the ground level, forcing a change of paradigm in BS deployments.

Despite the co-channel interference being a significant concern [21], backhaul provisioning poses another challenge in 5G small cell networks. A distributed architecture for ultra-dense cellular networks with single or multiple gateways was proposed in [22]. As opposed to 4G, where the HO is controlled by macrocell and picocell managers in the core network, the control plane and the user plane are split between tiers. In other words, the macro-cell tier would take care of the control plane traffic, whereas the small cells would be in charge of the data plane traffic. This architecture aims to alleviate the overhead caused by frequent user HOs for high-

speed mobile users. The authors conclude that ultra-dense 5G networks are not only interference-limited but also density-limited, meaning that, as the density of small cells per macrocell increases, the backhaul network capacity will decrease. Even so, universal access cannot be guaranteed while maintaining the same approaches to mobility management as in previous generations.

In summation, the two challenges in the mobility management that arise as the densification becomes extreme in 5G networks are:

1. Supporting mobility across increased network heterogeneity and
2. Determining appropriate cell association between tiers.

1.3 Contributions

The main contributions of this thesis are given as follows:

Chapter 3

- First, we propose an original HO algorithm based on predicted incomplete channel states from a Radio Environment Map (REM). In particular, we are interested in improving the mobility performance by reducing the overall number of HOs without sacrificing the network capacity. When applying a realistic timing, our results reveal a highly substantial improvement in the number of PP HOs in comparison to the LTE-HO algorithm without sacrificing QoS. For instance, we obtain at least an order of magnitude decrease in the PP rate at the expense of losing less than 9% in spectral efficiency. This work has been published as a conference paper *REM-Based Handover Algorithm for Next-Generation Multi-Tier Cellular Networks*.

- Second, we gauge the mobile backhaul traffic for different HO-skipping techniques found in the literature and our REM-based HO technique that exploits the geolocation-awareness. Then, we have employed a realistic 5G-ready environment concerning the network deployment and mobility traces to show the suitability of the proposed technique. The results highlight that our method

can deliver the same downstream traffic with 33% decrease in disconnections when compared to the conventional approach. At the same time, the backhaul traffic is reduced up to 68% against our counterparts. This work has been published as a conference paper *Low-Overhead Handover-Skipping Technique for 5G Networks*.

Chapter 4

- We develop an analytical framework for our proposed REM-HO algorithm that extends on the previous chapter. Based on the specifications for LTE and 5G-NR, we derive the probabilities of no handover, handover failure, and ping-pong handover in a two-tier HetNet as functions of the mobility parameters and geolocation information.

- We carry out an optimisation problem to fine tune our algorithm and validate our theoretical analysis through Monte Carlo simulations. To provide an insight into the impact of location errors in our proposed technique, we also compare it against the conventional LTE-HO algorithm. From the results, we show that our algorithm can avoid most of the PP HOs between tiers, for user speeds up to 120 km/h. However, location errors penalise the most, in terms of HF, due to the similar range between the errors and the distance travelled by the users during the HO process. Numerical results show that our REM-HO algorithm can drastically reduce the PP rate in most cases, maintaining it below 35%, an improvement of at least 10% over the LTE-HO standard and that the prediction time must be chosen adaptively to adjust to the HF rate.

The work in Chapter 4 has been published as a journal paper *Theoretical Analysis of REM-Based Handover Algorithm for Heterogeneous Networks*.

Chapter 5

- First, we derive the per-tier association probability under the REM-based cell selection, and the corresponding distance distributions to the serving cell, or

both the serving and the skipped cell for a given radius. Both functions are by nature probabilistic.

- Next, we determine the coverage probability in a fully-loaded network, where the coverage probability is defined as the probability that the signal-to-interference-plus-noise ratio (SINR) is above a given threshold. Computationally tractable expressions for coverage and rate are provided facing the impossibility of giving closed-form formulae.

- Finally, an optimisation problem is proposed based on the developed mathematical framework, where the optimal search radius is found for mobility users. A comparison between our proposed REM-based cell association with other cell-association policies follows concerning two metrics: average ergodic rate and backhaul traffic. Our strategy outperforms all of them in terms of the average ergodic rate employing half of the bandwidth that other schemes use and maintaining the same backhaul load as the traditional approach. In particular, it increases the average user throughput by 65% over the traditional approach, and it reduces the amount of overhead up to 68% over the other cell-association strategies.

The work in Chapter 5 has been submitted as a journal paper *Network Optimisation in 5G Networks: A Radio Environment Map Approach* and, after the first round of reviews, it has received major revisions.

1.4 Organisation of the Thesis

This chapter presents the background of the thesis as well as the challenges that motivate it. The main scenarios of each chapter are illustrated in Fig. 1.2. The rest of the thesis continues as follows:

In Chapter 2, we outline the pillars of this thesis: REMs and mobility management. Section 2.1 summarises the main efforts made in the radio environment mapping both in academia and industry. Section 2.2 gives an overview of mobility management in cellular networks and current challenges such as handover and cell

selection. We also introduce a taxonomy of handover algorithms based on a combination of the criteria and the technique used. Section 2.3 encompasses relevant uses of REM in cellular networks. Mobility management could benefit from REMs in different ways; in particular, we address the handover procedure in LTE networks and cell selection in dense cellular networks, which will be the focus of the next chapters.

In Chapter 3, we take an empirical approach to propose a REM-Based handover algorithm aimed to strike a balance between the number of unnecessary handovers and handover failures and evaluate its impact on the whole network. A first iteration of the algorithm is presented in Section 3.2, where fixed parameters are considered. This scenario comprises a first tier arranged in a hexagonal topology, complemented by a second tier randomly deployed around each macrocell. The density of cells for this first scenario is 198.94 cells/km^2 as per 3GPP guidelines. Based on the results obtained in Section 3.3, we decide to tweak the algorithm by using adaptive parameters that are more suitable for realistic deployments with real traffic flow in Section 3.5. In this case, the scenario resembles a typical European city centre where there is only one three-sectored macrocell on top of a building, and there are also 12 picocells installed on lampposts, which make an aggregate cell density of 70.22 cells/km^2. We also estimate the cost of our approach in terms of the average user throughput in the downlink and average network throughput between cells in Section 3.6.

In Chapter 4, we derive an analytical framework around the algorithm introduced in the previous chapter for heterogeneous networks with different tiers of cells, i.e. different transmit power. This power imbalance facilitates a geometric view of the coverage regions between tiers and leads to the system model discussed in Section 4.1. For tractability, we revisit the first scenario of Chapter 3, where a mixed topology of hexagonal grid and random deployment is considered for the two-tier network. Section 4.2 presents a set of probabilistic equations regarding different handover events and formulates a numerical optimisation problem for the optimal prediction time. The burden of positioning errors is considered in the formulation and assessed alongside other coetaneous algorithms in Section 4.3.

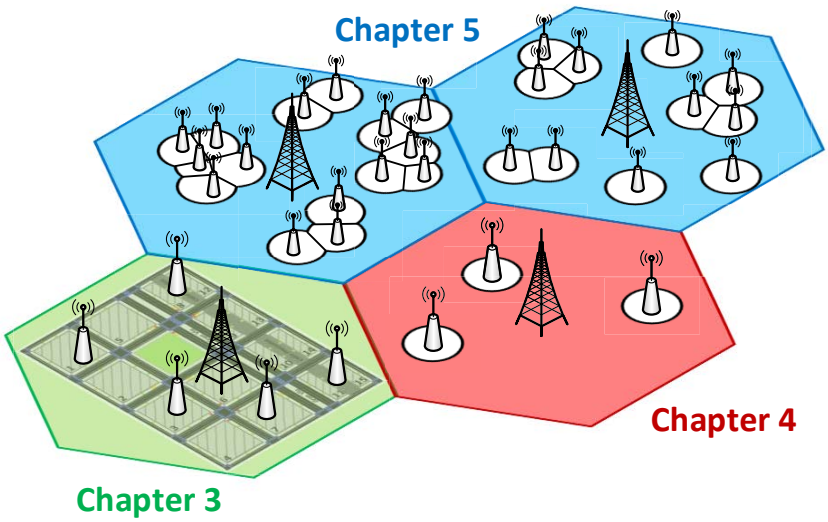

Figure 1.2: Scenarios of each chapter.

In Chapter 5, we broaden our scope from handover events to a dense cellular network altogether. We investigate a cell-selection technique that disregards specific associations to improve the user throughput. The association probabilities and distance distributions are analysed in Section 5.2. We found the coverage probability and spectral efficiency expressions through stochastic geometry in Section 5.3. A numerical optimisation problem follows in Section 5.4, targeted at maximising the user throughput and taking into consideration the penalty incurred by handovers.

In Chapter 6, we conclude the thesis and future directions are anticipated.

1.5 Summary

In this chapter, we have introduced the background of mobility management in 5G networks, the challenges that arise with network densification, and the motivation of this thesis. A summary of the contributions and organisation of the thesis is also given. In the next chapter, we will delve into radio environment maps and how they are applied to cellular networks to solve different problems.

Chapter 2

Literature Review

This chapter reviews the Radio Environment Map (REM) concept from an academic perspective and its applicability in industrial set-ups supporting cellular networks. Section 2.1 provides an overview of REMs. Section 2.2 elaborates on the current challenges in mobility management in cellular networks, namely handover and cell association. We also introduce a taxonomy of related work in handover and the limitations to solve these issues. For cell association, contemporary approaches fail to address the impact of advanced signal processing techniques in the backhaul. Section 2.3 shows the benefits of introducing REMs in terms of spectrum sharing, resource allocation, channel estimation, radio planning, and cell discovery within cellular networks.

2.1 Radio Environment Maps

The REM concept was firstly introduced by Zhao et al. [23] from the Virginia Tech team, where it is envisioned as a two-dimensional integrated database that contains multi-domain information on the radio environment but is not limited to:

- geographical features,
- available services,
- spectral regulations,
- locations and activities of radio devices,
- policies, and
- past experiences.

The REM stored information can be either derived from theoretical models [24] or obtained through measurement data [25]. The former uses a realistic three-dimensional urban electromagnetic wave propagation model fused with digital geographic map data (terrain altitude, building contours, etc.) to synthesise coverage maps down to 5-m resolution. The latter combines geo-tagged measurements reported by measurement capable devices (MCDs) with spatial interpolation techniques borrowed from geostatistics [26]. Nowadays, most handheld consumer electronics are equipped with at least one Global Navigation Satellite System (GNSS) that, combined with sensing capabilities, make them appropriate for the REM construction. However, both sensing and localisation errors play important roles in the final result, diminishing the expected gains [27, 28].

Attending to the time scale of the REM stored information, REM data can be classified as static, volatile, and derived. For example, static or quasi-static data correspond to the locations of TV towers, whereas volatile data mean that it is highly dynamic, e.g. spectrum usage information. Finally, derived information is determined after applying some processing techniques to the raw data regardless of their time scale, such as duty cycles [29]. At the same time, the data volatility

imposes an architecture division where efficient dissemination is crucial to prevent outdated or obsolete data from being used. Volatile data will preferably be stored as close as possible to the source in local REMs since it will increase the responsiveness of the system. On the contrary, static data is more suitable to be stored in global REMs, preferably in operator-centric scenarios [30].

The geo-tagged measurements are also timestamped, which means that, depending on the update rate and the granularity needed for a specific application, it might be impractical to construct REMs based on raw measurements only. For example, imagine the number of samples required to map a given area per unit of time, especially with volatile data in the order of minutes or seconds. Therefore, the traditional uniform spatial sampling, which requires time and effort to measure the radio environment at several locations, has been superseded by signal processing techniques like compressive sensing [31], where among all MCDs in a network, a subset of the MCDs perform measurements at a given time reducing the traffic overhead. Besides spatial and temporal dimensions, obtaining REMs in different frequency bands can be challenging due to the amount of time needed to scan the whole radio map or can be directly infeasible due to local spectrum regulations. In this context, spectral interpolation can alleviate the overhead that a direct-measurement multi-frequency REM would incur [32].

One of the first efforts to standardise REMs came from the Institute of Electrical and Electronics Engineers (IEEE) with its 802.22 specification aimed at the secondary access on the portion of the spectrum vacant after the analogue switch off, namely TV white spaces (TVWS) [33]. The IEEE 802.22 standard supports a two-tier network, where the primary users or incumbents have unrestricted channel access while the secondary users or licensees rely on opportunistic access without causing any harmful interference. To achieve this, all secondary users sense the radio spectrum and report their measurement to a central REM, which in turn derives a list of available channels and the maximum transmit power levels on each of them to minimise the interference towards the incumbents. Another joint academic and industrial effort towards broadening the REM concept is the European-funded Flexible and spectrum-Aware Radio Access through Measurements and modelling

In cognitive Radio systems (FARAMIR) project [34].

The vision of the FARAMIR project on REMs goes beyond a mere database that stores environmental data as in the IEEE 802.22 standard. Instead, their concept explores a holistic approach that encompasses a variety of use cases from operator-centric cellular networks to ad hoc networks. From a theoretical perspective, the task of obtaining radio environmental knowledge can be formulated as [25]:

> Given a finite number of localised radio measurement, how can we deduce the missing values of the measured quantity (the value of total received signal power on the considered frequency band) on the whole area of interest, with a given reliability degree?

The answer to this question comes from spatial interpolation; in particular, the FARAMIR project considered three methods: Kriging, modified Shepard's method (MSM) using inverse distance weighting (IDW), and gradient plus inverse distance squared (GIDS). The Kriging technique benefits from the spatial correlation inherently present in the radio propagation, correlated shadowing model, and is generally preferred because it generates the lowest interpolation error; however, its use in real-time set-ups is discouraged because its computational complexity grows as $\mathcal{O}(N^3)$ with the number N of measurements. Some advancements were done by reducing the number of samples required for interpolation by a third, exploiting Bayesian inference [35]. Similarly, in [36], the authors describe a fixed rank Kriging (FRK) model where the complexity is cut down to $\mathcal{O}(r^2N)$, where r is the number of deterministic spatial basis functions.

The contributions of the FARAMIR project were not limited to theory; an extensive body of work was also devoted to prototyping and putting into practice their theoretical framework. In [37], they constructed indoor REMS deploying a network of over 80 heterogeneous wireless spectrum sensors. They targeted two applications: mapping the indoor radio propagation conditions and the duty cycle of the primary users, where the main challenge was reconciling the significant variations in the data gathered by nearby sensors due to their different receiver characteristics. Focusing on the statistical characterisation of the primary user activity, a real-time spectrum selection technique is implemented in the Terrestrial Trunked

Radio (TETRA) band [38]. An emulated secondary network senses the channels of the downlink TETRA system and records the ON/OFF periods on a REM. Then, based on a first-order approximation, the secondary users are allowed to use the available channels, where the main objective is to minimise the number of spectrum HOs, i.e. change of channels.

A series of comprehensive measurement campaigns were carried out in Paris and London to analyse the spectrum use and radio environment dynamics in [39]. First, in Paris, they focused on frequency bands assigned to mobile network operators (MNOs) and described the interdependencies in spectrum use among bands, jointly with their spatial correlation characteristics. Second, in London, they studied the spectrum dynamics using both moving and stationary MCDs extending the previous models based on a local average to a distribution-wide approach. The results from Paris showed a strong spatial correlation in the RSS, and that these correlations can be captured using functions that depend solely on the distance between the measurement points. This benefits techniques that rely primarily on power levels such as collaborative energy detection or spatial interpolation for coverage prediction since data is sufficiently stationary to exploit spatial similarity efficiently.

On the contrary, the trend in the results from London indicates otherwise, where spatial correlation alone is not enough to describe changes in the received power distributions. The authors left a question open whether the complexity of the radio environment, especially at short distances, might make a dedicated MCD network economically infeasible because of the density required to capture their dynamics efficiently. At this point, they concluded that crowd-sourcing data from UEs might be the only possibility forward.

2.2 Mobility Management

Mobility management (MM) has been extensively studied in both industry and academia. How to ensure seamless connectivity for users has been a problem of the utmost importance throughout the history of wireless communications. Cellular networks are not an exception to the rule. Thus, it is worth clarifying some of

the current challenges in 4G and upcoming 5G networks. In 4G networks, one of the key technologies was the inclusion of small cells underlying the macro-only network layout. Depending on the radii of these cells, we can define microcells, picocells, and femtocells in a descending order. Generally, microcells and picocells are operator-owned, while femtocells are consumer-owned in an unplanned manner. In this context, low-cost zero-touch capabilities such as self-organising networks (SONs) were highly sought after in LTE networks [40].

The 3rd Generation Partnership Project (3GPP) established a series of simulation guidelines to assess improvements in seamless and robust mobility across HetNets in [4]. The principal key performance indicators (KPIs) in this document were the probability of RLFs and HFs, along with the probability of PP HOs. The first two KPIs are commonly used for measuring mobility performance as they indicate how smooth the transfers between cells are, i.e. without drops, whereas the last one reflects the signalling cost associated with unnecessary HOs. Therefore, strategies that can deliver low probability of these KPIs are said to be robust. In LTE HO, the probability of HF is proportional to the mobility speed of the UE and inversely proportional to the size of the HO region. For example, in 4G networks, the probability of HF is about 2.5% at 3 km/h, while it is about 31% at 120 km/h [18]. Recently, the 3GPP has segmented the LTE HO into two phases for 5G NR: network-controlled HO preparation and mobile-controlled HO execution, seeking an outage gain but also leading to a significant increase in signalling if not properly parametrised, for example, by SONs [19]. In summary, mobility robustness is an intricate problem because there is a trade-off between the HF rate and the PP rate.

Despite the importance of HO, the whole procedure, preparation and execution, takes place within the millisecond time scale. In the long term, cell selection/association determines the potential capacity gains for users. In 5G networks as opposed to 4G ones, it is expected that the increasing heterogeneity will be not only due to the cell sizes but also because of the many standards and spectrum bands coexisting [9]. Then, the optimal user association becomes a combinatorial optimisation problem that depends on user parameters (downlink SINR) as well as cell ones (cell load). One simple yet effective way of splitting users across HetNets

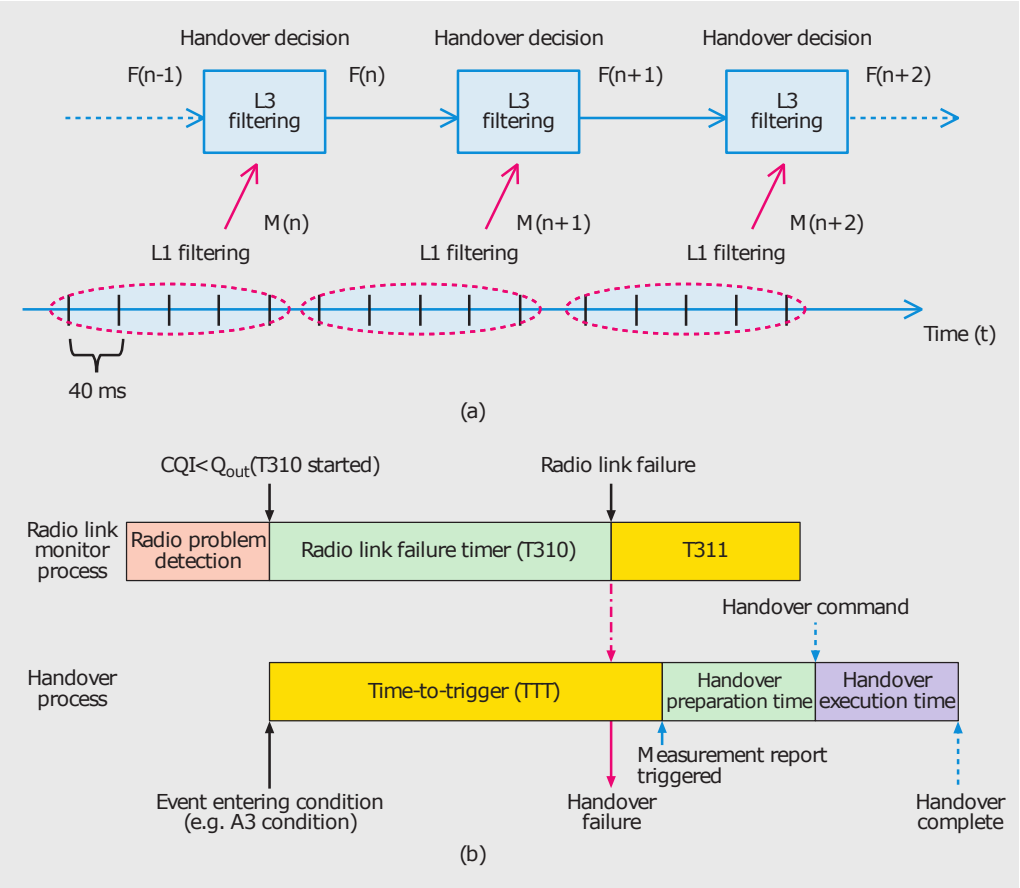

Figure 2.1: The handover procedure in the LTE-HO algorithm: a) L1 and L3 filtering processes; and b) Timers for RLF and HO procedures (extracted from [2]).

is biasing, which consists of virtually increasing the SINR experienced by users with small cells even when the macro tier turns out to be the best one available. Biasing has a positive effect in both tiers since it offloads the macro tier and provides more resources to the users that are now in the small tier since it usually is lightly loaded [41]. However, if these changes become too frequent, i.e. too many HOs, they counteract the foreseen capacity gains offered by the small tier because of the time needed to disconnect from one tier and reconnect to the other (hard HO). In this context, some authors have proposed topology-aware schemes aimed at maximising the user throughput by skipping certain cell associations [42, 43].

2.2.1 Handover

HO is the process by which a user transfers from its serving cell to a target one. It is typically associated with the best connection available, but the association might be

determined by other criteria such as load, delay or user speed. For instance, the LTE implements a hard HO approach that supports a wide range of association rules, known as events [2]. The LTE HO process consists of four phases: measurement, filtering, preparation, and execution (see Fig. 2.1, more details in Section 3.2). The first two take place at the user side. The UEs perform measurements of the Reference Signal Received Power (RSRP) over the cells included in their Neighbour Cell Lists (NCL) every 40 ms, and then average over five consecutive samples. This is known as Layer 1 (L1) filtering, and it is specifically targeted at removing the effects of fading. The result of this L1 filter, $M(n)$, is then averaged again through the second layer of filtering known as Layer 3 filtering, which deals with log-normal shadowing. The output value of this L3 filter, $F(n)$, is then, according to the event entry condition, sent as part of a measurement report. Once the serving cell receives this report, it starts the preparation stage, exchanging signalling with the target cell. During the execution phase, users are disconnected from the network before reattaching to the target cell. At the same time, the UEs are monitoring the channel quality. If the channel quality falls below a certain threshold, the UEs are said to be out of synchronisation, and the T310 timer is triggered (usually 1 s of duration). An HF is declared when this timer is running or expires during any of the stages of a HO. If it expires, an RLF ensues, and then, the T311 timer starts to re-establish the connection with the network.

Based on the LTE specifications, Lopez-Perez et al. [41] studied the effect of the range expansion bias on picocells' footprints and derived their boundaries as concentric circular regions. In [44], the same authors characterised the relation between HF and PP rates in a 3GPP HetNet scenario in closed-form expressions assuming that UEs follow linear trajectories. Vasudeva et al. [45] further extended this model to deal with fading, taking into account the L1 and L3 filtering. After collecting data from a 3GPP-compliant simulator, they concluded that fading could be incorporated in the formulation as a random variable on top of the measurement period. Lima et al. [46] followed a different approach where they characterised the outbound HF probability using tools from stochastic geometry. By considering a composite gamma-lognormal fading channel, the cell edges became probabilistic and

dependant on absolute power thresholds rather than the relative difference in power among BSs (SINR). Xu et al. [47] bridged previous works with stochastic geometry. They showed that the picocell coverage area is a circle and extended this result to a whole network employing the void probability of a Poisson point process (PPP). Then, the cross-tier HO rate is analysed in a simplified model with the random waypoint mobility (RWP) model. Similarly, the authors in [48] characterised the HO rate in a multi-tier HetNet with an arbitrary mobility model. An extension to this work can be found in [49], where the user data rate is also expressed in a closed form.

Beyond the 3GPP, a common criticism in the literature is the lack of tractability, most of the works below in HO decision algorithms present their results in the form of performance analysis, which may be insufficient to derive useful insights and provide mathematical results for the expected performance. For example, Kuang et al. [50] study the HF and PP HO rates based on a HetNet field-trial activity. Then the measured data are used as inputs to their simulation models. Despite its relevance, from a theoretical standpoint it is difficult to extend their conclusions to any other given network. Xenakis et al. [51] deliver a comprehensive survey of HO decision algorithms for femtocells in LTE-A, where the authors classify state-of-the-art algorithms according to the HO decision criterion using: a) received signal strength (RSS), b) speed, c) cost function, d) interference awareness, and e) energy efficiency. Nonetheless, they do not cover other approaches found in the literature such as f) context awareness, g) fuzzy logic, h) machine learning, i) location, and j) predictive methods. These criteria have their strengths and weaknesses that will not be discussed.

a) **RSS-based**

Most of the literature lies in here, including the LTE-HO algorithm through the A3 event: a neighbour becomes offset better than the server. Jung-Min and Dong-Ho [52] presented a method that combines the filtered RSS linearly from both the macrocell and the picocell involved in an HO. The linear combination is meant to overcome the uneven transmit power of the tiers, yet their technique yields a higher probability of HO to the femtocell without consider-

ing the signal quality, the number of HOs or the disconnection time. Aimed to reduce the disconnection time in high-speed trains (HSTs), Tian et al. [53] proposed a seamless HO scheme on top of the LTE that employs a relay and a dual-link system architecture. Using two antennae, they can execute the HO with one while the other remains connected to the serving BS, thus eliminating the need to forward data in the backbone. Moreover, all the passengers on board perform the HO at the same time through the relay, reducing the signalling overhead to about half of the LTE-HO algorithm. However, their proposed scheme relies on perfect channel state information (CSI), which is relatively idealistic, given that it is difficult to obtain at high speeds.

b) **Speed-based**

It is also common practice to restrict highly mobile users to macrocells, thereby lowering their rates. For instance, Zhang et al. [54] considered a low-overhead, low-complexity HO algorithm that adds a second condition to the well-known A3 event, allowing users to hand over to the femtocells only if their speed is below a speed threshold. Despite its backwards compatibility with the LTE-HO scheme, the selection of the threshold is not adequately investigated and remains as an ad hoc solution. Barbera et al. [55] proposed additional mobility enhancements to the existing LTE-HO algorithm by also preventing highly mobile users from accessing small cells. To that end, they modify the mobility state estimation (MSE), where all the HOs count the same amount, to a weighted sum depending on the serving and target cell characteristics. Based on this enhanced estimator, they develop two mechanisms: grey-listing solution and cell-dependent TTT scaling. The former avoids reporting grey-listed cells when in high mobility state, whereas the latter up or down-scale the TTT depending on the type of HO (co-tier or cross-tier).

c) **Interference-aware**

Xenakis et al. [56] introduce an HO decision algorithm for LTE that takes into account both the interference at the UE side and its battery life designed for indoor use. They optimise two HHMs: the first one skips cells that might

compromise service continuity, i.e. drops, whereas the second one identifies the cell with the minimum required UE transmit power. The method exchanges the interference at the UE side for the cell side and increases the utilisation of the femtocells, and with it, the HO probability. Another adaptive HHM approach can be found in [57], where the authors claimed that the shape of the femtocell coverage region is majorly affected by the SINR and not by the RSS. Under this assumption, they compare the SINR status from the serving and the target cells as well as the estimated path loss and modify the HHM to reduce the number of unnecessary HOs accordingly. The performance is only evaluated in a suburban scenario along a direct street with family houses on the sides at pedestrian walking speed, but further simulations in different set-ups would be desirable.

d) **Energy-efficient**

A policy aimed at minimising the UE power consumption exploiting the shorter distance from the femtocells is described in [58]. A user sends a measurement report when the HO triggering event is fulfilled; then the serving cell starts evaluating the average uplink transmission power required for a given SINR threshold that depends on the sustained QoS. This process is done sequentially with the help of a queue structure, where neighbouring cells that fail to satisfy the criterion are removed. The HO decision is made when all candidates cells have been evaluated, or the TTT goes off, whichever comes first. In the case of having found a suitable cell, the HO is allowed towards the neighbouring cell with the lowest UE power consumption. Otherwise, a reconfiguration procedure is triggered, i.e. a drop. Although the technique efficiently saves energy in both uplink and downlink streams, the overall number of HOs is increased. Besides, results on the HF and the PP probabilities are omitted.

e) **Cost-function based**

Lee et al. [59] combined some of the criteria already discussed into a cost function in the form of a weighted sum of normalised functions. This approach is quite common in the optimisation literature, where a multi-objective op-

timisation problem is converted to a scalar problem [60]. In particular, the authors considered the load difference between the target and serving cells, the velocity of UE, and the service type. Then, the value of the cost function is employed in deriving a flexible HHM. One of the novelties of this scheme is the user segmentation by service: real-time and non-real time, which permits the hand over of users based on their traffic dynamically. One of the drawbacks of this HO decision algorithm is the lack of hyperparameter optimisation, i.e. the values of the weights are chosen arbitrarily. In order to deal with that, Alhabo et Zhang [61] devised two weighting strategies based on the Technique for Order Preferences by Similarity to Ideal Solution (TOPSIS). The former employs an entropy-weighting technique, while the latter uses a standard-deviation weighting approach. Both methods fall under the category of multiple attribute decision making and take into consideration the Time of Stay (ToS), the user arrival angle to the target cell, and the SINR. Despite the reduction in HO rate and RLF as well as the enhancement of user throughput, these techniques may increase the computational complexity since they require real-time data from the candidate cells and perform matrix algebra.

f) **Context-aware**

Guidolin et al. [62] proposed an original Markov-based framework that exploits some parameters (e.g. the path-loss coefficients, the user speed, and the cell load factors among others) to derive an optimal TTT context-dependent parameter from limiting the number of HOs and also the signalling between the cells. They showed an improvement in the users capacity against fixed-TTT policies. Likewise, a Markov-based mobility prediction method is derived from diurnal mobility patterns (from home to work, then to a supermarket, such as from [63]) to predict the next cell and avoid coverage holes (tunnels) by buffering data beforehand. However, prior knowledge of the routes is needed. Calabuig et al. [64] proposed a context-aware, user-oriented radio-access technology selection mechanism in HetNets that uses fuzzy logic to evaluate available information such as user preferences, equipment capabilities, status, network

load, and operator's policies. Their scheme was compared against the LTE HO algorithm in an indoor environment, a 3-storey shopping centre, where users were free to roam. Results show a throughput gain, ranging from 12 to 86% as the traffic load also increases. Despite its low overhead since the calculations are made on the user side, it requires a high number of rules, 729, that might be cumbersome to manage.

g) **Fuzzy logic**

Similar to the cost-function based methods, fuzzy logic provides a framework to make multiple-criteria decisions, performing ratings and weights represented by linguistic variables. For example, Hussein et al. [65] considered the RSS, the number of available resource blocks, and the SINR of the candidate cells in a single-tier network, so its performance in a multi-tier network remains an open question. Da Costa Silva et al. [66] built their technique around mobile networks with dense small cells and proposed a fuzzy logic-based HO scheme exploiting the user's velocity and its radio channel quality to adapt an HHM in a self-organising manner. This dynamic adaptation minimises the number of redundant HOs and HFs. However, the intervals and granularity of the input parameters - namely speed, channel quality, and received power - are based solely on the 3GPP specifications [67], meaning that it only adapts for a very narrow range of networks. There is no method to adapt their definitions to any given network.

h) **Machine learning**

The advent of machine learning in a broad class of engineering problems is a reality. Jiang et al. [68] surveyed machine learning paradigms for next-generation wireless communications. In particular, to improve the QoE, regression analysis algorithms such as k-nearest neighbours and support-vector machine can be exploited to find location-specific configurations. For example, experiments yielded up to 90% successful prediction for energy demand, which could be applied for energy-saving algorithms. In a SON environment, Sinclair et al. [69] used a modified self-organising map, a type of unsupervised

neural network, to allow a femtocell to learn the locations of an indoor environment whether to permit or prohibit HOs. This neural network capitalises on previous experience to detect which regions led to unnecessary HOs, building a representation of the radio environment in the process, and is shown to be robust under positional errors. However, it would be interesting to see its scalability in outdoor environments. Chaudhuri et al. [70] proposed a self-optimising HO detection algorithm based on reinforcement learning. Their method is aimed at optimising HO decision parameters, namely TTT and HHM, by modelling a time-discrete Markov decision process. Results showed a high degree of adaptability to a wide range of scenarios, which is one of the critical features of SONs. However, there are several pitfalls. They did not present the optimal set of values for each scenario nor the convergence time. The former is essential since the LTE standard only allows a discrete set of values that needs to be encoded, while the latter is important to assess the feasibility of the method in a real environment. The amount of overhead required to send the decision parameters at each time step could outweigh the throughput gains, whose discussion is also missing.

Simsek et al. [71] addressed this problem in a holistic way: a short-term context-aware scheduler that relies on historical data (average rate and instantaneous speed) and a long-term load estimator that uses reinforcement learning. For the long-term solution, they considered two algorithms: a multi-armed bandit, that resembles slot machines, and a satisfaction equilibrium. Both algorithms perform better than the LTE-HO algorithm in terms of UE throughput, PP and HF probabilities; nonetheless, the convergence behaviour of the approaches is solely presented in the number of iterations for TTT = 480 ms, which is a high value only recommended for pedestrian walking speed. Handovers can also be triggered for more purposes than enhancing QoE, for instance, load balancing. Hasan et al. [72] presented a centralised SON algorithm that defines a resource block-utilisation ratio and minimises its standard deviation across the network. Their strategy employed an adaptive threshold for the A3 and A4 events, shifting edge users from neighbouring cells in a

controlled way to avoid PPs of load. Via simulations, they verified the load distribution in the network was evenly distributed instead of concentrated in a few cells. As a result, the user throughput increased due to having more resources available at each cell. The main critique of this method is its centralised approach, as the question of how many cells are required to find the optimal solution is left unanswered. A decentralised or hybrid scheme would be suboptimal, but it is more realistic that the proposed oracle-like solution.

i) **Location-based**

Po-Hsuan and Kai-Ten [73] designed an HO decision algorithm purely based on ranging measurements for the IEEE 802.16 series of standards, commercialised under the name Worldwide Interoperability for Microwave Access (WiMAX). In their paper, a Kalman filter is cascaded to smooth out the estimated location from raw measurements and to trace the estimation errors. Although the positional errors are high, tens of meters, the number of HOs is successfully reduced. A similar solution could be proposed for the LTE, but handheld devices possess GNSS capabilities that outperform any other ranging technology. Chen et al. [74] present a framework of HO decision in LTE networks under a high-speed mobility scenario, i.e. up to 500 km/h. They investigate a location-based HO decision algorithm that makes use of the information about the relative location between a train and cells down the tracks. By analysing the speed information sensed by the tachometer, the UE sends a measurement report of its current distance and velocity to the serving cell. Although the framework could be easily adapted to low-speed environments, the algorithm only considers a homogeneous network, where the cell edges correspond to the midpoint between cells. A similar topology is studied in [75], where the authors employed an adaptive beamforming technique changing the beamforming gain when the trains are located in the overlapping region between cells. To further improve the HO performance, the HHMs are dynamically scaled with the train speeds. Details on the beamforming scheme chosen or the feedback channel for reporting location are not given.

j) **Prediction-based**

In [76], for instance, the authors estimate the distance that a user traverses based on RSS measurements and calculate distance thresholds according to the probability of HF and PP HO. On a similar note, Becvar and Mach [77] propose an HO decision algorithm based on the estimation of throughput gain in case of handing over to femtocells. Coordination between macrocells and femtocells via backbone is exploited to mitigate redundant HOs. The increase in throughput is derived from an extrapolation of the previous measurements performed by UEs; then the HO is only executed if the gain is above a predefined threshold. However, their method has two significant drawbacks: first, the estimated gain relies on the prediction of the sojourn time within the cell, which in turn reduces the applicability of the algorithm to hand-in only; and second, the method is aimed at pedestrians.

All the algorithms mentioned are listed in Table 2.1.

2.2.2 Cell Association

An extensive body of work has been developed in recent years employing stochastic geometry as a way to provide a tractable model to evaluate a wide range of techniques in cellular communications [78–82]. Although the realm of stochastic geometry spans multiple disciplines, Andrews et al. [78] arguably develop the first model for the SINR in a single-tier cellular network using stochastic geometry. In this seminal work, they present a tractable set of expressions that can be easily computable in contrast to cumbersome system-level simulations that are hardly reproducible. They conclude that their model effectively acts as a lower bound of the coverage probability, whereas the grid model acts as an upper bound when compared to actual BS deployments. This work is further extended by Dhillon et al. [79] to K-tier HetNets for either open or closed access under the assumption that users connect to the BS that offers the highest instantaneous SINR.

However, users usually do not associate themselves to a BS instantaneously, but after several rounds of filtering to suppress the effects of fading from RSS measure-

Table 2.1: Taxonomy of HO decision algorithms.

a) RSS-based	**b) Speed-based**	**c) Interference-aware**	**d) Energy-efficient**	**e) Cost-function based**
Jung-Min and Dong-Ho [52]	Zhang et al. [54]	Becvar and Mach [57]	Xenakis et al. [58]	Lee et al. [59]
Tian et al. [53]	Barbera et al. [55]	Xenakis et al. [56]		Alhabo et Zhang [61]
f) Context-aware	**g) Fuzzy logic**	**h) Machine learning**	**i) Location-based**	**j) Prediction-based**
Guidolin et al. [62]	Hussein et al. [65]	Sinclair et al. [69]	Po-Hsuan and Kai-Ten [73]	Xiaohuan et al. [76]
Kuruvatti et al. [63]	Da Costa Silva et al. [66]	Chaudhuri et al. [70]	Chen et al. [74]	Becvar and Mach [77]
Calabuig et al. [64]		Simsek et al. [71]	Zhao et al. [75]	
		Hasan et al. [72]		

ments [2]. In this regard, Jo et al. [80] present a mathematical framework for SINR analysis in K-tier HetNets for open access where users connect to the BS that offers the highest long-term averaged SINR. They propose a flexible cell association using bias factors that can dynamically shift users from one tier to another regardless of the RSS. Singh et al. [81] elaborate on this idea in a multi-tier multi-radio-access technology network to offload the cellular traffic onto Wi-Fi. They show that the optimum bias depends on the metric to be maximised, namely SINR coverage or rate coverage. Moreover, Zhang et al. [83] proved that the strategy presented in [80] always outperforms the scheme introduced in [79] on multi-slot coverage probability, i.e. considering the spatial correlation of the SINR while moving, showing the effect of interference on the HO procedure.

A system-level and interference-aware optimisation criterion of the bias is introduced by Lu and Di Renzo [82] in a single-tier cellular network with relay nodes. One of the key findings drawn is that, in general, optimisation problems in the context of stochastic geometry do not show closed-form solutions, despite the simplicity of the utility functions. Another example can be found in [84], where Yang et al. analysed the performance of an ultra-dense millimetre-wave network with control and user plane separation architecture. The main focus is to find the optimal cell density that reduces the HO cost, constrained by a certain coverage probability. The problem is found not to be monotonically increasing nor a convex function with respect to cell densities. Therefore a numerical solution ensues. These solutions were different depending on the selected architecture. On the one hand, for conventional network architectures, the HO cost can be minimised by adding macrocells. On the other hand, including more small cells reduces the HO cost in split architectures like 5G [19].

Mobility management has suffered from the same lack of tractability. One of the first works to address the user mobility in a Poisson-Voronoi single-tier cellular network was carried out by Lin et al. [85]. Applying Rayleigh-distributed transition lengths to the well-known RWP mobility model, they analysed the HO rate and the sojourn time in two BS scenarios: a hexagonal grid (deterministic) and a Poisson-Voronoi network (random). Bao and Liang [49] found a stronger result, the

trajectory followed by an active user is irrelevant, i.e. it might be arbitrary when deriving the rates of all HO types (horizontal and vertical) in a multi-tier HetNet. They conduct a comparison between the user mobility trace data and their analysis to demonstrate its correctness. Since HOs become more frequent as network density intensifies and user speed increases, several works have pointed out the necessity of skipping HOs. These strategies aim to find a balance between the benefits in the capacity of smaller cells but also considering disconnections as a penalty [42, 43, 86].

Arshad et al. [86] proposed the femto-skipping (FS) and the femto-skipping with interference cancellation (FS-IC) strategies in two-tier HetNets. In both algorithms, FS and FS-IC, users skip femtocells alternatively along their trajectories. The skipping pursues reducing the HO rate, i.e., the disconnection time for the users. When a user skips a femtocell, the second and the third strongest cells perform cooperative transmission (JT CoMP [8]), intra- or inter-tier. Since the interference from the skipped femtocell, the strongest one, might be overwhelming, interference cancellation (IC) is also enabled [87]. The same authors extended their work in [42], where they proposed adding location awareness to the skipping decision. In the location-aware with IC (LA) strategy, a user skips any cell if the distance between the user and the target cell is above a threshold. Once an HO is skipped, both the JT CoMP and IC are assumed to be following the same principles as FS-IC. Similarly, Demarchou et al. [43] studied two HO techniques: an HO skipping technique based on the upcoming BS's topology and a cooperative scheme based on three consecutive cells in the user's trajectory for single-tier cellular networks. In the first technique, HOs are skipped according to three different criteria: the area of the cell, the chord length of the cell, or the distance from the cell edge. The threshold is set as a factor of the expected value of each criterion. In the second cooperative scheme, the users are always served by the two closest BSs in the network.

Although the user side benefits from these HO skipping techniques, it is not clear how the network side is affected by them. As important as the user throughput is the backhaul, which some skipping techniques in the literature based on JT CoMP fail to address. Cooperative transmission certainly improves the spectral efficiency of users, especially those in harsh conditions; nonetheless, some strategies harden users'

conditions purposefully by skipping HOs as long as JT CoMP is their safety net without acknowledging that the system bandwidth is effectively halved. Besides, the authors in [42, 86] consider perfect cancellation which is an optimistic assumption. In [87], the authors conclude that for users connected to the BS that offers the strongest long-term RSS, IC is only attractive in the case of weak signal conditions, i.e. cell edge.

2.3 Applications of REMs in Cellular Networks

In the FARAMIR project, it was envisioned operator-centric cellular networks where REMs could play an important role, providing spatial awareness. We list some of the main applications of REMs in cellular networks below:

Spectrum sharing

Since REMs were conceived for cognitive radio, it seems natural to adopt them in cellular networks for spectrum sharing. From the FARAMIR project, Grimoud et al. [88] used a REM, which stores the RSS and cell load, to optimise the power mask in a soft frequency reuse (SFR) scheme. The addition of propagation and traffic knowledge allows a genetic algorithm to improve the expected throughput by 13%. Furthermore, Dwarakanath et al. [89] modelled interference maps for Licensed Shared Access (LSA) in LTE networks, where they devised a spectrum sharing scheme to combat the interference induced by an LSA licensee on an LTE incumbent. Although REMs produced a substantially improved performance over the basic scheme, their technique required a dedicated sensor network alongside the network infrastructure, which increased the cost of the scheme. Holland and Dohler [90] led a major trial in the UK to assess the availability of channels in the TVWS bands to enhance spectrum sharing for 5G. Based on the UK/EU regulations regarding spectrum mask, they concluded that small cells able to aggregate multiple non-contiguous channels would be reasonably viable using a geolocation database-based architecture, i.e. a REM architecture.

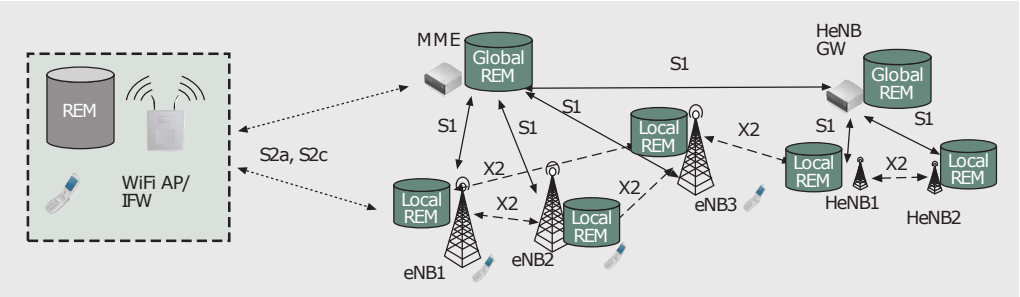

Figure 2.2: Layered REM architecture integrated in the LTE networks (extracted from [3]).

Network architecture

We can distinguish two approaches in the literature: REMs as enablers to bring LTE to TVWS [91] and REMs to support interference management optimisation in HetNets [3]. In the former, the authors discussed an ad hoc functional REM architecture, where different network entities are needed to acquire, store, process, and exploit radio environmental data. Besides the MCDs making measurements, there are the REM storage and acquisition unit as a data broker, the REM manager in charge of the processing tasks, and the REM users such as radio resource management (RRM) entities, policy managers, or mobile operators. In the latter depicted in Fig. 2.2, the authors mapped the REM functionalities to specific network elements in LTE networks. For example, the MCDs will become the mobile terminals and the cells, the REM manager will reside in the cells, and the storage and acquisition will be further split into two: acquisition at the small cells, and storage at either the MM entity or the gateway.

Resource allocation

Xue and Wang [92] studied the resource sharing problem among multiple Device-to-Device (D2D) links underlaying TVWS based on REMs. By storing the up-to-date available channel information and other relevant parameters in the REM, they performed resource allocation in two stages: spectrum assignment with interference minimisation as well as power control and admission control. Another example, Zaaraoui et al. [93] introduced the concept of a forecast scheduler for users with

high mobility employing SINR values provided by a REM, where the UEs have the capability of positioning using either a GNSS or an LTE network-assisted technique along with the measurement reports, already supported by the Minimization of Drive Test (MDT) in LTE.

Channel estimation

Hou et al. [94] exploited the fact that trains travel along a constant route, which is regular, repetitive, and predictable to estimate the Doppler shift experienced by HSTs in LTE Railway networks. At such high speed, the Doppler shift estimation is challenging, so they constructed a REM via field tests. Then they proposed an a priori estimator based on the raw measurements and an a posteriori method that also exploits the cyclic prefix (CP) structure of orthogonal frequency-division multiplexing (OFDM).

Radio planning

Radio planning tools such as simulators have been historically used to decide the best locations for new cell deployments. As mentioned in Section 2.1, REMs can be synthesised from propagation models. In this context, Letourneux et al. [95] presented a real model for realistic and large-scale HetNet performance evaluation. Such a model is site-specific and employs a ray tracer named Volcano by SIRADEL, a French company. This tool gathers a myriad of heuristic parameters and drive tests from mobile operators, so it is said to be pre-calibrated. In this work, they found that closed-access femtocells cause dead zones for non-subscribers in 15% of multi-storey indoor areas.

Similarly, Galindo-Serrano et al. [96] harvested MDT data to automatically identify the number, location, and shape of coverage holes. They converted a coverage map in power units to a binary map after defining a minimum RSS threshold. Then using image processing techniques, they replaced the tedious manual process of the coverage hole analysis by an automated solution.

Cell discovery

Prasad et al. [97] considered reducing the power consumption of users in mobility using a fingerprinting-based scheme. Since mobile terminals need to send measurement reports periodically, they can match these reports against REMs and instruct users to perform inter-frequency measurements only in the vicinity of small cells, providing an energy-efficient discovery mechanism. Despite the slow fading fragmenting of the small cells' coverage area, their results show gains of more than 98% in terms of the battery saving.

2.4 Summary

In this chapter, we have presented a literature review related to REMs from their inception in cognitive radio to their application in cellular networks. We have stressed two principal challenges in mobility management, such as handover and cell association. Also, a classification of handover-decision algorithms is delivered attending to the primary criterion or the framework employed. Some drawbacks of the current state-of-the-art approaches have been exposed like lack of tractability and halving the bandwidth. In the rest of the thesis, original work will address these limitations.

Chapter 3

Evaluation of Radio Environment Maps in 4G and 5G

The strongest-cell criterion has been extensively used for handover algorithms during the last cellular-network generations. When network topologies become multi-layered, it results in abrupt behaviours such as the ping-pong effect as a consequence of the power gap between tiers and their irregular deployment. This effect not only affects users' quality of experience but also introduces a significant network overhead. Therefore, we propose an original handover algorithm based on predicted incomplete channel states from a Radio Environment Map to reduce this effect in Section 3.2. The proposed algorithm is user-triggered, network-assisted, and fully backward compatible with LTE. Moreover, we evaluate the performance of our proposed algorithm against LTE in a two-tier cellular network for different user speeds following the guidelines outlined by the 3GPP on diverse matters such as channel, mobility, and wrapping in Section 3.3. When applying realistic timing, our results reveal a highly substantial improvement in the number of ping-pong handovers regardless of the handover policy adopted in comparison to LTE without sacrificing too much users' experience; for instance, we obtain at least an order of magnitude decrease in the ping-pong rate at the expense of losing less than 9% in spectral efficiency.

Invisible to the users, mobile network operators need to provision backhauling to include advanced interference mitigation techniques. In this chapter, we modify

our REM-aided handover management technique aiming to mitigate the number of disconnections without overloading the backhaul unnecessarily in Section 3.5. The proposed technique exploits a REM that stores the reception information along with geolocation data, commercially available on any handheld device. Finally, we have benchmarked several state-of-the-art handover schemes for 5G networks against ours in a realistic urban environment with user mobility trace data in Section 3.7. The results highlight that our method can deliver the same downstream traffic with 33% of decrease in disconnections when compared to the conventional approach. At the same time, the backhaul traffic is reduced up to 68% against our counterparts.

3.1 HetNet System Model

In this chapter, we assume that REMs are stored and managed by the mobile network operator. For example, in [3] the authors discuss possible implementations in different network entities within an LTE network. They introduce a layered architecture that consists of local and global REMs, where the coordination between local REMs can be done through the X2 interface while the coordination between local and global REMs must be done through the S1 one. REMs are typically geolocation databases that store some Radio-Frequency (RF) relevant parameters. The cost, field measurements mostly, of the maps is not considered in this chapter. So as to create a map, we can deploy MCDs that perform measurements (UEs and sensors) and apply spectrum cartography techniques as in [31], or we can use a realistic 3D urban electromagnetic wave propagation fused with digital geographical map data such as terrain altitudes, and building contours to synthesise coverage maps (up to 5-m resolution) as detailed in [95].

Also, users must be able to measure the band of interest and report those measurements to their serving cell in a similar fashion to the current LTE UE. Moreover, we need UEs to have the capability of positioning using either a GNSS or an LTE network-assisted technique. In the former group is included the GPS, GLONASS or GALILEO positioning systems, whereas in the latter Observed Time-Difference Of Arrival (OTDOA) and Enhanced Cell-ID techniques are used. The impact of these systems on the proposed algorithm is beyond the scope of this chapter. However, Chapter 4 delves into this matter.

We assume a HetNet composed of evolved Node B (eNB) and Home eNB (HeNB) in open-access mode. Both tiers belong to the same MNO, whose allocated frequency bands compose the set $\mathcal{F}$. Additionally, they operate in the same band $f \in \mathcal{F}$. As we evaluate the handover performance, from now on, we are solely focused on the downlink. Let $\mathcal{C}$ denote the set of cells operating in f, regardless of the tier, and $\mathcal{U}$ the set of users. As a consequence, the SINR of a user $u \in \mathcal{U}$ camping on its serving

cell $s \in \mathcal{C}$ can be expressed as

$$\gamma_{s,u} = \frac{P_s |h_{s,u}|^2}{\sum\limits_{c \in \mathcal{C} \setminus \{s\}} P_c |h_{c,u}|^2 + \sigma_u^2}, \tag{3.1}$$

where P_s is the transmit power of the cell s, P_c is the transmit power of the cell c, $h_{s,u}$ is the channel gain from cell s to user u, $h_{c,u}$ is the channel gain from cell c to user u, and σ_u^2 is the noise power at user u. Nonetheless, the LTE standard defines two different UE measurements: Reference Signal Received Power (RSRP) and Reference Signal Received Quality (RSRQ). Without loss of generality, in our approach a user u only measures the RSS from a cell $c \in \mathcal{C}$, defined as $\mathrm{RSS}_{c,u} = P_c |h_{c,u}|^2$.

LTE caters for mobility with event-triggered reporting, using both intra- and inter-frequency measurements whose values and thresholds are in dBm/dB. The entry condition must be met for at least the TTT period, generally configured by the network and further scaled by the user, depending on its speed to control the ping-pong effect. A relative offset also helps to adjust the timing when the handover is executed: a low value might lead to a too-early handover while a high value may end up with a too-late handover or even an RLF. Substituting the RSRP for the RSS as aforementioned we can describe this handover policy as follows:

$$c^* = \underset{c \in \mathcal{C}}{\operatorname{argmax}} \ \mathrm{RSS}_{c,u}(t) \mid \mathrm{RSS}_{s,u}^{\mathrm{TTT}} < \mathrm{RSS}_{c,u}^{\mathrm{TTT}} - \mathrm{HHM}, \tag{3.2}$$

where c^* corresponds to the strongest cell, $\mathrm{RSS}_{c,u}^{\mathrm{TTT}}$ is the $\mathrm{RSS}_{c,u}$ during the TTT, and HHM corresponds to the relative offset. We want to emphasise the time dependence, which is not commonly made explicit since our proposed algorithm to be introduced in the next section will depend specifically on time. From (3.2) it is clear that the current algorithm promotes cells with higher power/channel gain regardless of any other criteria such as SINR, cell load, and UE power consumption. In the remainder of this chapter, cell detection is assumed to be done under the time constraints specified in 3GPP TS 36.133 [98]. Therefore we will only focus on the handover itself.

3.2 REM Handover Algorithm

While the LTE handover policy has shown itself to be robust enough only in macrocell scenarios, with HetNets it becomes more challenging due to the higher interference under co-channel deployment, Neighbour Cell Lists (NCL) rapidly changing when femtocells appear and disappear. This is especially true for users who pass through an area under the overlapped coverage of different tier cells because of the number of ping-pong handovers increases and, thus, the network signalling. Furthermore, the higher the UE speed is, the more complicated the handover decision stage becomes. Our main objective is to reduce the overall number of ping-pong handovers between tiers using the spatial information provided by REMs without compromising the QoS of the users.

The proposed algorithm scheme relies on the same event-triggered mechanism as does LTE, although it is not limited to it. Thus it can be seamlessly adapted to current state-of-the-art UEs. As REMs will only be stored on the network side, the proposed algorithm avoids any extra overhead due to the exchange of information between the REM database and the UE. However, users must be requested to send their location along with the measurement reports, as already happens in the MDT in LTE [99]. It is worth noting that REM is not a technology to enhance from 4G to 5G. Instead, it can be applied to both to increase the performance.

Once the measurement report is triggered, our proposed algorithm predicts the user's position in a timespan Δt, assuming a simple uniform linear motion described by $\mathbf{r}(t + \Delta t) = \mathbf{r}(t) + \mathbf{v}\Delta t$, where $\mathbf{r}$ and $\mathbf{v}$ are position and velocity respectively. Even if the trajectory of the user is either accelerated or not linear, provided that the timespan is not too long the trajectory can be approximated by a set of adjacent segments where each follows a uniform linear motion. The endpoint is then introduced in the corresponding REMs to get an expected RSS value for a given cell. In order to reduce the number of queries, there is another algorithm-related parameter, R, which defines a searching radius whose centre is the predicted position. An example of this predicted position and the searching radius is depicted in Fig. 3.1. This parameter allows us to set an upper bound on the number of cells to

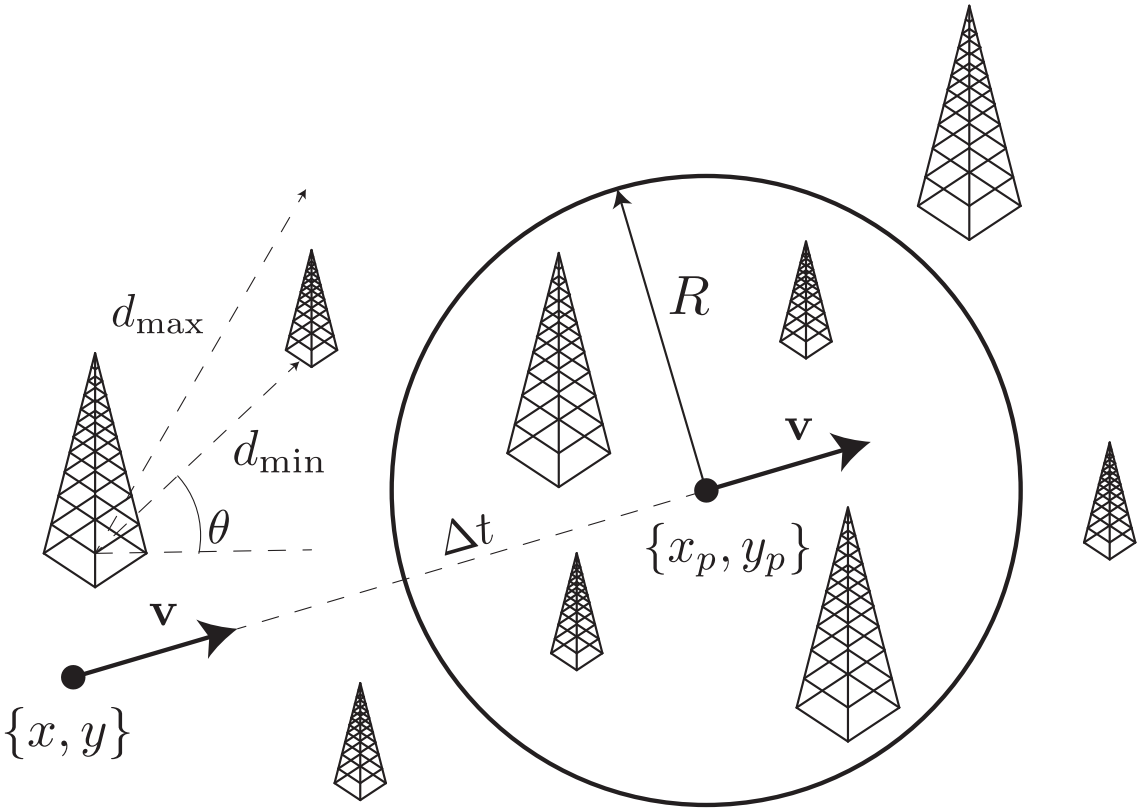

Figure 3.1: The analysed scenario for proposed REM handover algorithm.

be considered in the prediction calculations.

At this stage, even though we could pick the strongest predicted cell in Δt, it is preferable to obtain a more unbiased measurement like the SINR. Besides, the expected QoS of the user will depend on the capacity of the channel rather than just the highest received power. Taking all the previous parameters into account, our proposed policy to determine the strongest cell for handover can be expressed as

$$c^* = \underset{c \in \mathcal{B}}{\operatorname{argmax}} \ \gamma_{c,u}(t + \Delta t) \mid \mathrm{RSS}_{s,u}^{\mathrm{TTT}} < \mathrm{RSS}_{c,u}^{\mathrm{TTT}} - \mathrm{HHM}, \tag{3.3}$$

where all parameters from (3.2) remain, and $c \in \mathcal{B}$ means cells within the searching radius ($\mathcal{B} \subset \mathcal{C}$). What this policy accomplishes is that a user will hand over to the strongest cell only if that same cell has the highest SINR according to the user's trajectory. Note that (3.1) is a pessimistic evaluation of the SINR since the cell traffic load is not considered (all cells are fully loaded) and hence we could avoid some handovers towards heavily-loaded cells. This effect might increase the spectral

efficiency and the global performance, but this approach is not the actual focus of this chapter.

For instance, we can imagine a high-speed user crossing an area under the coverage of a macrocell and several femtocells. Even when the strongest-cell policy might suggest that the best option is handing over to a femtocell, after several seconds, the same user will be handed over back to the macrocell. In our approach, we avoid such handovers, remaining camped on the macrocell. If we are dealing with a slowly-moving user, the current strongest cell will most likely have the best SINR in the future since the user will not have left its coverage. This introduces a second condition to perform a handover that, eventually, will lead to a reduction in the total number of handovers. The different steps of the proposed algorithm are shown in Algorithm 1.

The procedure of the UE REM-HO takes place at the User Equipment, and it is identical to what is currently used in the LTE standard. Similarly, the second procedure labelled BS REM-HO is run on the operator's side. On the user's side, the values used to trigger the events are not the raw physical-layer measurements but a filtered version using what is known as L3 filtering [100]. This recursive filter is located in the Radio Resource Control (RRC) layer and is expressed as

$$F_n = (1-a)F_{n-1} + aM_n, \tag{3.4}$$

where $a = 2^{-fc/4}$ is the filter coefficient with parameter fc, F_n is the filtered value (e.g. RSRP, RSRQ, etc.) and M_n is the raw measurement provided by the PHY layer. In our case, F_n is the RSS while the filter coefficient is optionally signalled by the network (the default value is $fc = 4 \rightarrow a = 0.5$). Similarly, the RSS values stored in the REMs only represent the effect of path loss and shadowing, since fast-fading is averaged out over several measurements.

3.3 Numerical Results for HetNets

This section provides numerical results for evaluating the performance of the proposed REM-HO algorithm and, for comparison, the standard LTE-HO algorithm in

Algorithm 1 REM-based handover algorithm with fixed prediction time

procedure UE REM-HO(RSS_c, TTT, HHM)
  if $\mathrm{RSS}_s^{\mathrm{TTT}} < \mathrm{RSS}_t^{\mathrm{TTT}} - \mathrm{HHM}$ **then**
    UE sends a measurement report with the target cell t, user's location $\{x, y\}$ and velocity $\{v_x, v_y\}$.
  end if
end procedure

procedure BS REM-HO(t, $\{x, y\}$, $\{v_x, v_y\}$, Δt, R, REM_c)
  if Measurement report received **then**
    Predict the user's position in Δt.
    $\{x_p, y_p\} \leftarrow \{x, y\} + \{v_x, v_y\} \cdot \Delta t$
    Find all cells within R.
    $c \in \mathcal{B}$ where $\mathcal{B} := (x - x_p)^2 + (y - y_p)^2 \leq R^2$
    Rank cells according to their expected SINR using the values stored in the REMs.

$$\gamma_c \leftarrow \frac{\mathrm{REM}_c(x_p, y_p)}{\sum\limits_{k \in \mathcal{B} \setminus \{c\}} \mathrm{REM}_k(x_p, y_p) + \sigma^2}$$

    if $t = \underset{c \in \mathcal{B}}{\operatorname{argmax}}\ \gamma_c$ **then**
      BS sends the handover command back to the UE.
    end if
  end if
end procedure

a HetNet. The simulation environment used for carrying out the simulations has been developed entirely using MATLAB. It comprises a scenario generator based on hexagonal grids [101] for deploying base stations and users, a radio simulator following WINNER's Phase II Model implementation but using 3GPP 3D channel models [102] (see values in Table 3.1) where we obtain the RSS for each pair BS-UE and, finally, an algorithm workbench where we can test different HO algorithms on the same radio simulation instance. The baseline scenario is based on the European-funded Mobile and wireless communications Enablers for the Twenty-twenty Information Society 5G (METIS) project [103] that also includes mobility models. We have also included geographical distance-based wrapping following the 3GPP guidelines in [104]. Therefore, we do not have less interference at the border of the network. Table 3.1 lists the major simulation parameters. Macrocells, the first-tier network, follow the classic 19-site layout with an Inter-Site Distance (ISD) of 200 m, while picocells, the second-tier network, are deployed following the next Probability Density Functions (PDF) using polar coordinates (r, θ) relative to their macro station [105]:

$$p_r(r) = \frac{2(r - d_{\min})}{(d_{\max} - d_{\min})^2} \qquad d_{\min} \leq r \leq d_{\max}, \tag{3.5}$$

$$p_\theta(\theta) = \frac{1}{2\pi} \qquad 0 \leq \theta < 2\pi, \tag{3.6}$$

where $d_{\min}$ is the closest distance admissible between tiers, which is equal to 55 m, and $d_{\max}$ corresponds to the cell edge which depends on the angle θ (see details in Fig. 3.1). The UEs are also scattered according to (3.5) and (3.6) but there is a change of the minimum distance to 35 m instead of 55 m [103]. For the baseline scenario, we have deployed 8 picocells and 5 users per macro sector unless otherwise stated. Each UE moves linearly in a direction randomly chosen between $[0, 2\pi)$, and its speed of motion is constant. During the simulation, the UE's position is updated every 100 ms, and we obtain a channel realisation every 10 ms, which corresponds to the LTE frame duration. The propagation conditions (Line- and Non-Line-Of-Sight, LOS/NLOS) are assigned at the beginning according to the 3GPP formulae [102] and kept fixed for the rest of the simulation.

Table 3.1: Simulation Parameters

Items	**Macrocell**	**Picocell**
Path-loss model	3GPP TR 36.873 (3D-UMa)	3GPP TR 36.873 (3D-UMi)
Shadow fading std	LOS = 4 dB NLOS = 6 dB	LOS = 3 dB NLOS = 4 dB
Correlation distance SF	LOS = 37 m NLOS = 50 m	LOS = 10 m NLOS = 13 m
Fast-fading model	Geometry-based stochastic modelled	
BS antenna height	25 m	10 m
BS/UE antenna pattern	Omnidirectional	
BS EIRP	49 dBm	30 dBm
Carrier frequency/BW	2 GHz/ 20 MHz	
Inter-site distance	200 m	20 m
UE height	1.5 m	
Sampling period	10 ms	
Total simulation time	300 s	

Similarly, the LTE-HO algorithm has been extracted from [4], including realistic timing such as the intra-frequency measurement period, handover preparation and execution times. The RLF recovery has been bounded to occur within 120 ms, including the RRC procedure delay. In this case, we assume that the target cell is sufficiently strong to be detected in the first correlation attempt [106]. A UE is said to be out of synchronisation when its wideband SINR is below the threshold Q_{out} and to be back in synchronisation when above the threshold Q_{in}. An RLF is declared when a UE is out of synchronisation for longer than the RLF Time (T310

Table 3.2: HO and RLF Parameters

Item	**Value**
Q_{out}	-8 dB
Q_{in}	-6 dB
RLF Time	1 s
RLF Recovery Time	120 ms
HO Preparation Time	40 ms
HO Execution Time	50 ms
Minimum ToS	1 s

timer in 3GPP terms, typically 1 s). Subsequently, a handover failure happens if: a) RLF occurs before TTT duration, b) T310 is running when the handover command is sent, or c) the wideband SINR in the target cell is below Q_{out} when the handover-complete message is sent. Finally, the Time of Stay (ToS) is defined as the duration between two consecutive successful handovers. If these handovers are performed between the same two cells in less than the minimum ToS, it is considered as a ping-pong handover. Ping-pong handovers reduce the efficiency of the network, so it is crucial to reduce their numbers while keeping a satisfactory QoS. Table 3.2 reflects the parameters involved in both handover and RLF.

REMs have been built using the worst-case scenario for both macro and pico-cells, in effect, NLOS, where the path loss and large-scale fading can be predicted but small-scale fading cannot, due to its nature. If we were able to build REMs from real measurements, this workaround would not be needed since the measurements themselves inherently contain the propagation conditions. Finally, we assess the proposed algorithm and its counterpart by evaluating 4 different sets of configuration parameters as shown in Table 3.3, ranging from less to more aggressive (lower to higher mobility as well), extracted from [4]. We have decided to keep the specific REM-HO parameters constant on purpose so that we can evaluate them in

Table 3.3: Configuration Sets

Profile	**Set 1**	**Set 2**	**Set 3**	**Set 4**
TTT [ms]	160	160	80	40
HHM [dB]	3	2	1	-1

Table 3.4: Average ping-pong rate (%) with 8 picocells per macrocell sector and $\Delta t = 2.5$ s

	Speed [km/h]	**Set 1**	**Set 2**	**Set 3**	**Set 4**
LTE-HO	3	0	1.6721	19.8882	58.6097
	30	2.1754	4.0750	8.7126	25.5029
	60	4.2724	7.3409	11.8169	21.6473
	120	3.8307	6.9485	18.1408	26.0302
REM-HO	3	0	0	0.4562	1.9008
	30	0.0867	0.1725	0.4497	1.2736
	60	0	0	0.1077	0.2356
	120	0	0	0.0249	0.0598
REM-HO with 3 candidates	3	0	1.5751	19.0726	56.3074
	30	1.0745	2.2814	5.4542	16.0515
	60	0.2964	1.8212	3.9878	9.4934
	120	0.0924	0.6767	1.4164	4.7515

Subsection 3.3.2. R in Algorithm 1 is 200 m to coincide with the ISD and Δt is 2.5 s, which is a compromise for the different speeds considered (3, 30, 60, 120 km/h).

3.3.1 Ping-pong Handovers

Table 3.4 shows the ping-pong rate percentage defined in [4] as

$$\text{Ping-pong rate (\%)} = \frac{\text{number of ping-pongs}}{\text{total number of successful handovers}} \times 100. \tag{3.7}$$

It can be seen that in our proposed algorithm, this rate is below 2 per cent in any configuration set regardless of the user's speed. The reason behind such a considerable reduction is the incomplete channel states stored in the REMs. Our technique double-checks if a target cell spotted by a user would still be a right choice in Δt seconds, so avoiding virtually any possibility of hopping over two cells in less than Δt. The users with the lowest speed suffer from a marginally higher rate because they require more time to cross the same area. An adaptive timespan will be considered according to the user's speed, enunciating an optimisation problem in Chapter 4.

If we relax the constraint of picking the BS with the highest SINR and we increase the candidate list up to the first K cells with the highest SINR, our proposed technique will tend to behave like LTE. As K increases, both algorithms become indistinguishable. For example, in Table 3.4 we have set K equal to 3. Again, the lowest-speed users are the most affected by this change, with rates similar to LTE for configuration sets 3 and 4 (see the set details in Table 3.3). The rest of the sets do not increase at the same pace due to the longer TTT.

The decrease in the ping-pong rate has a definite impact on the number of handovers. Table 3.5 shows the average number of events where REM-HO events are substantially diminished. The grey rows represent the ratio of ping-pong handovers to the total. The difference in the number of handovers is not only attributed to the ping-pong avoidance; in this regard, our algorithm postpones handovers *as long as possible* until a strong cell which will stay strong for at least Δt seconds shows up. This effect is translated into a higher occurrence of RLFs but is still comparable to LTE for the most aggressive sets, as shown in Table 3.6. There is a trade-off between the ping-pong rate and the number of RLFs, controlled by the size of the candidate list. As previously mentioned, being less conservative and allowing more cells to be selected can reduce RLFs while increasing the ping-pongs.

Table 3.5: Average number of handovers per user per second (HO/UE/s) with 8 picocells per macrocell sector and $\Delta t = 2.5$ s

	Speed [km/h]	**Set 1**	**Set 2**	**Set 3**	**Set 4**
LTE-HO	3	0.0014	0.0024	0.0056	0.0190
		0	0	0.0011	0.0111
	30	0.0034	0.0058	0.0130	0.0213
		0.0001	0.0002	0.0011	0.0054
	60	0.0031	0.0053	0.0168	0.0260
		0.0001	0.0004	0.0020	0.0056
	120	0.0031	0.0050	0.0171	0.0266
		0.0001	0.0003	0.0031	0.0069
REM-HO (grey rows 1E-4 ×)	3	0.0010	0.0013	0.0019	0.0024
		0	0	0.0858	0.4600
	30	0.0009	0.0014	0.0028	0.0034
		0.0078	0.0234	0.1248	0.4366
	60	0.0005	0.0008	0.0022	0.0026
		0	0	0.0234	0.0624
	120	0.0005	0.0009	0.0031	0.0039
		0	0	0.0078	0.0234

3.3.2 Impact on Spectral Efficiency

Preventing users from handing over also brings a loss in a user's spectral efficiency, as in Fig. 3.2 and Fig. 3.3. In these figures we have the average channel spectral efficiency for configuration set 3 (TTT = 80 ms, HHM = 1 dB) for 60 km/h users. In Fig. 3.2 we keep all the parameters fixed and sweep only Δt. The obtained loss in spectral efficiency compared to LTE can be easily explained. LTE picks

Table 3.6: Average number of RLFs per user per second (RLF/UE/s) with 8 picocells per macrocell sector and $\Delta t = 2.5$ s

	Speed [km/h]	**Set 1**	**Set 2**	**Set 3**	**Set 4**
LTE-HO	3	0.0027	0.0024	0.0020	0.0018
	30	0.0090	0.0082	0.0042	0.0033
	60	0.0145	0.0142	0.0079	0.0061
	120	0.0177	0.0176	0.0117	0.0099
REM-HO	3	0.0024	0.0022	0.0020	0.0020
	30	0.0080	0.0076	0.0063	0.0059
	60	0.0122	0.0119	0.0106	0.0102
	120	0.0148	0.0144	0.0123	0.0116

the strongest cell at any time after TTT seconds, whereas we double-check if that cell will maintain its status after Δt seconds. Therefore, if the timespan becomes smaller, the filtered measurements and the predicted values stored in the REMs will be similar because of the spatial correlation in large-scale fading. For instance, our algorithm almost perfectly overlaps LTE when $\Delta t = 0$. Selecting the right Δt for each speed is key to controlling the trade-off between the reduction in the ping-pong handovers and the loss in spectral efficiency. As an example, for $\Delta t = 2.5$ s, which corresponds to a prediction distance of 41.67 m, we reduce the ping-pong rate to 0.01% (11.82% for LTE-HO) but, at the same time, we lose approximately 9% of spectral efficiency (1.14 b/s/Hz against 1.25 b/s/Hz).

In Fig. 3.3, we benchmark the performance of the LTE-HO and the proposed REM-HO algorithms under different picocell densities. Although the gap increases with density, it will not go further than approximately 0.1 b/s/Hz. Here we observe the trade-off of using our technique instead of the current LTE handover approach. The slight loss of spectral efficiency is due to the smaller overall number of handovers, by around an order of magnitude. However, we ensure an acceptable QoS while

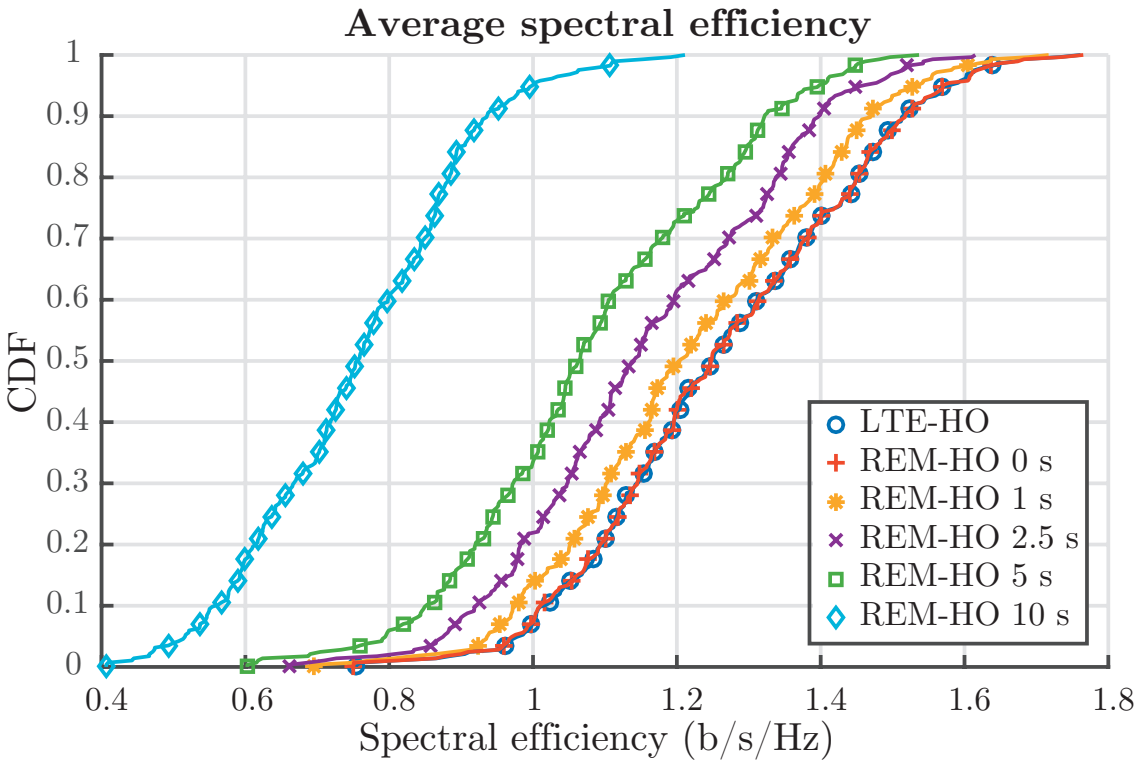

Figure 3.2: CDF of channel spectral efficiency for configuration set 3, 60 km/h, 8 picocells and $\Delta t = \{1, 2.5, 5, 10\}$ s.

introducing a smaller amount of overhead in the network.

Regarding the network overhead, the UEs only send a few extra bits of information compared to the LTE-HO algorithm (location and velocity although they are parameters already included in the standard), which we might consider negligible. Besides, the signalling between BSs will depend on the specific algorithm; as detailed in [3], it is estimated that the REM signalling requirement is about 68 bits/s per cell for an inter-cell interference minimisation technique. The update frequency of the databases is not discussed.

3.4 Madrid Grid

In Section 3.1, we presented a synthetic deployment scenario broadly accepted in the literature. Nonetheless, some of the assumptions are definitely unrealistic. For example, mobile terminals do not travel at a constant speed on a straight line or the radio environment is not isotropic. In this regard, realistic deployment scenarios

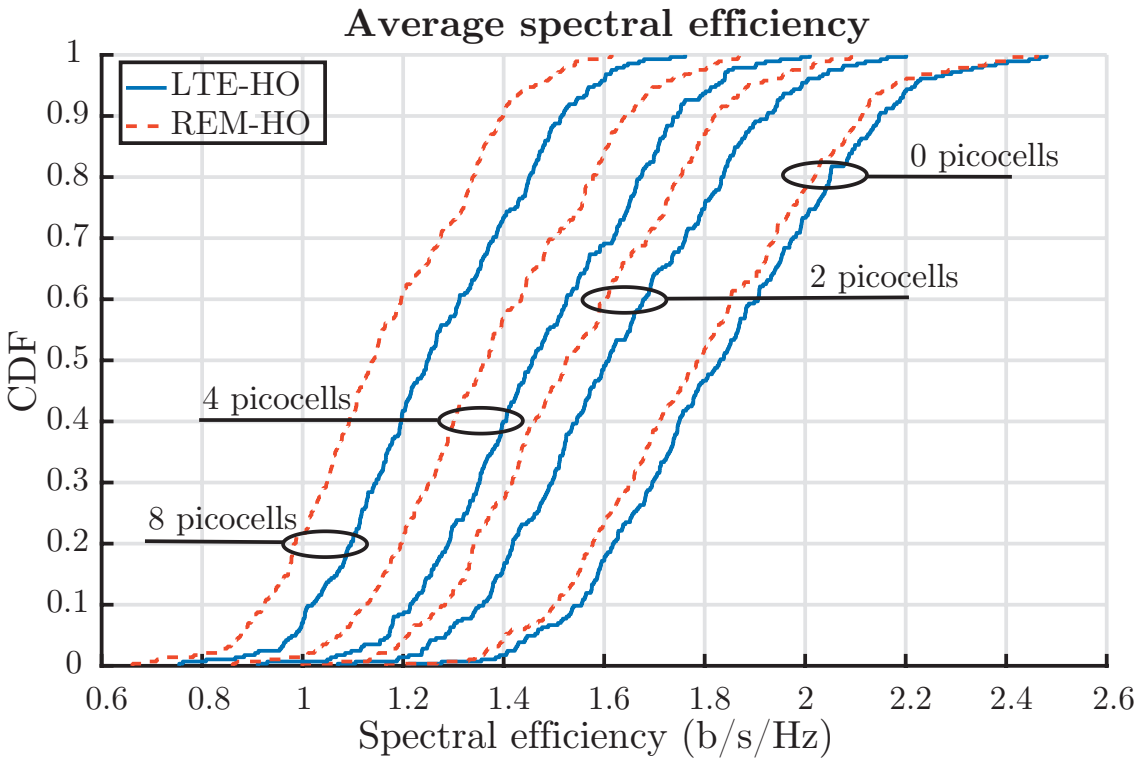

Figure 3.3: CDF of channel spectral efficiency for configuration set 3, 60 km/h, $\Delta t = 2.5$ s and $\{0, 2, 4, 8\}$ picocells.

such as a Manhattan grid can provide invaluable information of real-world KPIs. We consider the Madrid grid model from the METIS project [103] for our simulations. Total dimensions for Madrid grid are 387 m (west-east) and 552 m (north-south); however, to limit border effects, a wrap-around of 9 identical copies is considered.

3.4.1 Deployment

There is an orthogonal deployment of picocells complementing the macrocell tier. There is only one macro site with three sectors on the edge of a building top, and there are also 12 pico cells installed on lampposts. Their locations are indicated in Fig. 3.4 while their parameters are summarised in Table 3.7.

3.4.2 Mobility Model

Mobility traces have been generated with the open-source, microscopic, and continuous road agent-based traffic simulation package *Simulation of Urban MObil-*

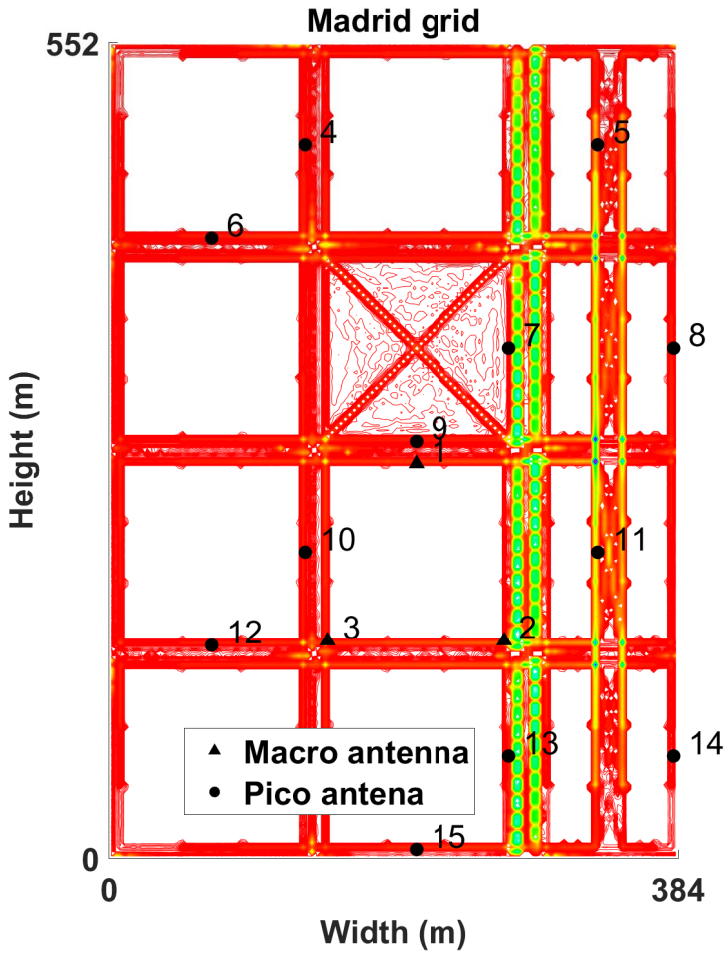

Figure 3.4: Deployment for Madrid grid with a heatmap of the mobility traces.

Table 3.7: Deployment Parameters

	Macro	**Pico**
Carrier frequency [MHz]	800	2600
Bandwidth [MHz]	20	80
Maximum Tx power (per 10 MHz) [dBm]	43	30
Antenna height [m]	52.5	10
Antenna configuration	4 TX/RX MIMO	2 TX/RX MIMO
Antenna type	Sector	Omnidirectional
Azimuth from x-axis [°]	{90, 330, 210}	-
Mechanical tilt [°]	{7, 18, 18}	-
Map resolution [m]	3	3

ity (SUMO) developed by the Institute of Transportation Systems at the German Aerospace Centre [107]. It allows modelling with high detail road traffic and pedestrians too. METIS provides a publicly available, generous dataset of traces whose parameters are collected in Table 3.8.

3.5 REM Handover Skipping Adaptive Algorithm

Our proposed HO skipping technique relies on a REM, which is primarily a database that stores spectrum information. In [24], the authors create REMs via an urban electromagnetic wave propagation model intended for radio planning, which predicts the field strength within 5–8 dB root-mean-square error (RMSE). In his PhD dissertation, Sato [108] focuses on measurement-based REMs using Kriging interpolation. Over three months, he found a correlation of roughly 0.94 in a 10-m-resolution map of a suburban area with the 90^{th} percentile of the residual error around 7 dB. In both these works, maps are generated with similar errors that follow a log-normal distribution with zero mean for each point. In our simulations, we assume that the ray-tracing based path-loss maps provided by METIS [103] are the ground truth.

Table 3.8: Mobility Model Parameters

	Cars	Buses	Pedestrians
Dimensions [m]	1.8×4.3	12×2.5	-
Maximum speed [km/h]	50	50	3
Acceleration [m/s^2]	2.9	1.2	-
Deceleration [m/s^2]	7.5	4	-
Minimum gap [m]	2.5	4	-
Number of traces	420	320	1500
Time [s]	3600	43–135	600
Trace resolution [s]	1	1	1

Thus we calculate HOs based on them. On the contrary, our radio-environment maps have been created by taking these maps and adding errors to mimic the limitations of the current methods.

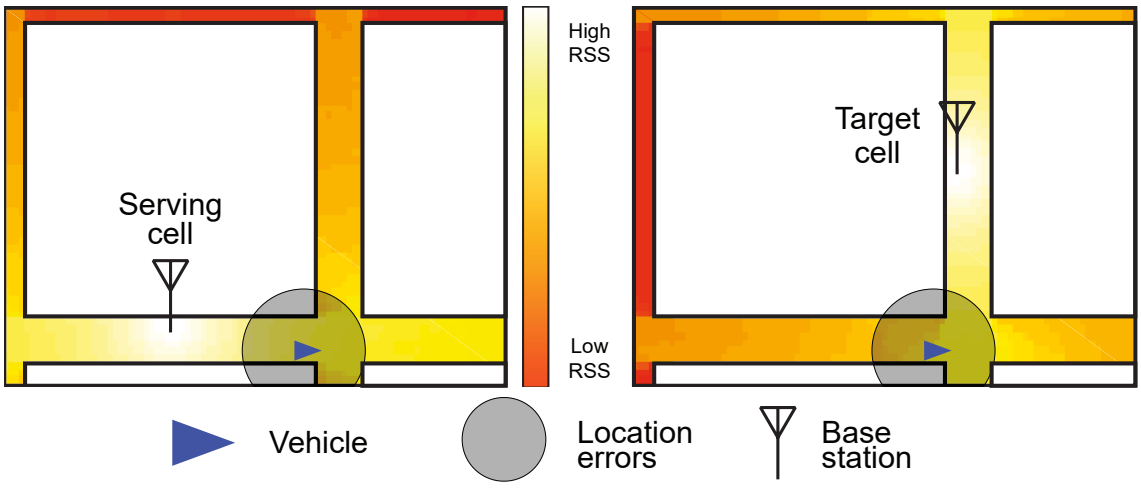

Figure 3.5: A vehicle is going through a city. Even though the target cell seems like the right choice, the trajectory indicates to us that it is not. Thanks to the REM, we avoid it. The circle represents the location errors.

The first two steps of our proposed algorithm REM-HO in Section 3.2 [109] are identical to the LTE HO process. When users send a measurement report to start the preparation stage, they also piggyback their location and velocity (not just speed) information. This extra traffic can be quantified in 32 bytes: longitude, latitude, and

the velocity vector (4 doubles). This amount of data is much smaller than the user data, and its effect on the overall traffic is negligible as the exchange of channel-state information in CoMP [110]. Consider $\mathbf{x}$ and $\mathbf{v}$ to be the location and the velocity of a user when reporting, respectively. We can predict the user's position assuming that the user does not change their trajectory abruptly, for example, cars and public transport. Although pedestrians may be unpredictable, inherent location errors are more prominent. Then, we can write the predicted location $\mathbf{x_p}$ as,

$$\mathbf{x_p} = \mathbf{x} + \mathbf{v} \times \Delta t + \varepsilon, \tag{3.8}$$

where $\Delta t = L/|\mathbf{v}|$ is the prediction time and is chosen adaptively according to a threshold L as in [42], and to the user speed (magnitude of $\mathbf{v}$). We assume that location errors ε follow a bivariate normal distribution like Global Positioning System (GPS [111]). It might be argued that the velocity is also prone to errors; nonetheless, the time correlation between samples when determining the velocity cancels the error, resulting in a more reliable estimation [112].

During the signalling exchange, the predicted location is plugged into both the serving cell's REM and the target cell's REM to extract the predicted RSS from each cell. The HO is skipped with no collaboration between cells whatsoever, if and only if the predicted RSS from the target cell is above the predicted RSS from the serving cell,

$$\mathrm{RSS}_{\mathrm{target}}(\mathbf{x_p}) > \mathrm{RSS}_{\mathrm{serving}}(\mathbf{x_p}). \tag{3.9}$$

This way, we ensure that the upcoming HO is worth doing since the sojourn time in the new cell will be at least Δt. We exploit not only the location of the user but also the trajectory as shown in Fig. 3.5, where we show the REMs of the serving cell (left) and the target cell (right), respectively. For example, a user is in a vehicle going through a city, and it measures a target cell at an intersection due to the street canyon effect. If we only checked the distance, it would seem the right choice. However, if the vehicle keeps driving straight, the burden is two-fold: there are two HOs with their corresponding disconnections impacting negatively on the quality of experience (QoE) and BSs need to send data over the backhaul.

3.6 Handover Cost and Backhaul Traffic Estimation

In this section, we present evaluation metrics that will be discussed in the results section. The first one is meant for the user side and represents the normalised average time disconnected from the network as defined in [86]. The HO cost $\mathcal{D}$ for K tiers, which is 2 in our case, is described as

$$\mathcal{D} = \sum_{i}^{K} \sum_{j}^{K} H_{ij} \times d_{ij}, \tag{3.10}$$

where H_{ij} represents the HO rate between tiers i and j, and d_{ij} denotes the delay associated with the type of HO. For instance, the delay incurred by a macro-macro HO is shorter than a macro-pico HO since the backhaul connection of macrocells is usually fibre optic, whereas picocells are not. Hence, for the METIS dataset, it can be further simplified to

$$\mathcal{D}^{sch} = H_{mm}^{sch} \times d_m + (H_{mp}^{sch} + H_{pp}^{sch}) \times d_p, \tag{3.11}$$

where the subscript m means macro, p pico, and the superscript sch alludes to the HO strategy followed. We do not distinguish the HO order, i.e., we have merged handover from/to a macro cell to/from a picocell in H_{mp} because the associated delay is the same.

The second one is meant for the network's side and quantifies both upstream and downstream backhaul traffic, whether using CoMP or not. LTE has two logical interfaces: S1 and X2. The S1 interface is a star network that links the advanced gateway with each cell and carries the sum of all user data, whereas the X2 interface is a mesh network that enables signalling exchange among cells. Traffic on the X2 interface remains smaller than S1 traffic unless cooperation is allowed because downlink data to one single user must be simultaneously transmitted over several links (JT CoMP [113]). Inspired by [110], S1 traffic is given by

$$S1^{sch} = \sum_{M} \eta(M) \times B(M) \times \rho^{sch}(M), \tag{3.12}$$

where $\eta(M)$ denotes the transmission mode spectral efficiency, $B(M)$ the transmission mode bandwidth, and $\rho^{sch}(M)$ is the transmission mode probability that

depends on the HO strategy. We define transmission mode as macrocell, picocell, and two cells in cooperation (macro-macro, pico-pico, or macro-pico). Overhead, due to tunnelling protocols and HO events, is estimated at 14% [110], then X2 upstream traffic can be written as

$$X2_{up}^{sch} = (0.14 + \bar{x}^{sch}) \times S1^{sch}, \tag{3.13}$$

where $\bar{x}^{sch}$ represents the inter-site ratio, i.e., the X2 interface is only used when cells at different sites cooperate. For instance, if no cooperation is needed as in the BC strategy, $\bar{x}^{BC} = 0$. Equation (3.13) is also the total upstream traffic considered because upstream user data are ignored.

In the downstream, X2 carries data shared by all cooperating cells and is equal to

$$X2_{down}^{sch} = (0.14 + \bar{x}^{sch}) \times \sum_{M} [S(M) - 1] \times \eta(M) \times B(M) \times \rho^{sch}(M), \tag{3.14}$$

where $S(M)$ is the transmission mode cluster size, which is limited to 1 or 2 in our case (no cooperation or cooperation). Finally, we can combine (3.11), (3.12), and (3.14) to express downstream traffic denoted by $\mathcal{T}$ as

$$\mathcal{T}^{sch} = (1 - \mathcal{D}^{sch}) \times (1.1 \times S1^{sch} + X2_{down}^{sch}). \tag{3.15}$$

3.7 Numerical Results for Madrid Grid

We evaluate two versions of our proposed algorithm as well as BC [80], FS and FS-IC [86], LA [42] and LA with geolocation errors (LA-GPS). The first version, REM, considers GPS errors, but we have perfect knowledge of the RSS map, while the second version, REM-ERR, includes both map errors and location errors. The environment used is MATLAB, where we have processed the ray-tracing based path-loss maps provided by METIS [103] and added the maximum transmit powers in Table 3.7, so we obtain RSS maps. After that, we have calculated spectral efficiency maps for each transmission mode $\eta(M)$ in (3.12). The transmission modes are macro, pico, macro-macro, pico-pico, and macro-pico. The last three modes can be with or without IC. As a result, we have eight different 3-m resolution maps, one per

transmission mode, for the spectral efficiency in the Madrid grid. The bandwidth of the cooperative modes is the minimum of the two cells that are cooperating.

The mobility traces have also been treated with MATLAB to infer the transmission mode probabilities $\rho^{sch}(M)$ in (3.12). We have recorded for each time sample the transmission mode and counted the number and type of HOs for each. We took special care in ignoring random respawns of users as HOs, e.g., when a pedestrian enters a building, they will appear at another building or metro entrance randomly at the next time sample. Then, the probabilities are calculated by dividing the amount of time in each mode over the trace simulation time and averaging for each type of user, i.e., cars, buses, or pedestrians. The inter-site ratio $\bar{x}$ in (3.12) is equal to the sum of all the transmission mode probabilities that involved cooperation between sites, i.e., macro-pico and pico-pico. Note that macro-macro is intra-site cooperation. Similarly, the HO rates H_{ij} in (3.11) have been computed as the number of HOs divided by the trace simulation time and averaged for each type of user and HO. The rest the parameters are listed in Table 3.9.

Table 3.9: Simulation Parameters

Name	**Symbol [unit]**	**Value**
Distance threshold [42]	L [km]	$2.56/\lambda$
BS intensity of Madrid grid	λ [km^{-2}]	70.22
Prediction time	Δt [s]	$36.44/\lvert\mathbf{v}\rvert$
Std of GPS errors [111]	σ_{XY} [m]	12.3
RMSE of map errors [24]	σ_S [dB]	6
Macro-macro HO delay [86]	d_m [s]	0.35
Pico-related HO delay [86]	d_p [s]	$2d_m$
Simulation drops	N	1000

3.7.1 Spectral Efficiency η

When a user skips a picocell, the second and the third strongest cells do cooperate [113], intra- or inter-tier. We assume that the cells are sorted in descending order concerning their RSS ($\text{RSS}_i \geq \text{RSS}_{i+1}, \forall i$). Therefore, the signal-to-interference ratio (SIR) γ in the downlink at the user is

$$\gamma = \frac{\left|\sqrt{P_2 h_2 r_2^{-\alpha}} + \sqrt{P_3 h_3 r_3^{-\alpha}}\right|^2}{\sum_{i>3} P_i h_i r_i^{-\alpha} + P_1 h_1 r_1^{-\alpha}}, \tag{3.16}$$

where P_i is the transmit power of cell i, and h_i and $r_i^{-\alpha}$ denote the channel gain and the path-loss gain from the i-th cell, respectively. Since the interference from the skipped cell $P_1 h_1 r_1^{-\alpha}$ (the strongest one) might be overwhelming, interference cancellation is also enabled. However, we do not assume that such cancellation is performed with probability one as [42,86]. The success probability to cancel the n-th strongest signal is characterised in [87] and depends on the SIR. In particular, the success probability of cancelling the first strongest signal in the rest of this chapter will be equal to

$$\mathbb{P}_{\text{s,can}}(\gamma) = \frac{1}{1 + \sqrt{\gamma} \times \arctan(\sqrt{\gamma})}. \tag{3.17}$$

In Fig. 3.6, we depict the empirical CDF of the spectral efficiency for each transmission mode. The methods that do not use interference cancellation experience lower SIR, affecting their spectral efficiency negatively. Even when two macro sectors cooperate (macro-macro IC), their spectral efficiency is below 3 bps/Hz. On the contrary, cooperation between tiers (macro-pico IC) and picocells (pico-pico IC) seem like a reasonable compromise, where the spectral efficiency is reduced at the expense of reducing the total number of HOs. We can also observe that approximately 65% of the time, two cells from different tiers collaborating (macro-pico IC) can achieve better spectral efficiency than one single picocell (pico).

As recommended by the Next Generation Mobile Networks Alliance and discussed in [110], results for the mean (50^{th} percentile) and the peak (95^{th} percentile) spectral efficiency of JT CoMP are considered.

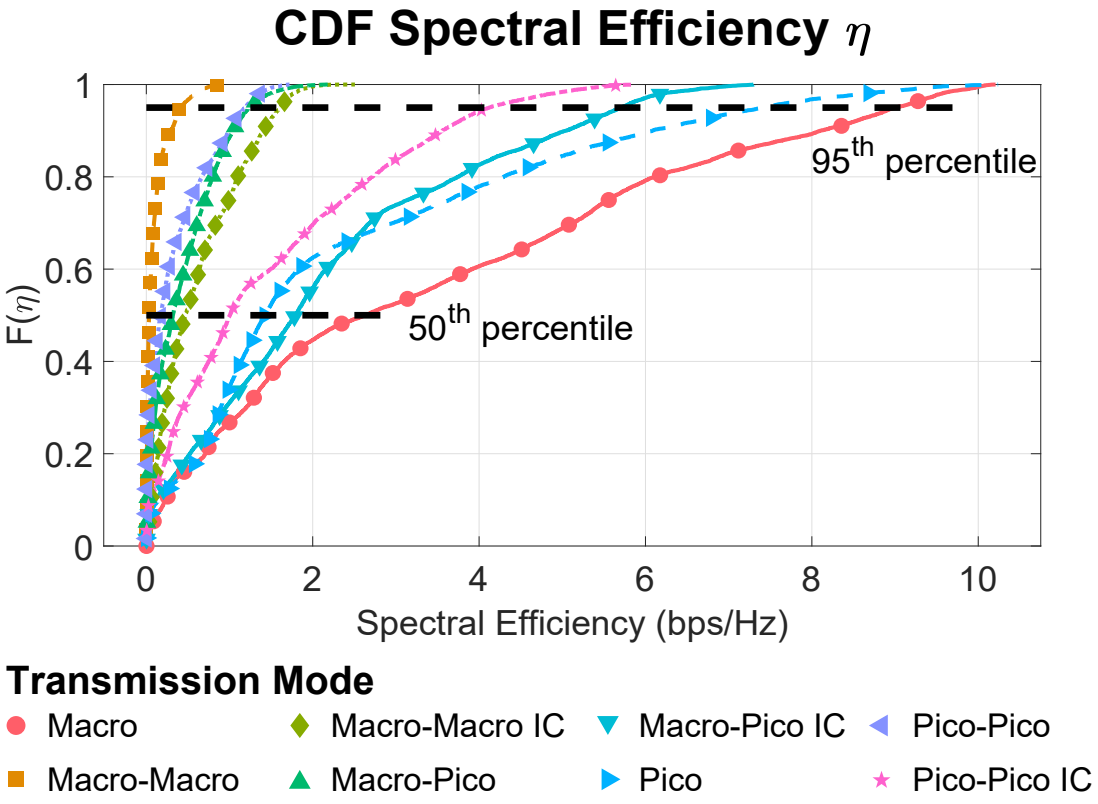

Figure 3.6: Coverage probability for each transmission mode.

3.7.2 Handover Cost $\mathcal{D}$

In Table 3.10, we show the results for the HO cost (3.11), where we can agree that all the skipping strategies improve the baseline technique (BC). In particular, both our proposals with a reduction between 33–50% in the disconnection time are behind alternative skipping (FS and FS-IC, 40–56% reduction), and location-aware skipping (LA and LA-GPS, 56–65% reduction). This result was expected since our decision not only depended on the user's location but also on the user's velocity. Depending on the prediction time Δt, which changes dynamically with the current user speed, there are HOs that our strategy flags as worth doing and the other techniques skip more aggressively. Results show that location errors on average barely affect the performance of the strategies that use location because of the nature of the errors, circularly-symmetric bivariate normal distribution.

Table 3.10: Handover Cost [%]

	Buses	**Cars**	**Pedestrians**
BC [86]	3.78	1.20	1.35
FS [86]	2.12	0.72	0.60
FS-IC [86]	2.12	0.72	0.60
LA [42]	1.55	0.54	0.47
LA-GPS	1.54	0.53	0.47
REM	2.30	0.80	0.67
REM-ERR	2.30	0.80	0.67

3.7.3 Backhaul Traffic

Results for the downstream backhaul traffic (3.15) needed for each HO skipping strategy are depicted in Fig. 3.7. Note that the downstream backhaul traffic is equal to the downstream user throughput, whereas the upstream backhaul traffic is just overhead due to each technique, i.e., not user data. Regarding the mean value, 50^{th} percentile, in the downstream, it is observed that all strategies seem to

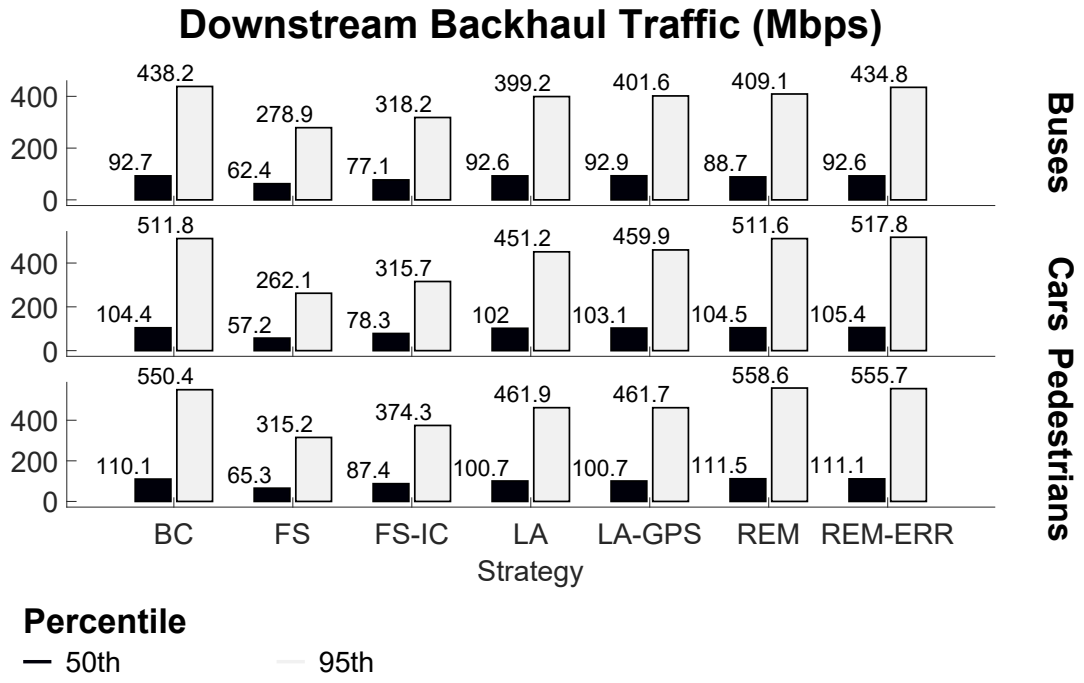

Figure 3.7: Downstream backhaul traffic for 50^{th} and 95^{th} percentiles.

perform substantially the same except for FS and FS-IC. As observed in [42], location awareness outperforms alternative skipping even when interference cancellation comes into play. This effect is even more apparent when looking at peak rates, 95^{th} percentile. However, our technique is superior to LA and LA-GPS within 8–17% because of the extra information stored in REMs. For example, LA would blindly skip an HO when the distance is greater than a threshold, but REM would check if the HO is worth skipping in Δt seconds. This way, we allow a dynamic HO skipping strategy. On top of that, LA and LA-GPS do not always succeed in cancelling the main interferer following (3.17).

The main difference regarding traffic can be seen in the upstream backhaul traffic (3.13) in Fig. 3.8. FS, LA, and derivative methods incur losses in a significant 61–68% overhead increment when compared to our strategy that employs neither CoMP nor SIC. Here is where the possible gains of these techniques in the downstream do not compensate for the drawbacks. We believe that CoMP and SIC could be useful in specific scenarios, e.g., cell edge, mainly when the two strongest cells cooperate. However, there are situations where, even with perfect cancellation, they

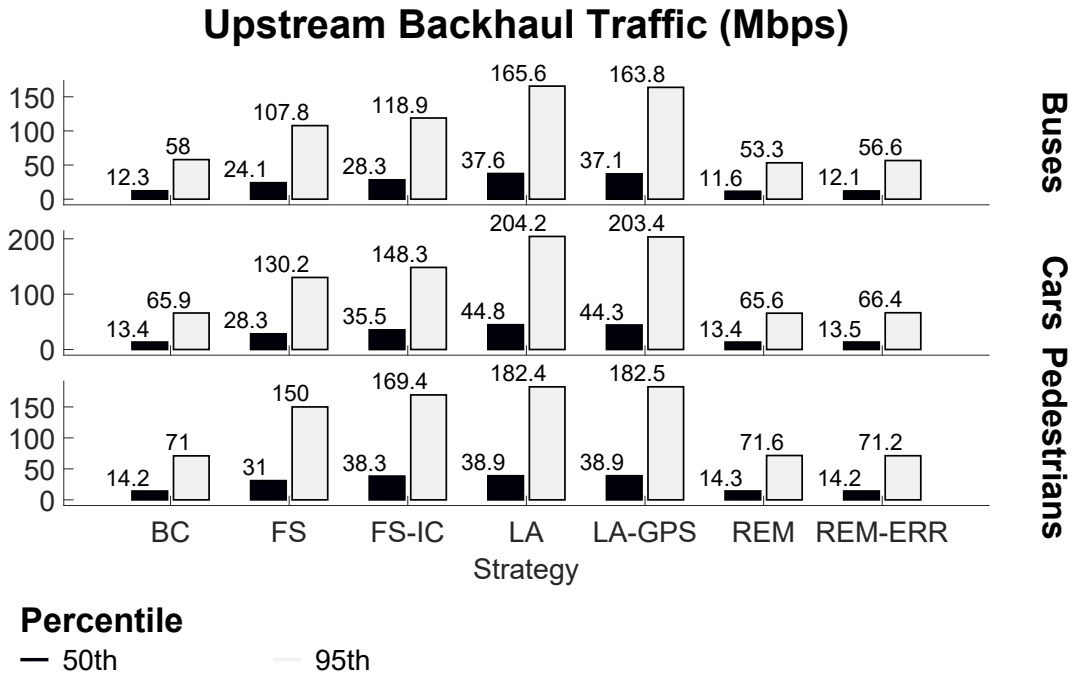

Figure 3.8: Upstream backhaul traffic for 50^{th} and 95^{th} percentiles.

are not worth it (see Fig. 3.6). Besides, SIC is particularly attractive for upstream and, although it is also suitable for downstream, its impact on the user's autonomy is not studied [87].

3.8 Summary

In this chapter, we have introduced the idea of using REMs in the handover decision-making as a way of predicting QoS. We have also presented a handover algorithm which takes advantage of REMs' spatial information in multi-tier cellular networks by preventing users from handing over too early. We have simulated our proposed algorithm and the LTE-HO algorithm where we have shown a significant reduction in the number of ping-pong handovers independently of the hysteresis margin applied. At the same time, the overall number of handovers is also cut down while maintaining a reasonable channel spectral efficiency.

Moreover, we have compared the backhaul traffic for several handover-skipping techniques in a realistic dense urban environment. We have shown that location awareness represents an improvement over the conventional handover strategy on

the user side. However, on the network side, skipping strategies can introduce a considerable amount of overhead at the same time. We present a low-overhead handover skipping scheme that uses REMs to support measurement reports on the field. The results show that our technique finds a balance between the conventional method and other skipping strategies. Our technique does not overload the upstream, reducing in more than 61% of the required data exchange between base stations, while maintaining the same quality of service in the downstream with at least 33% less time disconnected from the network because of the handovers.

Chapter 4

Analysis of REM-Based Handover Algorithm for Heterogeneous Networks

Handover has been a widely studied topic since the beginning of the mobile communications era, but with the advent of another generation, it is worth seeing it with fresh eyes. Data traffic is expected to keep growing as new use cases will coexist under the same umbrella, e.g. vehicle-to-vehicle or massive-machine-type communications. Heterogeneous networks will give way to multi-tiered networks, and mobility management will become challenging once again. Under the current approach, based uniquely on measurements, the number of handovers will soar, so will the signalling.

We propose a handover algorithm that employs multidimensional radio-cognitive databases, namely Radio Environment Maps, to predict the best network connection according to the user's trajectory. Radio Environment Maps have been extensively used in spectrum-sharing scenarios, and recently, some advances in other areas have been supported by them, such as coverage deployment or interference management. We also present a geometric model that translates the 3GPP specifications into geometry and introduce a new framework that can give useful insights into our proposed technique's performance. We validate our framework through Monte Carlo simulations, and results show that a drastic reduction of at least 10% in the ping-

pong handovers can be achieved, thus reducing the signalling needed.

Section 4.1 presents an overview of the system model employed. Section 4.2 explains the REM-HO algorithm and presents the set of equations used to describe the proposed algorithm. In Section 4.3, we validate our theoretical approach by numerical evaluation and discuss how some relevant parameters affect the performance of our proposed algorithm. We also show a performance comparison with the LTE-HO algorithm, and state the main findings of this chapter.

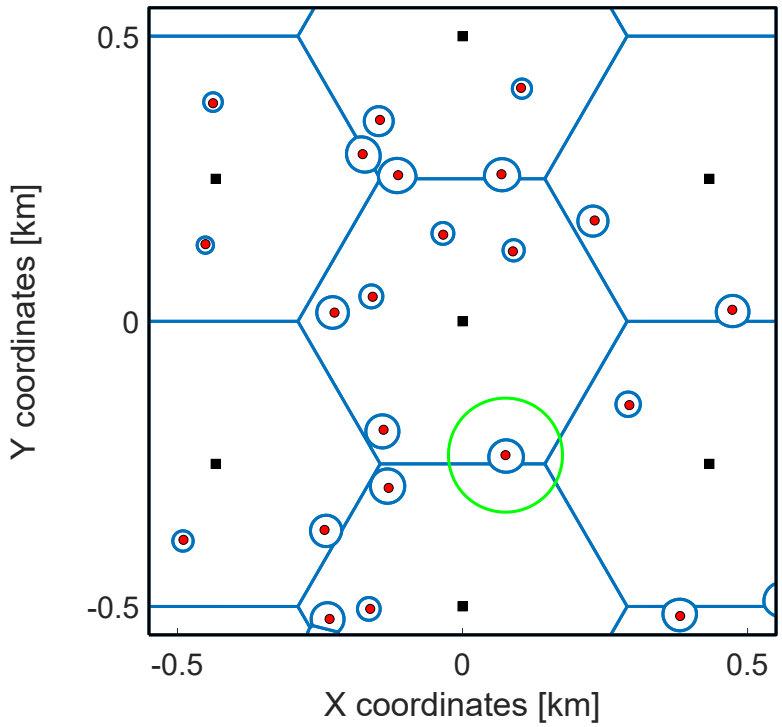

Figure 4.1: Coverage regions (blue lines) in a two-tier cellular network. Macrocells (black squares) are in a hexagonal grid with ISD = 500 m and picocells (red circles) are uniformly deployed. Users bounce within the green circle with radius = 100 m as per 3GPP specifications [4].

4.1 System Model

In this section, we provide a model so that we can describe the handover regions analytically. We consider the long-term cell association based solely on the path loss (fading is averaged out [47, 80]). Moreover, we introduce the location error model focusing on the Global Positioning System (GPS) [111]. Hereafter, we describe the main models needed for a clear understanding of our proposed approach.

4.1.1 Geometric Model

We consider a two-tier HetNet comprised of a macrocell tier (tier m) and a picocell tier (tier p). We assume that both tiers operate on the same spectrum. Following the 3GPP specifications [4] (see Table 4.1), the macrocell tier is arranged in a hexagonal grid whereas the picocell tier is uniformly deployed within the coverage areas of macrocell BSs as shown in Fig. 4.1. Considering that the BSs in the same tier

$i = \{m, p\}$ have the same transmit power $P_{t,i}$ and antenna gain G_i, the received signal strength $P_{r,i}$ at a distance d_i can be expressed as the following:

$$P_{r,i} = P_{t,i} G_i K_i d_i^{-\gamma_i}, \tag{4.1}$$

where K_i is the attenuation at the reference distance and γ_i is the path-loss exponent that takes into account the specific characteristics of the propagation environment, i.e. the frequency, the antenna height, among others. A macrocell UE will start the HO procedure to the picocell when $P_{r,m}$ drops below $P_{r,p}$ plus a certain HHM α, namely A3 event (a neighbour becomes offset better than the server [100, Ch. 17]):

$$P_{r,m} < P_{r,p} + \alpha. \tag{4.2}$$

In this scenario, under the assumption that the macrocell has a transmit power significantly higher than the picocell (16–22 dB difference [47]), the handover region converges to a circle [41, Theorem 1]. Without loss of generality, we assume that a macrocell BS is at the origin, and a picocell BS is at location $\mathbf{x_p} = (0, d)$, then the picocell coverage area is a circle with the centre $\mathbf{x_c}$ and the radius R_c given as follows:

$$\mathbf{x_c} = \left(0, \frac{\mathcal{Z}}{\mathcal{Z} - 1} d\right), \text{ and} \tag{4.3}$$

$$R_c = \frac{\sqrt{\mathcal{Z}}}{\mathcal{Z} - 1} d, \tag{4.4}$$

where $\mathcal{Z} = \left(\frac{\alpha P_{t,m} G_m K_m}{P_{t,p} G_p K_p}\right)^{2/\gamma_p}$. For simplicity, we assume that $\gamma_m = \gamma_p$. Similar expressions can be obtained for the general case when $\gamma_m \neq \gamma_p$ as presented in [44,47], but comes at the expense of more involved expressions.

Similarly, a handover failure is declared when the macrocell UE's wideband signal-to-noise-plus-interference ratio (SINR) is below a threshold $Q_{\text{out}} = -8$ dB. Hence we can define the macrocell handover failure circle with the centre $\mathbf{x_f}$ and the radius R_f given as:

$$\mathbf{x_f} = \left(0, \frac{\mathcal{Z}_f}{\mathcal{Z}_f - 1} d\right), \text{ and} \tag{4.5}$$

$$R_f = \frac{\sqrt{\mathcal{Z}_f}}{\mathcal{Z}_f - 1} d, \tag{4.6}$$

where $\mathcal{Z}_f = \mathcal{Z} Q_{\text{out}}^{-2/\gamma_p}$. In the case of homogeneous networks or horizontal HO, where the BSs in the same tier $i = \{m, p\}$ have the same transmit power $P_{t,i}$ and antenna gain G_i, then $\mathcal{Z} = \alpha^{2/\gamma}$, which means that the HHM is the only parameter that affects the shape of the circle. Depending on the value of α, we can have:

1. $\alpha \neq 0$ dB $\rightarrow \{\mathcal{Z}, \mathcal{Z}_f\} \neq 1$, then (4.3)–(4.6) represent circles, and our algorithm can be normally applied.

2. $\alpha = 0$ dB $\rightarrow \{\mathcal{Z}, \mathcal{Z}_f\} = 1$, then (4.4) represents a circle with infinite radius, i.e. a straight line. To be precise, it becomes the bisector of the segment that links two given BSs. For example, in Fig. 4.1, the hexagonal grid is the superposition of different segment bisectors among the macrocells. The macrocell handover failure circle would remain. Our algorithm could still be applied but it would not give any significant advantage over LTE in terms of PP HO since there is no coverage circle to avoid.

4.1.2 Mobility Model

We assume that the macrocell UEs move with a constant speed v on an arbitrary trajectory within a concentric circle around a picocell (green circle in Fig. 4.1) whose radius is larger than the radius of the picocell coverage circle. The starting position is chosen randomly on the circumference of the circle; then the UE follows a random linear trajectory towards the picocell until it becomes a chord of the circle, i.e. a straight line whose endpoints both lie on the circumference. Its arrival angle to the picocell coverage area β in Fig. 4.2 is uniformly distributed in $\left[-\frac{\pi}{2}, \frac{\pi}{2}\right]$. Let $d(\beta) = 2R_c \cos(\beta)$ denote the length of the chord formed by the entry and exit points of a UE crossing the picocell coverage area, and r be the distance from the

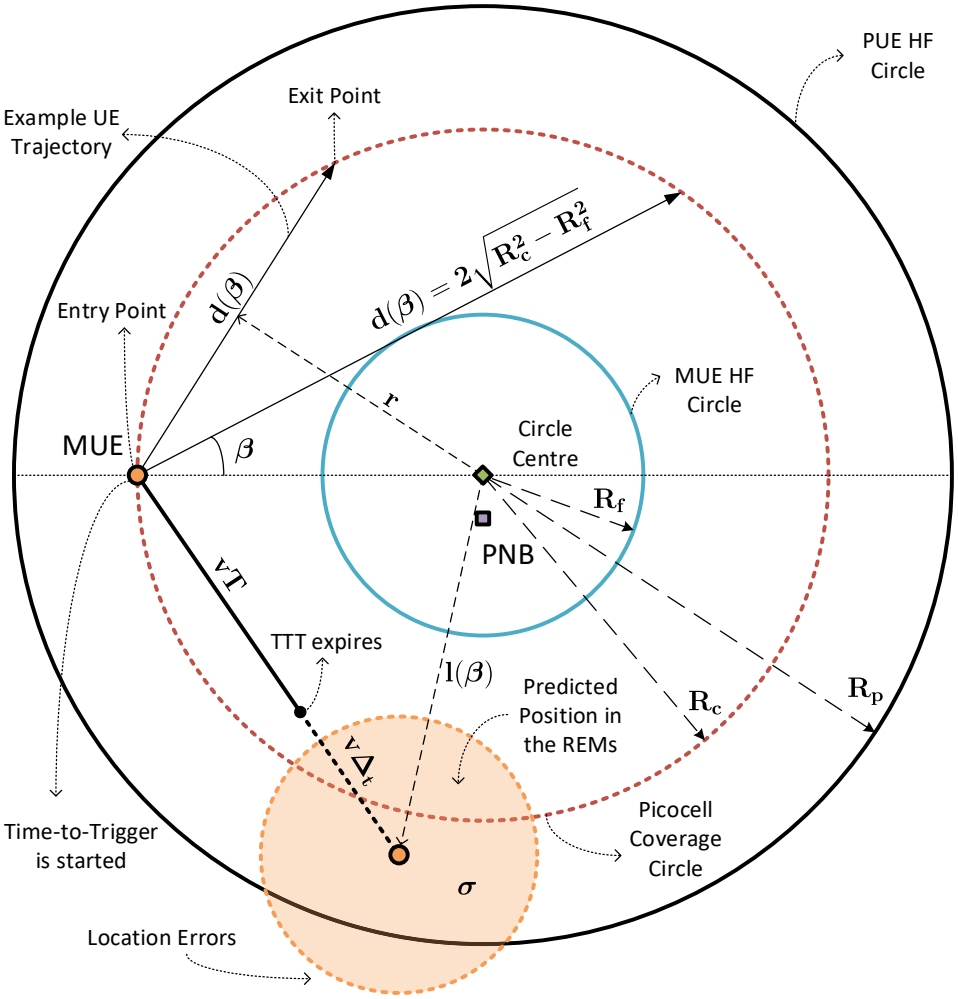

Figure 4.2: Models for picocell coverage area and macrocell and picocell HF areas.

centre of the picocell area to the chord $d(\beta)$. The probability density function (PDF) of r follows [44]:

$$f(r) = \frac{2}{\pi\sqrt{R_c^2 - r^2}}, \quad 0 \leq r \leq R_c. \tag{4.7}$$

Therefore, the probability of the chord being between two given lengths d_1 and d_2, with $d_1 < d_2$ is given by:

$$\mathbb{P}(d_1 < d(\beta) < d_2) = \frac{2}{\pi} \arctan\left(\frac{r}{\sqrt{R_c^2 - r^2}}\right) \Bigg|_{\sqrt{R_c^2 - d_1^2/4}}^{\sqrt{R_c^2 - d_2^2/4}}. \tag{4.8}$$

When UEs send measurement reports to their serving macrocell to perform an HO to the picocell [4], we assume that they also send back their location and velocity information. In this context, the UE's position provided by either a GNSS or a cellular network-assisted technique is altered by location errors. Nowadays, the most universally available system is GPS. Therefore our analysis considers it as a baseline. The GPS error model can be seen as a bivariate normal (Gaussian) distribution $\boldsymbol{\varepsilon} \sim \mathcal{N}_2(0, \boldsymbol{\Sigma})$, where $\boldsymbol{\varepsilon} = (x, y)$ is a random vector which describes the location errors and the positive-definite covariance matrix $\boldsymbol{\Sigma}$ is given by

$$\boldsymbol{\Sigma} = \begin{pmatrix} \sigma_X^2 & \rho\sigma_X\sigma_Y \\ \rho\sigma_Y\sigma_X & \sigma_Y^2 \end{pmatrix}, \tag{4.9}$$

where σ_X and σ_Y represent the standard deviations of the errors in the North-South and the East-West directions, and ρ is the correlation factor between them [112]. For simplicity, we consider them to be independent in both the x and y directions and equal , i.e. $\rho = 0$ and $\sigma_X = \sigma_Y = \sigma$. Hence, the distance from the centre of the picocell area to the reported location by the UE follows a Rice distribution $\kappa \sim \text{Rice}(\nu, \sigma)$, where ν denotes the true position of the UE. The cumulative distribution function (CDF) of κ is given as:

$$\mathbb{P}(\kappa < K) = 1 - Q_1\left(\frac{\nu}{\sigma}, \frac{K}{\sigma}\right), \tag{4.10}$$

where Q_1 is the Marcum Q-function [114]. Finally, GPS errors are also temporally and spatially autocorrelated, meaning that two consecutive position samples taken close in space and in time have similar errors, thus cancelling out when calculating averages [112]. The probabilities of no handover (NHO), handover failure (HF) and ping-pong handover (PP) will be derived based on (4.8) and (4.10).

4.2 REM-Based Handover Algorithm

Once we have described the different models needed, we are in a position to introduce our proposed algorithm (Algorithm 2). We propose a REM-based HO algorithm

aimed to reduce the number of ping-pong HOs without compromising the number of HFs. A REM is a spectrum database that stores the spatial distribution of the average RSS per cell [31]. Exploiting the stored RSS values and geolocation, we can pre-emptively classify an HO as worth doing according to the current UE's location. Since we could flag all the triggered HOs as unnecessary, we have to take the risk of possible HFs (drops) as well. Note that Algorithm 2 is written from the macrocell's point of view. From the picocell's perspective, we default to the standard LTE-HO algorithm.

When the user arrives at the border between the two cells, it starts a timer called Time-To-Trigger (TTT) of duration T [67]. Once the TTT expires[a] (see line 3 in Algorithm 2), our proposed algorithm predicts the user's position in a timespan Δ_t (line 8). This predicted point is then introduced in the macrocell and picocell REMs (each BS has one) to get the stored RSS values. Since our model only considers path loss, the handover region where the picocell RSS is higher than the macrocell RSS is exactly the circle defined in (4.3–4.4). Therefore, our policy allows the UE to hand over to the picocell only if the predicted point lies within the circle (lines 9–10). Otherwise, it will remain connected to the macrocell.

Nonetheless, an HF is declared if the UE's SINR is below Q_{out}, i.e. its trajectory intersects the HF circle. In the following, we derive the probabilities of NHO, HF for both macrocell and picocell UEs, and PP HOs. Such probabilities are conditioned on the distance between the macrocell and the picocell, which is uniformly distributed in an annulus with major and minor radii denoted by $r_{\max}$ and $r_{\min}$ [115]. In order to obtain the probabilities for the whole network, the probabilities must be weighted by the following PDF [105]:

$$f(x) = \frac{2\,(x - r_{\min})}{(r_{\max} - r_{\min})^2}, \quad r_{\min} \leq x \leq r_{\max}. \tag{4.11}$$

Algorithm 2 REM-Based Handover Algorithm with optimum prediction time

procedure UE REM-HO($P_{r,m}, P_{r,p}, \alpha, T$)
  if $P_{r,m} + \alpha < P_{r,p}$ for T **then**
    UE sends a measurement report with the user's location $\mathbf{x_u} = (x_u, y_u) + \boldsymbol{\varepsilon}$, and velocity $\mathbf{v} = (v_x, v_y)$.
  end if
end procedure

procedure BS REM-HO($\mathbf{x_u}$, $\mathbf{v}$, Δ_t, $\mathrm{REM}_m, \mathrm{REM}_p$)
  if Measurement report received **then**
    Predict the user's position in Δ_t.
    $\mathbf{x_p} = \mathbf{x_u} + \mathbf{v} \cdot \Delta_t$
    if $\mathrm{REM}_p(\mathbf{x_p}) > \mathrm{REM}_m(\mathbf{x_p})$ **then**
      BS sends the handover command back to the UE.
    end if
  end if
end procedure

4.2.1 Probability of No Handover

The probability of NHO represents the probability of a user leaving the handover region before the TTT expires without having a handover failure, i.e. intersecting the macrocell HF circle, which means that the chord must be shorter than the tangential chord ($2\sqrt{R_c^2 - R_f^2}$ in Fig. 4.2). Based on the distance that a macrocell UE can go across during a TTT of duration T, vT, we can distinguish two different cases. If vT is longer than the tangential chord, regardless of the prediction, the probability of NHO becomes the probability of the chord being between $0 < d(\beta) < 2\sqrt{R_c^2 - R_f^2}$ (4.8) as shown in Fig. 4.3 in the case of $v_1 T_1$. In the case that vT is shorter, both the TTT and the prediction time determine if there will be an HO. There will not be any HO if either the TTT expires outside the HO region ($0 < d(\beta) < vT$) or the TTT does expire within the HO region, but the prediction

[a] We disregard the handover preparation and execution times [4].

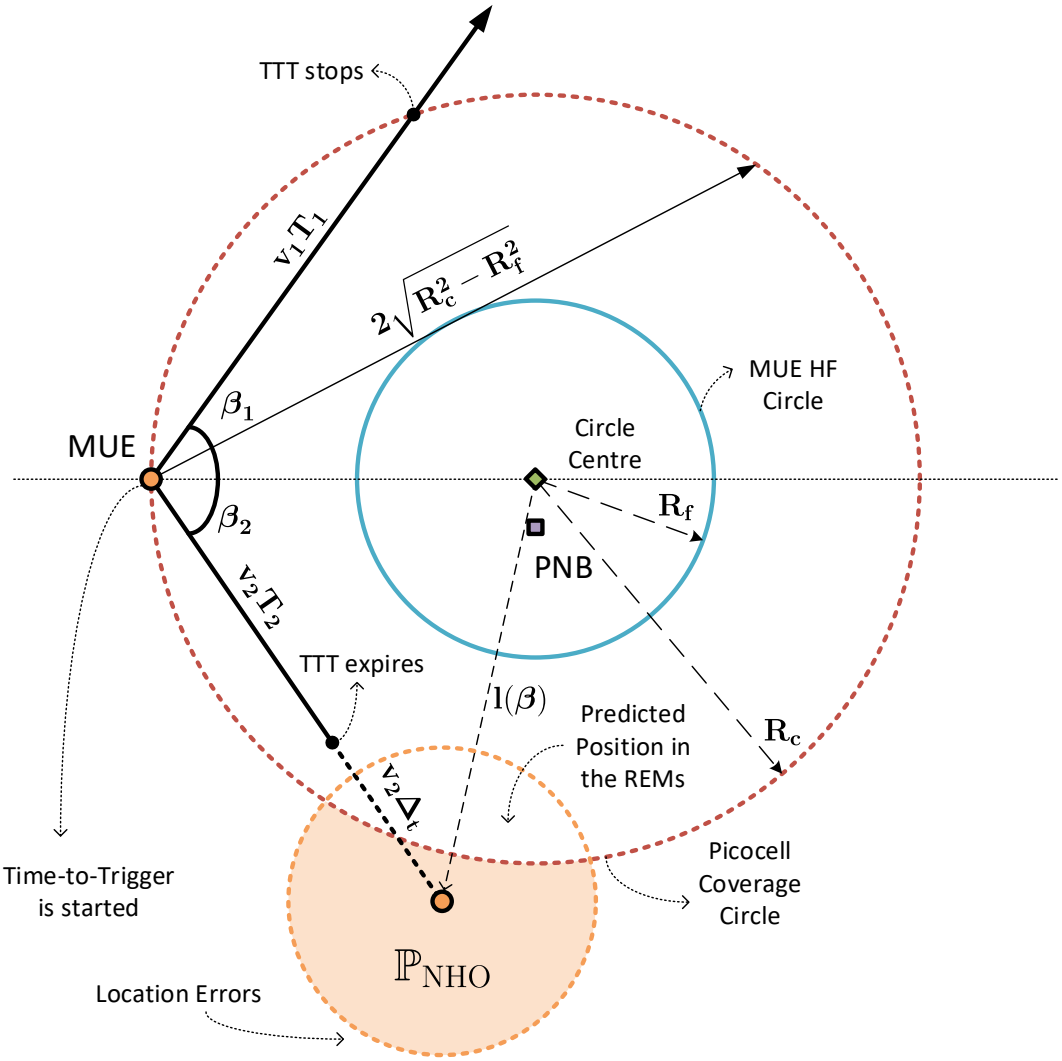

Figure 4.3: Probability of No Handover.

is outside without suffering from an HF. In Fig. 4.3, we show the case of v_2T_2 where T_2 can be either just the TTT or the addition of the TTT and the prediction time. Note that the prediction is affected by location errors. However, we can derive the centre of the distribution as:

$$l(\beta) = \sqrt{v^2 \left(T + \Delta_t\right)^2 + R_c^2 - 2v \left(T + \Delta_t\right) R_c \cos(\beta)}. \tag{4.12}$$

To avoid intersecting the macrocell HF area, the UE's trajectory must be between

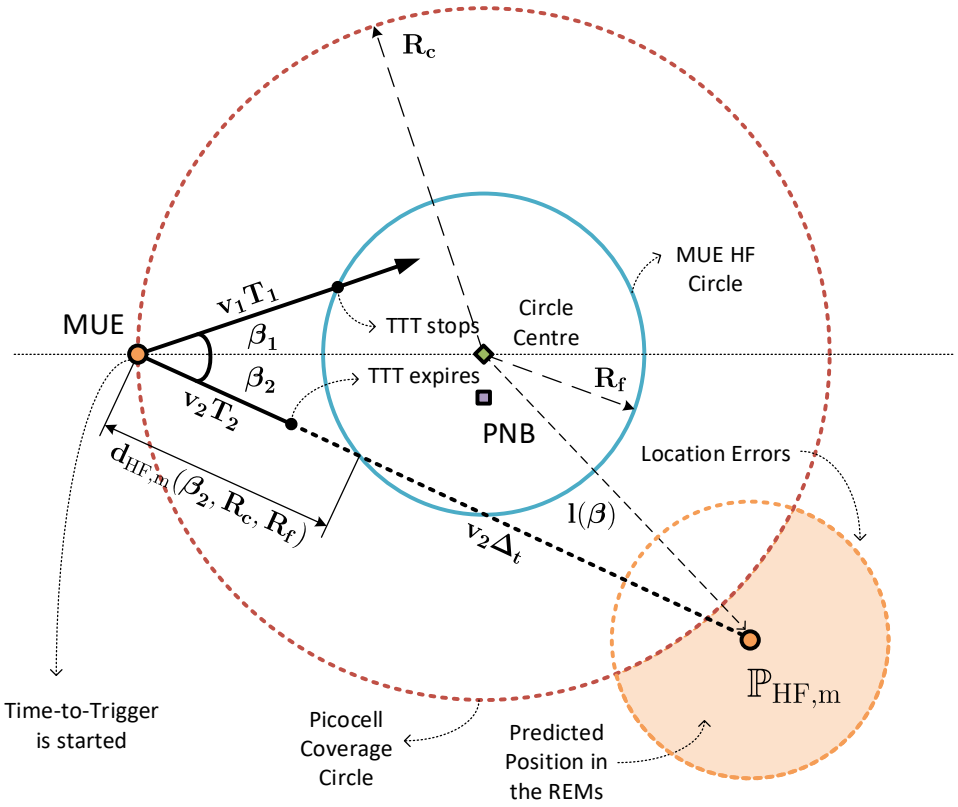

Figure 4.4: Probability of Macrocell Handover Failure.

$\arcsin\left(R_f/R_c\right) < \beta \leq \arccos\left(vT/2R_c\right)$. Thus using (4.10), we can obtain

$$\mathbb{P}\left[l(\beta) > R_c\right] = \frac{2}{\pi} \int_{\arcsin\left(R_f/R_c\right)}^{\arccos(vT/2R_c)} Q_1\left(\frac{l(\beta)}{\sigma}, \frac{R_c}{\sigma}\right) \mathrm{d}\beta. \tag{4.13}$$

Taking everything into account, we can write:

$$\mathbb{P}_{\mathrm{NHO}} = \begin{cases} \mathbb{P}\left[d(\beta) < 2\sqrt{R_c^2 - R_f^2}\right] & \text{if } vT \geq 2\sqrt{R_c^2 - R_f^2}, \\ \mathbb{P}\left[d(\beta) < vT\right] + \mathbb{P}\left[l(\beta) > R_c\right] & \text{if } vT < 2\sqrt{R_c^2 - R_f^2}, \\ & \arcsin\left(R_f/R_c\right) < \beta \leq \arccos\left(vT/2R_c\right). \end{cases} \tag{4.14}$$

4.2.2 Probability of Macrocell Handover Failure

If the chord length is longer than the tangential one, it means the user's trajectory intersects the macrocell HF circle, and the possibility of handover failure is real. In

our proposed algorithm, depending on where the TTT expires, two possible events might end up in a handover failure. The first one is the same as in LTE; in the case that the user reaches the macrocell HF circle before the TTT expires, an HF is declared as can be seen in Fig. 4.4 with v_1T_1. The user reaches the macrocell HF circle if the distance during the TTT is longer than the distance between the starting point and the circle. It can be expressed as

$$vT \geq d_{\mathrm{HF,m}}(\beta, R_c, R_f), \tag{4.15}$$

where $d_{\mathrm{HF,m}}(\beta, R_c, R_f) = R_c\cos(\beta) - \sqrt{R_f^2 - R_c^2\sin^2(\beta)}$. For example, in Fig. 4.4 the distance is labelled as $d_{\mathrm{HF,m}}(\beta_2, R_c, R_f)$. Then, the probability of a UE reaching the macrocell HF circle is [44]:

$$\mathbb{P}\left[vT \geq d_{\mathrm{HF,m}}(\beta, R_c, R_f)\right] = \begin{cases} 1 & \text{if } vT \geq \sqrt{R_c^2 - R_f^2}, \\ \dfrac{\arccos\left[\frac{(vT)^2 + R_c^2 - R_f^2}{2vTR_c}\right]}{\arcsin\left(\frac{R_f}{R_c}\right)} & \text{if } R_c - R_F \leq vT \leq 2\sqrt{R_c^2 - R_f^2}, \\ 0 & \text{if } vT < R_c - R_f. \end{cases} \tag{4.16}$$

The second event that may lead to an HF is related to our proposed algorithm: even though the TTT expires before reaching the macrocell HF circle, if the prediction is not within the handover region, an HF will be declared since we skip that HO mistakenly only for trajectories between $0 \leq \beta \leq \arcsin\left(R_f/R_c\right)$. This can be observed in Fig. 4.4 with v_2T_2 and $v_2\Delta_t$. Similarly to the NHO probability, the centre of the distribution is $l(\beta)$ in (4.12), but now we are interested in the UE's trajectories that intersect the macrocell HF area, i.e. $0 \leq \beta \leq \arcsin\left(R_f/R_c\right)$. Thus, the total probability of macrocell HF is given by:

$$\begin{aligned} \mathbb{P}_{\mathrm{HF,m}} = {} & \mathbb{P}\left[d(\beta) > 2\sqrt{R_c^2 - R_f^2}\right] \cdot \mathbb{P}\left[vT \geq d_{\mathrm{HF,m}}(\beta, R_c, R_f)\right] + \\ & \mathbb{P}\left[l(\beta) > R_c\right] \cdot \mathbb{P}\left[vT < d_{\mathrm{HF,m}}(\beta, R_c, R_f)\right] \quad \text{if } 0 \leq \beta \leq \arcsin\left(R_f/R_c\right). \end{aligned} \tag{4.17}$$

4.2.3 Probability of Picocell Handover Failure and Ping-pong Handovers

There is a successful HO to the picocell if the TTT of duration T expires inside the picocell coverage area and the prediction is also inside, without touching the picocell HF circle. Once the macrocell UE has performed a successful HO to the picocell, the roles are reversed. As soon as the user leaves the picocell coverage area, it will enter the macrocell coverage area again so, if it reaches the picocell HF circle, a picocell HF is declared. We can define the distance between the picocell HF circle and the HO one as:

$$d_{\mathrm{HF,p}}(\beta, R_c, R_p) = R_c \cos(\beta) + \sqrt{R_p^2 - R_c^2 \sin^2(\beta)} - d(\beta). \tag{4.18}$$

As in the macrocell case, we base our analysis on the distance that the user is capable of going across the TTT (4.24), vT. We can distinguish three cases:

1. If $vT \geq \sqrt{R_c^2 - R_f^2}$:

   In this case, the UE either leaves the picocell without performing an HO or experiences an HF based on (4.14) and (4.17). Therefore, both the probability of picocell HF and PP are $\mathbb{P}_{\mathrm{HF,p}} = \mathbb{P}_{\mathrm{PP}} = 0$.

2. If $\sqrt{R_c^2 - R_f^2} < vT < 2\sqrt{R_c^2 - R_f^2}$:

   In this case, in order to have a successful HO to the picocell, the chord length must be between $vT < d(\beta) < 2\sqrt{R_c^2 - R_f^2}$, i.e. $\arcsin(R_f/R_c) < \beta < \arccos(vT/2R)$. Then, a picocell HF is declared if the UE reaches the picocell HF circle before the TTT expires. From (4.18), we obtain:

$$vT > d_{\mathrm{HF,p}}(\beta, R_c, R_p) \Rightarrow \beta_{\mathrm{HF,p}} < \arccos\left(\frac{R_p^2 - R_c^2 - v^2T^2}{2R_c vT}\right). \tag{4.19}$$

   Since $\arcsin(R_f/R_c) < \beta < \beta_p$ with $\beta_p = \min\left[(vT/2R_c), \beta_{\mathrm{HF,p}}\right]$, the probabil-

ity can be written as:

$$\mathbb{P}\left[l(\beta) < R_c\right] = \frac{2}{\pi} \int_{\arcsin\left(R_f/R_c\right)}^{\beta_p} 1 - Q_1\left(\frac{l(\beta)}{\sigma}, \frac{R_c}{\sigma}\right) \mathrm{d}\beta. \tag{4.20}$$

There is no point in using the prediction for the HO back to the macrocell because location errors could cause additional HFs. Besides, avoiding the HO to the picocell in the first place reduces the PP HOs. Ping-pong HOs happen when performing two successful consecutive HOs between the same two cells within a minimum time of stay (ToS) of duration T_{PP}. As a result, they reduce the efficiency of the network due to the frequent disconnections from the network. Note that LTE implements a hard HO. Besides, the exchange of signalling between the cells also introduces an undesirable amount of overhead, thus it is crucial to find a balance between the best connection available, hence the HO, and the number of unnecessary disconnections to keep a satisfactory QoS for the users. We obtain the angle β_{PP} (see Fig. 4.5) above which, for a given speed v, the user takes less time than T_{PP} to perform those two handovers, as:

$$2R_c \cos(\beta) < vT_{\mathrm{PP}} \Rightarrow \beta_{\mathrm{PP}} > \arccos\left(\frac{vT_{\mathrm{PP}}}{2R_c}\right). \tag{4.21}$$

Including this condition, the probability is:

$$\mathbb{P}\left[l(\beta) < R_c\right] = \frac{2}{\pi} \int_{\beta_r}^{\arccos\left(\frac{vT}{2R_c}\right)} 1 - Q_1\left(\frac{l(\beta)}{\sigma}, \frac{R_c}{\sigma}\right) \mathrm{d}\beta, \tag{4.22}$$

where $\beta_r = \max\left[\arcsin\left(R_f/R_c\right), \beta_{\mathrm{HF,p}}, \beta_{\mathrm{PP}}\right]$.

3. If $vT < \sqrt{R_c^2 - R_f^2}$:

   In this case, even when the chord length is $d(\beta) > 2\sqrt{R_c^2 - R_f^2}$, it is possible to HO successfully to the picocell if the UE does not reach the macrocell HF

circle. Then, we can divide the probability space into two. For $vT \leq d(\beta) < 2\sqrt{R_c^2 - R_f^2}$, it follows the same equation as (4.20), whereas for $2\sqrt{R_c^2 - R_f^2} \leq d(\beta) < 2R_c$, we obtain:

$$\mathbb{P}\left[l(\beta) < R_c\right] = \frac{2}{\pi} \int_0^{\beta_q} 1 - Q_1\left(\frac{l(\beta)}{\sigma}, \frac{R_c}{\sigma}\right) \mathrm{d}\beta, \tag{4.23}$$

where $\beta_q = \min\left[\arcsin\left(R_f/R_c\right), \beta_{\mathrm{HF,p}}\right]$. Combining (4.16) and (4.23), the total picocell HF probability is:

$$\mathbb{P}_{\mathrm{HF,p}} = \begin{cases} 0 & \text{if } vT \geq 2\sqrt{R_c^2 - R_f^2}, \\ \mathbb{P}\left[l(\beta) < R_c\right] & \text{if } \sqrt{R_c^2 - R_f^2} < vT < 2\sqrt{R_c^2 - R_f^2}, \\ & \arcsin\left(R_f/R_c\right) < \beta \leq \arccos\left(vT/2R_c\right), \\ \mathbb{P}\left[vT < d_{\mathrm{HF,m}}(\beta, R_c, R_f)\right] \times & \\ \mathbb{P}\left[l(\beta) < R_c\right] + & \text{if } vT \leq \sqrt{R_c^2 - R_f^2}, \\ \mathbb{P}_{\mathrm{HF,p}}\Big|_{\sqrt{R_c^2 - R_f^2} < vT < 2\sqrt{R_c^2 - R_f^2}} & 0 < \beta \leq \arcsin\left(R_f/R_c\right). \end{cases} \tag{4.24}$$

The PP probability for this case can also be divided into two. For $vT \leq d(\beta) < 2\sqrt{R_c^2 - R_f^2}$, it is the same equation as (4.22), whereas for $2\sqrt{R_c^2 - R_f^2} \leq d(\beta) < 2R_c$, it can be expressed as:

$$\mathbb{P}\left[l(\beta) < R_c\right] = \frac{2}{\pi} \int_{\beta_s}^{\arcsin\left(R_f/R_c\right)} 1 - Q_1\left(\frac{l(\beta)}{\sigma}, \frac{R_c}{\sigma}\right) \mathrm{d}\beta, \tag{4.25}$$

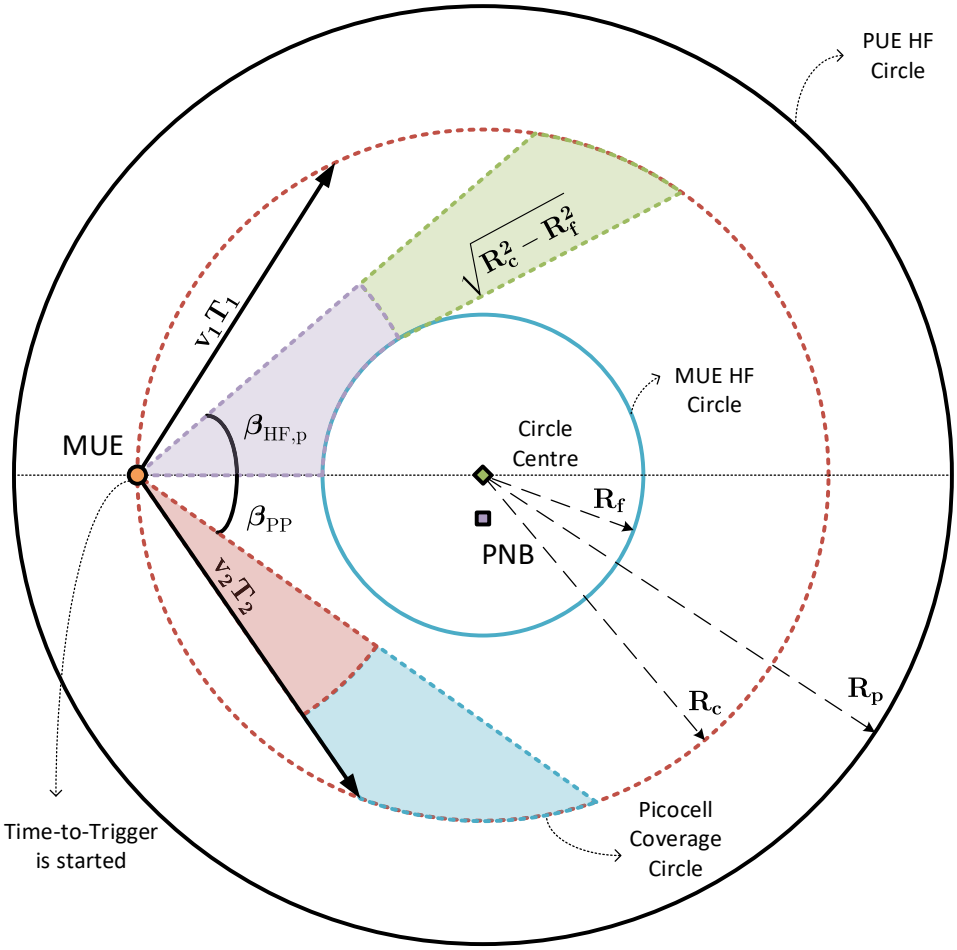

Figure 4.5: Probability of Picocell Handover Failure and Ping-pong Handovers.

where $\beta_s = \max[0, \beta_{\mathrm{HF,p}}, \beta_{\mathrm{PP}}]$. The final expression is given by:

$$\mathbb{P}_{\mathrm{PP}} = \begin{cases} 0 & \text{if } vT \geq 2\sqrt{R_c^2 - R_f^2}, \\ \mathbb{P}\left[l(\beta) < R_c\right] & \text{if } \sqrt{R_c^2 - R_f^2} < vT < 2\sqrt{R_c^2 - R_f^2}, \\ & \arcsin\left(R_f/R_c\right) < \beta \leq \arccos\left(vT/2R_c\right), \\ \mathbb{P}\left[vT < d_{\mathrm{HF,m}}(\beta, R_c, R_f)\right] \times & \\ \mathbb{P}\left[l(\beta) < R_c\right] + & \text{if } vT \leq \sqrt{R_c^2 - R_f^2}, \\ \mathbb{P}_{\mathrm{PP}}\Big|_{\sqrt{R_c^2-R_f^2}<vT<2\sqrt{R_c^2-R_f^2}} & 0 < \beta \leq \arcsin\left(R_f/R_c\right). \end{cases} \tag{4.26}$$

4.2.4 Optimal Prediction Times

The utility of this analysis is providing a set of equations to choose the optimum combination of prediction times for macrocell UEs based on their speed. Different optimisation problems can be proposed depending on the objective. As an example, we could define the following one:

$$\begin{aligned} &\underset{\Delta_t}{\text{minimise}} \quad \mathbb{P}_{\text{PP}}(\Delta_t) \\ &\text{subject to} \quad \mathbb{P}_{\text{HF}}(\Delta_t) \leq p_{\text{out}}, \end{aligned} \tag{4.27}$$

where p_{out} is the outage probability, Δ_t is the timespan for the prediction, and the functions involved are derived in Section 4.2. In (4.27) we try to minimise the probability of ping-pong handovers allowing a certain probability of outage. We have used MATLAB to solve (4.27), in particular, `fmincon` (Interior Point Method).

4.3 Numerical Results

In this section, we first validate the theoretical analysis derived in Section 4.2 with Monte Carlo simulations carried out in MATLAB. We assume omnidirectional antennae at both BSs and the user and, as in the whole chapter, only the path loss is considered in our analysis. Furthermore, we suppose that we have perfect knowledge of the UE RSS at any moment (geometry HO). Without the loss of generality, we consider a null HHM. In the case of increasing its value, the inbound HO region, macrocell to picocell, would become smaller since it is equivalent to an increase in the macrocell transmit power, and vice versa for the outbound HO region, picocell to macrocell, for the same reason. As depicted in Fig. 4.1, picocells are uniformly deployed under the coverage of a macrocell. We fix a macrocell at the origin and deploy a picocell according to (4.11), creating a bouncing circle around it (see green circle in Fig. 4.1). We have carried out 10^4 random picocell deployments. Then, we have positioned 10^3 users on the bouncing circle, connected to the macrocell at first, and make them move towards the picocell with a random angle as per 3GPP specifications [4]. For each user, the simulation ends when either an HF occurs or

Table 4.1: Simulation Parameters

Parameter	**Value**
Carrier frequency (f)	2 GHz
Macrocell BS transmit power ($P_{t,m}$)	46 dBm
Macro path loss model (K_m, γ_m)	$128.1 + 37.6 \log(R)$ dB (R in km)
Macro antenna gain (G_m)	14 dBi
Picocell BS transmit power ($P_{t,p}$)	30 dBm
Pico path loss model (K_p, γ_p)	$140.7 + 36.7 \log(R)$ dB (R in km)
Pico antenna gain (G_p)	5 dBi
ISD	500 m
Pico distribution radius ($r_{\max}$)	289 m
Minimum distance macro-pico ($r_{\min}$)	75 m
Minimum distance pico-pico	40 m
Mobile UE speed (v)	10 – 120 km/h
Time-To-Trigger (T)	{40, 80, 160, 480} ms
Minimum Time-of-Stay (T_{PP})	1 s
Handover Hysteresis Margin (α)	0 dB
HF threshold (Q_{out})	-8 dB
Location errors std (σ)	3 m
Probability of outage (p_{out})	1%
Number of simulations drops	10^7 per TTT-speed combination

the UE hits the other border of the bouncing circle, whichever comes first. The results shown in the next subsections consist of the probability of no handover, the probability of handover failure (macrocell and picocell together), and the probabil-

ity of ping-pong handover. Then, we compare our proposed algorithm with other algorithms found in the literature [44, 66]. Finally, we evaluate the performance of the REM-HO algorithm under the influence of different location errors. The rest of the simulation parameters are listed in Table 4.1.

4.3.1 Performance of REM-HO

In Fig. 4.6, we show the theoretical and the simulation results for Δ_t^* obtained from the optimisation problem in (4.27) versus different values of the UE speed. In general, a good match can be observed between the theoretical values and the simulation ones. The slight differences are due to the circles in the simulation not being concentric as they are in the theoretical model. In Fig. 4.6a, the probability of NHO is above 30% for all speeds considered regardless of the TTT. Note that not handing over does not imply the call is dropped. It means that the UE can safely avoid the HO without an HF. The product of UE speed v and TTT T determines how far the UE travels within the picocell. Therefore, as expected, the higher this product, the more likely the UE will skip the picocell. However, this is also true for the probability of HF. In Fig. 4.6b, we can observe that the probability of HF is above the required $p_{out} = 1\%$ for $T = 480$ ms, i.e. the solver has been unable to find a feasible solution for (4.27). After 85 km/h, $T = 160$ ms rises by 1% over the limit. Only $T = 40$ ms accomplishes the target, closely followed by $T = 80$ ms at around 1.5%.

On the contrary, the probability of PP HO follows the opposite trend in Fig. 4.6c. In most cases, the probability of PP is within 22 – 34% for highway-speed users whereas it is less than 10% for speeds below 80 km/h. The results of the optimisation problem are depicted in Fig. 4.7. It can be seen that the predictions are at least one order of magnitude larger than the TTTs considered, i.e. hundreds of milliseconds against tens of milliseconds, which cause the prediction times to look bundled up. The prediction time follows an inversely proportional trend to the UE speed as the longer the distance within the picocell, the higher the risk of an HF. In the case that we relax the constraints, we could skip HOs more aggressively while increasing the HF probability.

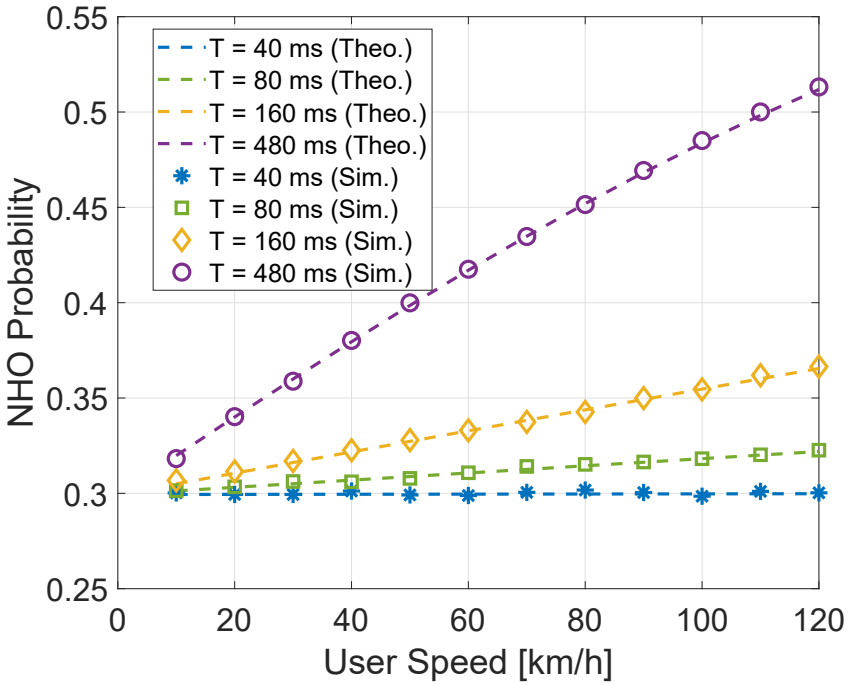

(a) Probability of no handover.

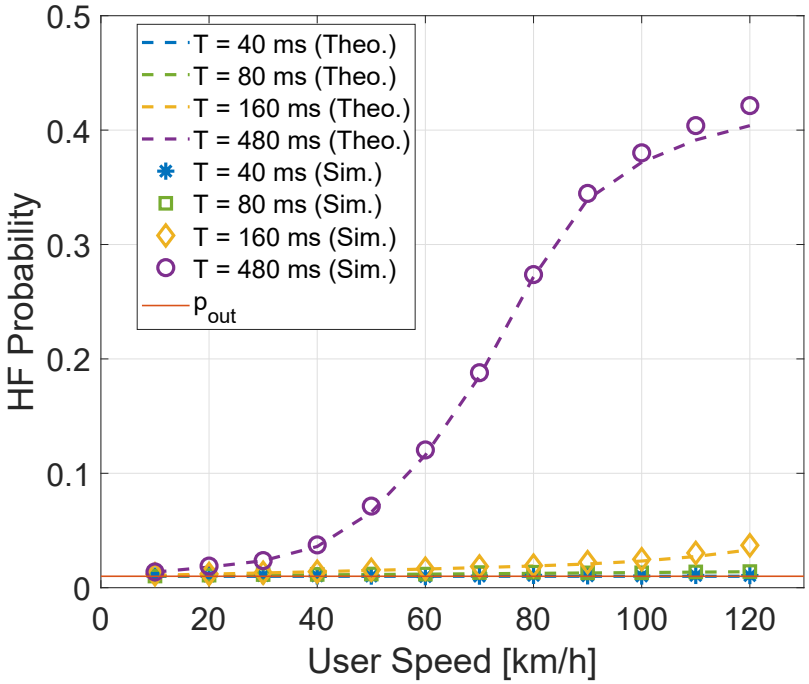

(b) Probability of handover failure.

Figure 4.6: REM-HO theoretical (dashed lines) and simulated (markers) results as a function of the UE speed for TTT = {40, 80, 160, 480} ms, and Δ_t^* from (4.27).

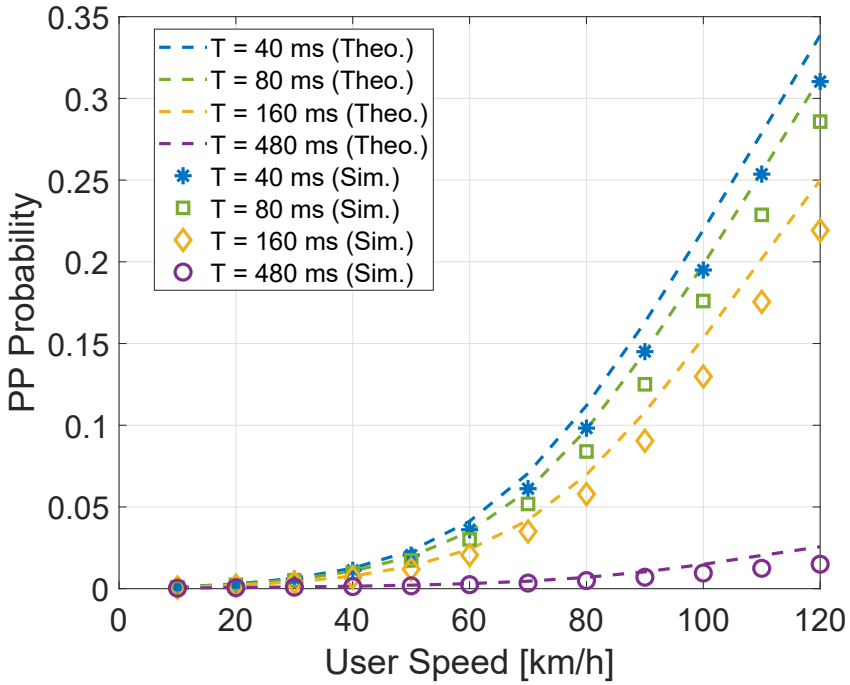

(c) Probability of ping-pong handover.

Figure 4.6: REM-HO theoretical (dashed lines) and simulated (markers) results as a function of the UE speed for TTT = {40, 80, 160, 480} ms, and Δ_t^* from (4.27).

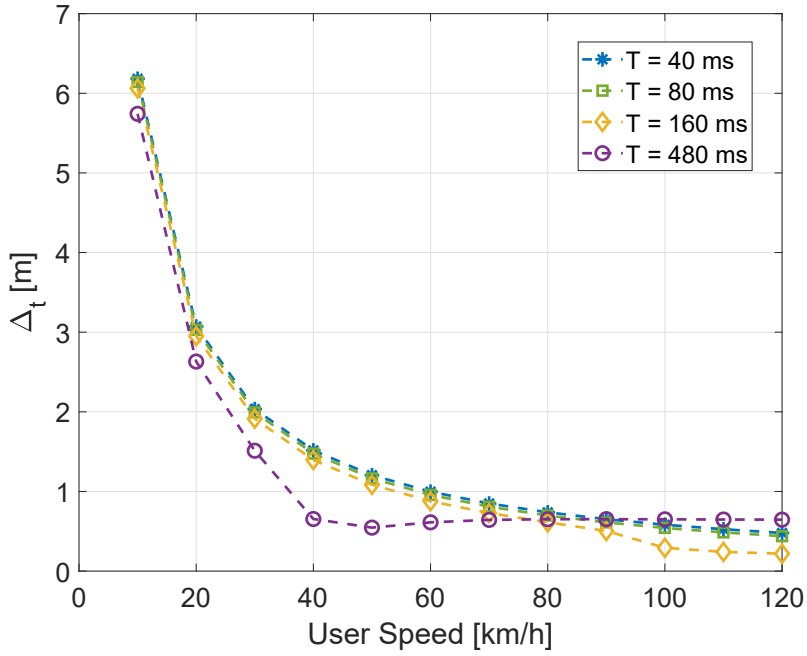

Figure 4.7: Optimal prediction times as a function of the UE speed for TTT = {40, 80, 160, 480} ms.

4.3.2 Comparison with Competitive Algorithms

After validating the theoretical model, we can compare our proposed REM-HO with other competitive schemes in the same scenario. The following algorithms implemented or evaluated for the comparison are considered:

- Best Connected (BC): the UE always connects to the BS with the highest RSS. It is equivalent to the LTE-HO algorithm with $T = 0$ ms and $\alpha = 0$ dB.
- LTE-HO: the UE waits for the TTT to perform an HO. Without loss of generality, we consider $\alpha = 0$ dB. We have verified the analytical work presented in [44], and have only evaluated the theoretical results.
- Adaptive HMM based on fuzzy logic (AHFL): defined in [66], it uses fuzzy logic to change the value of α.
- REM-HO with fixed prediction time (fREM): introduced in [109], the value of Δ_t could not be optimised due to the lack of analytical work. This algorithm was introduced in Chapter 3, and we include it to show the improvement of the new scheme.

In Fig. 4.8a, we can view how the probability of NHO increases for longer TTTs, as stated before. In this case, our algorithm shifts the probabilities proportionally to the product $v\Delta_t$. All REM-HO cases outperform the LTE-HO algorithm in terms of NHO. On the contrary, the BC scheme does not skip a single HO. Thus the probability of NHO stays at zero for all the speeds considered. Also, the majority of fREM cases and all the AHFL cases represent an improvement over the LTE-HO algorithm. Note that the probability of NHO implies that the UE can leave the picocell coverage area without experiencing a drop. However, the probability of HF for both schemes worsens dramatically for speeds above 20 km/h, as shown in Fig.4.8b. For example, the AHFL algorithm performs substantially worse than the rest of the algorithms for all the speeds. Adding up the probability of NHO and the probability of HF in the AHFL cases results in almost 1, which means that the totality of the HOs is either skipped (NHO) or dropped (HF). The fREM approach becomes as bad for speeds above 80 km/h.

On the contrary, the probability of HF is marginally higher for REM-HO in the region of low TTTs and high speed. This is because, although the TTT expires before reaching the HF macrocell circle, some predictions lie outside the picocell coverage circle, so the REM-HO method avoids the opportunity of HO. Since the UE's location is not perfect, there is always a remnant of the probability of HF that our proposed algorithm cannot eliminate. In particular, the HF probability is below 1.5% throughout the considered speeds as mentioned beforehand for $T = 40 - 160$ ms. For $T = 480$ ms, the distance travelled by the UE is large enough to hit the MUE HF circle, causing an HF. This effect is depicted in Fig. 4.4 with the example of $v_1 T_1$. The reason why the LTE-HO algorithm performs slightly worse for high-speed users is due to the lesser number of avoided HOs in Fig. 4.8a. It would seem that the BC algorithm is a good option because it does not experience any HF. As it can be seen in Fig. 4.8c, it has the highest probability of PP HO due to performing all possible HOs. It is a corner case that exemplifies the trade-off between HF and PP HO.

The LTE-HO scheme reduces the probability of PP HO as the TTT increases. For values of T from 40 to 160 ms, the PP HO follows an almost linear fashion. However, for $T = 480$ ms, the PP HO reaches a plateau for speeds above 60 km/h. In this case, this trend can be explained from the higher number of HF in Fig. 4.8b, i.e. if there is a drop, there are fewer chances of having a PP HO. Similarly, both the AHFL and the fREM algorithms do not experience any redundant HOs because of the high number of drops. This behaviour is another corner case, where these two algorithms can reduce the PP HO to zero by increasing the probability of HF. Finally, we show that for our proposed REM-HO, the probability of PP HO is significantly reduced by 10, 20, and 30% for 30, 60, and 120 km/h. Our algorithm focuses on avoiding as many HOs as possible in Fig. 4.8a, but without overly increasing the HF in both 40 and 80 ms cases (1%) in Fig. 4.8b. These results demonstrate that REMs can be successfully integrated into the HO decision process complementing the current industry standard since it is backwards compatible.

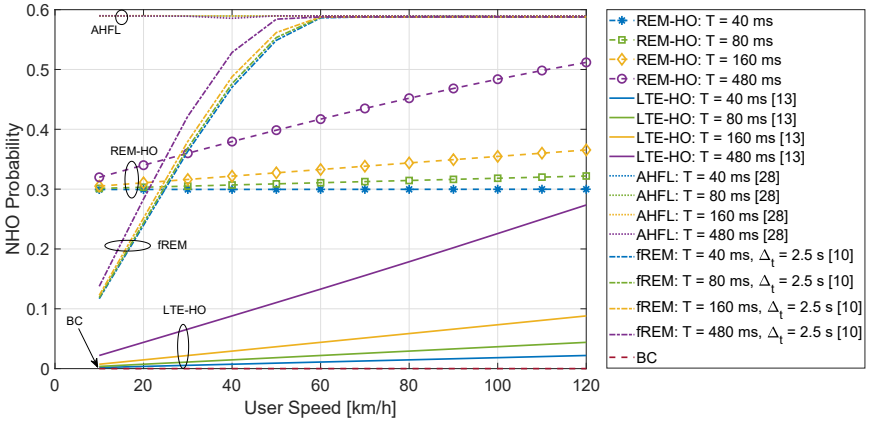

(a) Probability of no handover.

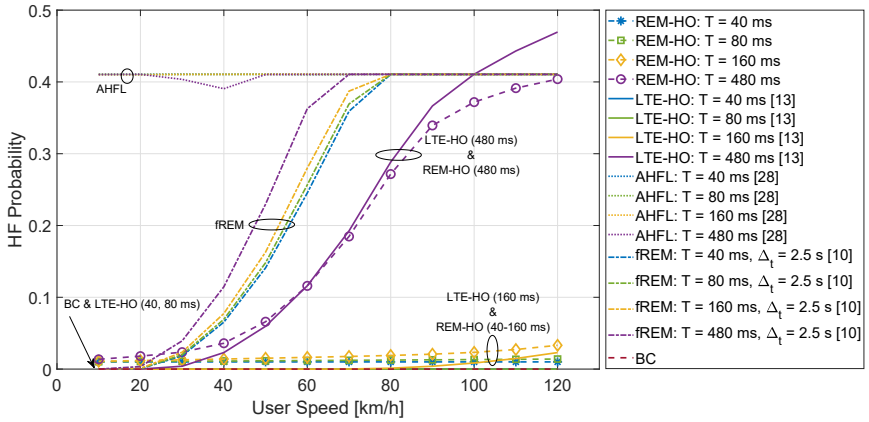

(b) Probability of handover failure.

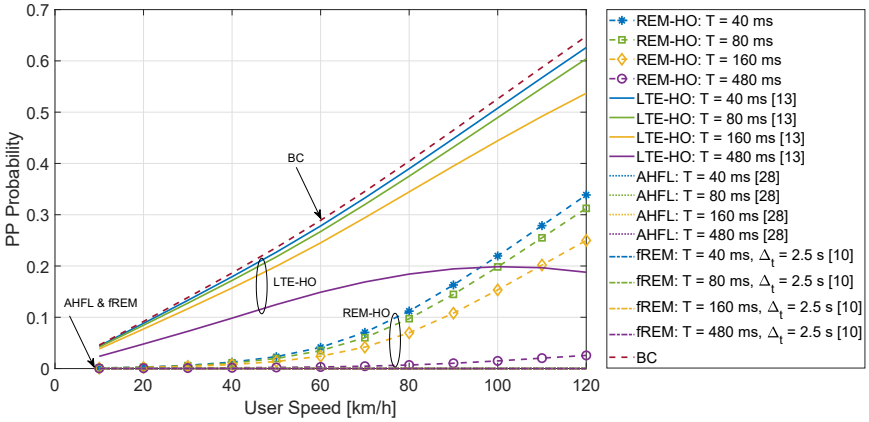

(c) Probability of ping-pong handover.

Figure 4.8: Comparison between REM-HO (dashed lines with markers), LTE-HO (solid lines), AHFL (dotted lines), fREM (dash-dot lines), and BC (dashed line without markers) results as a function of the UE speed for TTT = {40, 80, 160, 480} ms.

4.3.3 Location-error Effect

We want to assess the importance of the location errors, and to do so we have selected $T = \{40, 80\}$ ms because they can reduce the PP probability significantly without committing an excessive amount of HFs. Also, we sweep the location errors through σ from the 3-m case [112] to 99.9% availability at any time and location given by the 12-m case [111]. The probability of NHO depicted in Fig. 4.9, where the differences in performance between $\sigma = 3$ m and $\sigma = 6$ m are negligible. For $\sigma = 12$ m, we can skip more HOs at the expense of experiencing more HFs. In Fig. 4.9b, the probability of HF tends to be almost constant for the whole range of speeds considered. We notice that the probability of HF is 14% for $\sigma = 12$ m, which is intolerable, while it is reduced by 10% for $\sigma = 6$ m. When $\sigma = 3$ m, the probability of HF is almost zero. This makes it evident that our proposed technique is useful whenever the location is accurate to a certain degree, e.g. 6 m in our case. A standard GPS receiver can estimate its accuracy and forward it in the measurement reports. Thus, in case of poor conditions, our algorithm can always fall back to the standard LTE-HO by ignoring the prediction. The probability of PP is shown in Fig. 4.9c. We can see that the performance does not very rapidly increase to LTE-HO levels in any case. Note that when location errors increase, the probability of PP decreases due to the higher likelihood of experiencing an HF.

4.3.4 Discussion

It is important to highlight that the location errors σ are out of our control because they are intrinsically related to the GPS device coverage. Location errors in the range of 3 m $\leq \sigma \leq$ 6 m are nearer to a realistic scenario. If we put a focus on Fig. 4.6b, we can spot that TTTs from 40–80 ms are the least affected by the location errors, while 160 ms could be acceptable in certain situations too. We would like to stress the importance of the prediction time Δ_t that has an essential effect on the achieved performance in the REM-HO. Note that the prediction time allows us to mitigate the impact of the PP HO in Fig. 4.6c, and it is fundamental to set its value accordingly to the UE speed. Overall, our proposed algorithm can achieve a

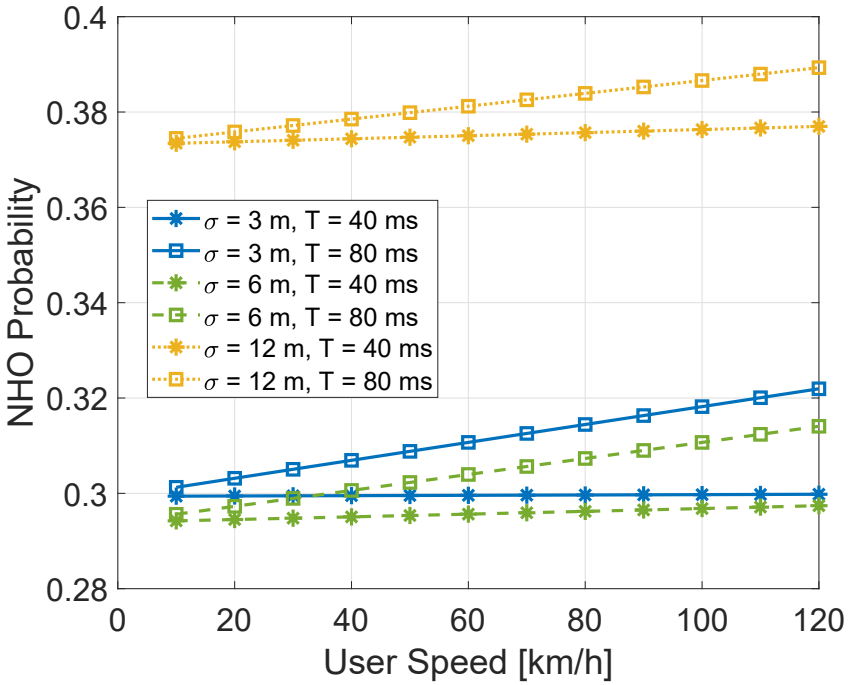

(a) Probability of no handover.

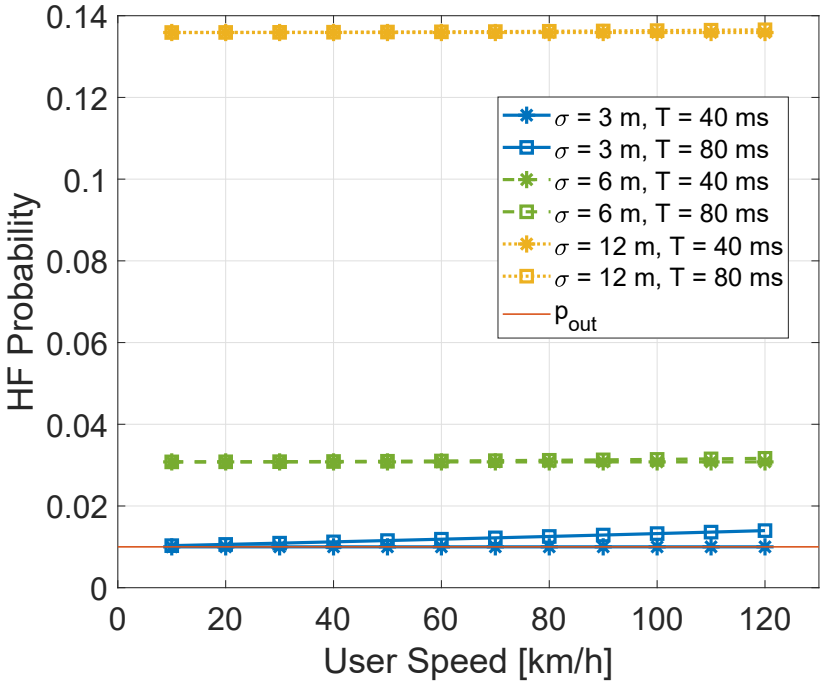

(b) Probability of handover failure.

Figure 4.9: REM-HO results for TTT = {40, 80} ms, and σ = {3, 6, 12} m.

low probability of HF and, at the same time, can reduce the PP HOs to acceptable rates. This verifies our previous works and also demonstrates that breaking the

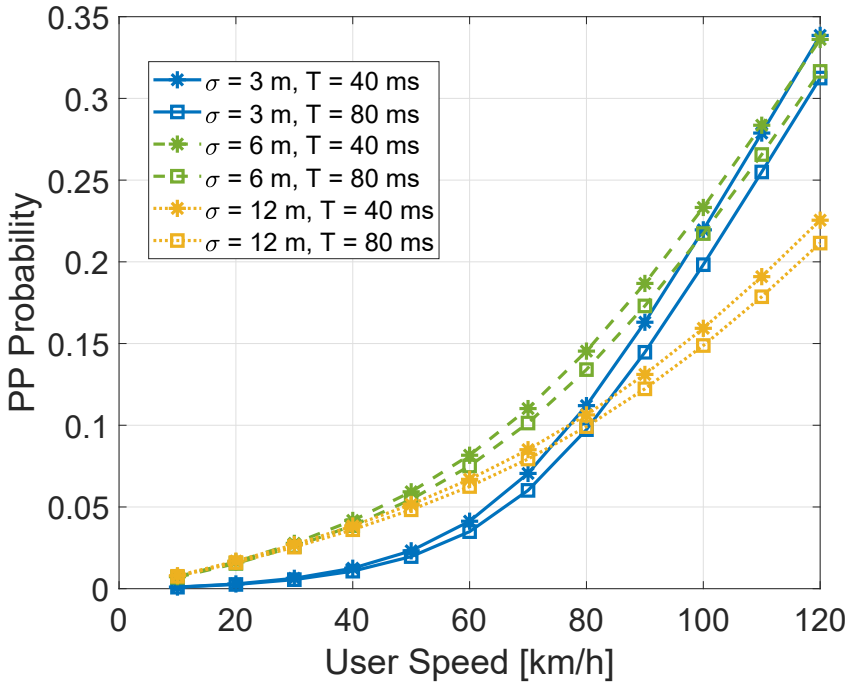

(c) Probability of ping-pong handover.

Figure 4.9: REM-HO results for TTT = {40, 80} ms, and σ = {3, 6, 12} m.

LTE-HO procedure into two stages, measurements and prediction, is an excellent option to find a compromise between performance and backwards compatibility. Moreover, this approach is in line with the CHO approach, where we have replaced the condition for a query into a database.

4.4 Summary

In this chapter we have presented an HO algorithm that uses REMs as a tool to reduce the number of PP HOs without incurring too many HFs, therefore ensuring a reduction on the HetNet network signalling and future multi-tier cellular networks. Since our proposed algorithm uses the UE's geolocation capabilities, we have also derived a framework that allows us to obtain a better understanding of the expected HO performance under location errors. This framework has been validated through Monte Carlo simulations for a wide range of cases. Numerical results show that our REM-HO algorithm can drastically reduce the PP rate in most cases, maintaining it below 35%, an improvement of at least 10% over the LTE-HO standard and that

the prediction time must be chosen adaptively to adjust the HF rate. In the next chapter, we will tune the prediction time through an optimisation problem that takes into account the HO performance obtained in this chapter and the network performance as a whole, for example, maximising the users' QoS.

Chapter 5

Network Optimisation in 5G Networks: A Radio Environment Map Approach

Network densification can boost capacity in 5G networks. However, prospective gains could be undermined by inefficient cell-association policies, outdated radio planning solutions or backhaul topologies. In this chapter, we propose a strategy for cell association based on radio environment maps (REMs) for dense 5G networks. By exploiting the stored channel states and user location, we connect cellular users to the optimal tier dynamically. Based on stochastic geometry, the association probability and the coverage probability have been derived for dense 5G networks, where the base station locations follow Poisson Point Processes. Moreover, the user throughput and backhaul traffic are evaluated to assess their performance in dense 5G networks. The proposed technique is validated via Monte Carlo simulations and compared to different cell-association techniques. Results show that our scheme finds a balance between the coverage probability and the handover rate by numerical optimisation. In particular, it increases the average user throughput by 65% over the traditional approach, and it reduces the amount of overhead by up to 68% over the other cell-association strategies.

5.1 System Model

We consider a cellular network comprised of two tiers whose locations are modelled as independent homogeneous Poisson point processes (HPPP) $\Phi_k \subset \mathbb{R}^2$ with intensity λ_k, $k = \{1, 2\}$, operating in the same band. We assume that every base station (BS) in the k^{th} tier shares the same transmit power P_k as well as the same bias factor B_k. The channel includes path loss with different path-loss exponents $\alpha_k > 2$, Rayleigh fading with unit power $h \sim \exp(1)$, and additive white Gaussian noise (AWGN) with power σ_n^2. It is worth noting that the analysis derived in this paper is deducted from the stationary case as in [86]. The mathematical notation used throughout this chapter is in Table 5.1.

5.2 REM-Based Cell-Association Strategy

We propose a novel REM-based cell-association strategy that aims to connect cellular users to the optimal tier based on their location. A REM is a spectrum database that stores the spatial distribution of the average received signal strength (RSS) per cell [31]. Exploiting the stored RSS values and geolocation, we allow cellular users to skip HOs on their best interest. Our policy does not only rely on the location or velocity alone, but a fusion of both. For example, a simple distance threshold could prevent HOs at cell edges at the expense of triggering multiple HOs during the sojourn time, or a speed threshold could impede high-speed users to perform HOs neglecting that they could be heading towards the centre of the cell. On the other hand, obtaining cellular users' positioning allows us to geolocate them on a REM and to select the best connection available according to their current trajectory at once. In Fig. 5.1, we illustrate how our strategy works; for example, in Fig. 5.1b, the typical user at the origin connects to the closest macrocell represented by the green square despite the existence of a picocell even closer due to the difference in transmit power. However, after a small modification in the position of the closest picocell represented by the purple circle in Fig. 5.1c, even though the typical user would connect to the same macrocell under the traditional approach, the search circle favours the connection to the closest picocell. We introduce this search circle

Table 5.1: Mathematical Notation

Notation	**Description**
Φ_k	HPPP of BSs in the k^{th} tier
λ_k	Intensity of BSs in the k^{th} tier
P_k	Transmit power of BSs in the k^{th} tier
B_k	Bias factor of BSs in the k^{th} tier
α_k	Path-loss exponent of BSs in the k^{th} tier
h	Channel gain with unit power
σ_n^2	AWGN power
$P_{\text{r},k}$	Biased RSS of the strongest BS in the k^{th} tier
L_0	Path loss at the reference distance $r_0 = 1$ m
R_k	Distance from the nearest BSs in the k^{th} tier
Δ_k	Search radius in the REM for the k^{th} tier
$P^e_{\text{r},k}$	Stored RSS in the REM of the strongest BS in the k^{th} tier
ρ_k	RSS estimation error in the REM for the k^{th} tier
σ_k	Standard deviation of the RSS error in the REM
Φ^e_k	Equivalent HPPP of BSs in the k^{th} tier
λ^e_k	Equivalent intensity of BSs in the REM for the k^{th} tier
$\mathcal{A}_k\,(\mathcal{A}^s_k)$	Association probability of the k^{th} tier (after skipping)
$\mathcal{C}_k\,(\mathcal{C}^s_k)$	Coverage probability of the k^{th} tier (after skipping)
$\mathcal{R}_k\,(\mathcal{R}^s_k)$	Spectral efficiency of the k^{th} tier (after skipping)
$\mathcal{T}$	Average user throughput
$\mathcal{D}$	HO cost
$\mathcal{W}$	System bandwidth
H_{kj}	HO rate between tiers k and j
d_k	HO delay for k^{th} tier

in the next subsection.

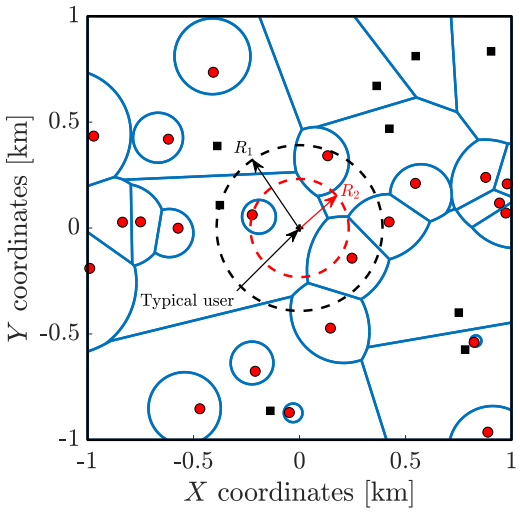

(a) The closest macrocell and the closest picocell are at R_1 and R_2, respectively. The typical user (at the origin) will camp on one or another depending on the search radii.

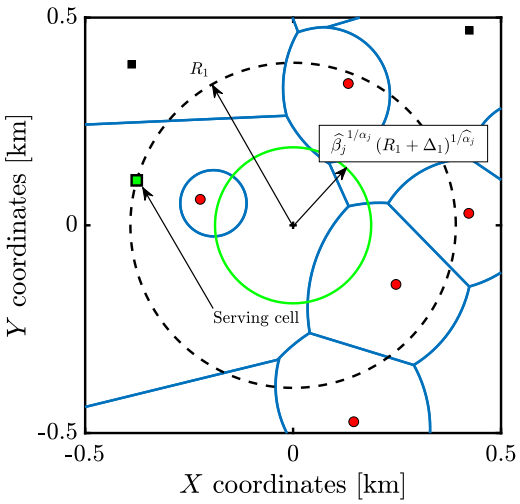

(b) The serving cell is the macrocell (green square) because the search circle (green circle) is empty.

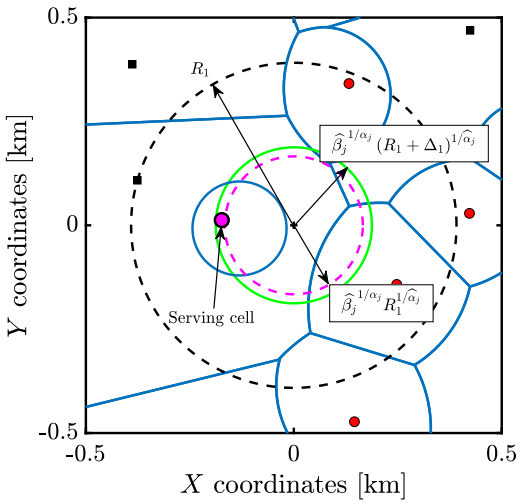

(c) The serving cell is the picocell (purple circle) because the search circle (green circle) is not empty.

Figure 5.1: Coverage regions (blue lines) in a two-tier cellular network. Both macrocells (black squares) and picocells (red circles) are independent HPPPs with $\{\lambda_1, \lambda_2\} = \left\{\frac{2}{\pi 500^2}, \frac{4}{\pi 500^2}\right\}$ m^{-2}, $\{\alpha_1, \alpha_2\} = \{3.76, 3.67\}$, $\{P_1, P_2\} = \{46, 30\}$ dBm, and $\{B_1, B_2\} = \{1, 1\}$.

5.2.1 Association Probability

We assume that cellular users firstly try to communicate with the BS that provides the strongest long-term averaged biased RSS $P_{\mathrm{r},k}$ defined as

$$P_{\mathrm{r},k} = P_k L_0 \left(R_k / r_0\right)^{-\alpha_k} B_k, \tag{5.1}$$

where L_0 is the path loss at the reference distance $r_0 = 1$ m, and R_k is the distance from the typical user to the nearest BS in the k^{th} tier. Once a user shares its geolocation, the strongest BS can decide whether to allow such connection petition or derive it to another tier, skipping the nearest BS. The decision is made by fetching data from the BS's REM and making sure that there is no BS from another tier within a radius Δ_k. This radius Δ_k is a tuning parameter that can be dynamically adjusted to associate users with different tiers according to their speed, to reduce the HO rate, and increase the average user throughput of the network.

Evidently, the accuracy of the stored RSS values affects our ability to choose the best connection. Denote $P^e_{\mathrm{r},k} = P_{\mathrm{r},k}\rho_k$ as the stored RSS values in the map, where ρ_k characterises the estimation error. The authors in [116] found that the estimation error approximately follows a log-normal distribution with zero mean and standard deviation σ_k. Therefore, the estimation error can be seen as shadowing on top of the stored RSS values in the REM. In [117, Lemma 1], it is shown that the shadowing transforms a HPPP $\Phi_k \subset \mathbb{R}^2$ with density λ_k into another HPPP $\Phi^e_k \subset \mathbb{R}^2$ with intensity $\lambda^e_k = \lambda_k \mathbb{E}\left[\rho_k^{2/\alpha_k}\right]$ as long as $\mathbb{E}\left[\rho_k^{2/\alpha_k}\right] < \infty$. This implies that REMs can be seen as equivalent to HPPPs $\Phi^e_k \subset \mathbb{R}^2$ with intensity

$$\lambda^e_k = \lambda_k \exp\left[\frac{1}{2}\left(\frac{\ln 10}{5}\frac{\sigma_k}{\alpha_k}\right)^2\right] = \lambda_k \rho_k. \tag{5.2}$$

We are now in a position to provide the per-tier association probability of our strategy $\mathcal{A}_k$ in the following lemma.

Lemma 1. *The probability that a typical user is associated with the nearest BS in the k^{th} tier with the REM cell-association strategy is:*

$$\mathcal{A}_k = 2\pi\lambda_k \int_0^\infty r_k \exp\left\{-\pi \sum_{j=1}^{2} \lambda_j \widehat{\beta}_j^{\,2/\alpha_j} \left(r_k + \delta_{jk}\right)^{2/\widehat{\alpha}_j}\right\} \mathrm{d}r_k, \tag{5.3}$$

where, for ease of notation, $\delta_{jk} = \Delta_k \mathbb{1}_{j\neq k}$, $\widehat{\beta}_j = \frac{P_j B_j}{P_k B_k}$, and $\widehat{\alpha}_j \triangleq \frac{\alpha_j}{\alpha_k}$.

Proof. We follow similar steps as in [80, Lemma 1], but adapt our association rule. The joint distribution of R_k and R_j is given as:

$$f_{R_k,R_j}(r_k, r_j) = (2\pi)^2 \lambda_k \lambda_j r_k r_j \exp\left(-\lambda_k \pi r_k^2\right) \exp\left(-\lambda_j \pi r_j^2\right). \tag{5.4}$$

In order to be associated with the k^{th} tier, the $P_{\text{r},k}$ of the typical user at $R_k + \Delta_{r_k}$ must be higher than $P_{\text{r},j}$ at R_j $\forall j \neq k$. This is equivalent to impose that there must not be any cell from the j^{th} tier in the circle of radius $\widehat{\beta}_j^{\,1/\alpha_j} (R_k + \Delta_k)^{1/\hat{\alpha}_j}$, where

$$\widehat{\beta}_j = \frac{P_j B_j}{P_k B_k},\ \widehat{\alpha}_j \triangleq \frac{\alpha_j}{\alpha_k}. \tag{5.5}$$

Then,

$$\begin{aligned}
\mathcal{A}_k &\triangleq \mathbb{E}_{R_k,R_j}\left[\mathbb{P}\left[R_j > \widehat{\beta}_j^{\,1/\alpha_j} (R_k + \Delta_k)^{1/\hat{\alpha}_j}\right]\right] \\
&= \int_0^\infty \int_{\widehat{\beta}_j^{1/\alpha_j}(r_k+\Delta_k)^{1/\hat{\alpha}_j}}^\infty (2\pi)^2 \lambda_k \lambda_j r_k r_j \exp\left(-\lambda_k \pi r_k^2\right) \exp\left(-\lambda_j \pi r_j^2\right) \mathrm{d}r_j \, \mathrm{d}r_k \\
&= 2\pi\lambda_k \int_0^\infty r_k \exp\left\{-\pi\lambda_j \widehat{\beta}_j^{2/\alpha_j} (r_k + \Delta_k)^{2/\hat{\alpha}_j} - \pi\lambda_k r_k^2\right\} \mathrm{d}r_k.
\end{aligned} \tag{5.6}$$

Defining δ_{jk}, we obtain the result in (5.3). ■

In the case $\{\alpha_j\} = \alpha$, the probability reduces to a closed-form expression as in the following corollary.

Corollary 1. *When $\{\alpha_j\} = \alpha$, the probability that a typical user is associated with the nearest BS in the k^{th} tier with the REM cell-association strategy is:*

$$\mathcal{A}_k|_{\{\alpha_j\}=\alpha} = \kappa \exp\left(-\pi\mu\Delta_k^2\right)\left[1 - \pi\nu\Delta_k \exp\left(\pi\nu^2\Delta_k^2\right) \operatorname{erfc}\left(\sqrt{\pi}\nu\Delta_k\right)\right], \tag{5.7}$$

where $\mu = \lambda_j \widehat{\beta}_j^{\,2/\alpha}$, $\nu = \frac{\mu}{\sqrt{\lambda_k + \mu}}$, and $\kappa = \frac{\lambda_k}{\lambda_k + \mu}$.

Proof. If $\{\alpha_j\} = \alpha$, then $\hat{\alpha}_j = 1$ $\forall j \in \{1, 2\}$. Thus,

$$\begin{aligned}
\mathcal{A}_k &= 2\pi\lambda_k \int_0^\infty r \exp\left\{-\pi \sum_{j=1}^{2} \lambda_j \widehat{\beta}_j^{\,2/\alpha} (r + \delta_{jk})^2\right\} \mathrm{d}r \\
&= K \int_n^\infty r \exp\left\{-ar^2 - br - c\right\} \mathrm{d}r.
\end{aligned} \tag{5.8}$$

Completing the square in the exponent, we obtain two integrals. Employing the change of variables $u = r + b/2a$ in the first integral and $t = \sqrt{a}(r + b/2a)$ in the second one gives

$$\mathcal{A}_k = \frac{K \exp\left(\frac{b^2}{4a} - c\right)}{4a^{3/2}} \left[2\sqrt{a} \exp\left[-\frac{(b+2an)^2}{4a} \right] - b\sqrt{\pi}\, \mathrm{erfc}\left(\frac{b+2an}{2\sqrt{a}} \right) \right]. \quad (5.9)$$

Further algebraic manipulation provides the result in (5.7). ■

Remark. *The radius Δ_k acts as a weighting function over the association probability given by (5.3) and (5.7). When $\Delta_k \to \infty$, $\mathcal{A}_k \to 0$ due to the probability of not having an interfering BS belonging to any other tiers in an infinite circle tends to zero, thus we would skip too many HOs penalizing coverage. On the contrary, when $\Delta_k \to 0$, it reduces to the association probability under generalised cell selection [117, Lemma 2], i.e. the REM contains errors ρ_k.*

We have yet to explain what happens when users skip the strongest BS. In that case, users camp on the strongest BS of the other tier, e.g. if a user skips the strongest BS in the macro tier, it will connect to the strongest BS in the pico tier, and vice versa. This will cause a reduction of the potential capacity. However, we avoid performing so many HOs and reduce the number of disconnections from the network. The per-tier association probability after skipping the j^{th} tier of our strategy $\mathcal{A}_k^s$ is given in the following lemma.

Lemma 2. *The probability that a typical user is associated with the nearest BS in the k^{th} tier after skipping the j^{th} tier with the REM cell-association strategy is:*

$$\mathcal{A}_k^s = 2\pi\lambda_k \int_0^\infty r_k \theta_j(r_k) \exp\left(-\pi\lambda_k r_k^2\right) \mathrm{d}r_k, \quad (5.10)$$

where $\theta_j(r_k)$ is defined as:

$$\theta_j(r_k) = \begin{cases} 1 - \exp\left\{ -\pi\lambda_j \widehat{\beta}_j^{\,2/\alpha_j} r_k^{2/\widehat{\alpha}_j} \right\} & \text{if } 0 \le r_k < \Delta_j^{\widehat{\alpha}_j} / \widehat{\beta}_j^{\,1/\alpha_k}, \\ \exp\left\{ -\pi\lambda_j \left(\widehat{\beta}_j^{\,1/\alpha_j} r_k^{1/\widehat{\alpha}_j} - \Delta_j \right)^2 \right\} - \exp\left\{ -\pi\lambda_j \widehat{\beta}_j^{\,2/\alpha_j} r_k^{2/\widehat{\alpha}_j} \right\} & \text{if } \Delta_j^{\widehat{\alpha}_j} / \widehat{\beta}_j^{\,1/\alpha_k} \le r_k \le \infty. \end{cases} \quad (5.11)$$

Proof. In the case there is at least one cell of the j^{th} tier in the circle of radius $\widehat{\beta}_j^{\,1/\alpha_j}\left(R_k\ +\Delta_k\right)^{1/\hat{\alpha}_j}$, the typical user connects to the j^{th} tier, i.e. $R_j \leq \widehat{\beta}_j^{\,1/\alpha_j}\left(R_k+\Delta_k\right)^{1/\hat{\alpha}_j}$. Rearranging this inequality, we obtain the lower bound for the distance to the k^{th} tier: $R_k \geq \widehat{\beta}_j^{\,-1/\alpha_k} R_j^{\hat{\alpha}_j} - \Delta_k$. The upper bound comes from the fact that R_k cannot be greater than $\widehat{\beta}_j^{\,-1/\alpha_k} R_j^{\hat{\alpha}_j}$, otherwise the user would have tried to connect to the j^{th} tier in the first place instead of skipping the default association. Swapping the indices j and k and integrating (5.4) yields

$$\begin{aligned}\mathcal{A}_k^s &\triangleq \mathbb{E}_{R_k,R_j}\left[\mathbb{P}\left[R_j \leq \widehat{\beta}_j^{\,1/\alpha_j}\left(R_k+\Delta_k\right)^{1/\hat{\alpha}_j}\right]\right] \\ &= 2\pi\lambda_k \int_0^{\infty} r_k \exp\left(-\pi\lambda_k r_k^2\right)\,\mathrm{d}r_k\ \times 2\pi\lambda_j \int_{\widehat{\beta}_j^{1/\alpha_j} r_k^{1/\hat{\alpha}_j}-\Delta_j}^{\widehat{\beta}_j^{1/\alpha_j} r_k^{1/\hat{\alpha}_j}} r_j \exp\left(-\pi\lambda_j r_j^2\right)\,\mathrm{d}r_j.\end{aligned} \tag{5.12}$$

Note that the lower limit of the integral in r_j is negative when $\widehat{\beta}_j^{1/\alpha_j} r_k^{1/\widehat{\alpha}_j} < \Delta_j$. That is why we define the piecewise auxiliary function $\theta_j(r_k)$ in (5.11) and the result in (5.10) follows. ■

When $\{\alpha_j\} = \alpha$, the probability is simplified to:

Corollary 2. *When $\{\alpha_j\} = \alpha$, the probability that a typical user is associated with the nearest BS in the k^{th} tier after skipping the j^{th} tier with the REM cell-association strategy is:*

$$\begin{aligned}\mathcal{A}_k^s|_{\{\alpha_j\}=\alpha} = 1 - \exp\left(-\pi\xi\Delta_j^2\right) - \kappa + \kappa\exp\left(-\pi\xi\Delta_j^2\right) \times \\ \left[1 - \pi\zeta\Delta_j \exp\left(\pi\kappa\xi\Delta_j^2\right)\operatorname{erfc}\left(\sqrt{\pi\kappa\xi}\Delta_j\right)\right],\end{aligned} \tag{5.13}$$

where $\xi = \lambda_k \widehat{\beta}_j^{\,-2/\alpha}$, $\zeta = \frac{\lambda_j}{\sqrt{\lambda_j+\xi}}$, $\mu = \lambda_j \widehat{\beta}_j^{\,2/\alpha}$ and $\kappa = \frac{\lambda_k}{\lambda_k+\mu}$.

Proof. If $\{\alpha_j\} = \alpha$, $\hat{\alpha}_j = 1\ \forall j \in \{1,2\}$, we have to divide the integral based on the definition of $\theta_j(r_k)$. When $0 \leq r_k < \Delta_j^{\widehat{\alpha}_j}/\widehat{\beta}_j^{\,1/\alpha_k}$, there are two immediate exponential integrals. Then, when $\Delta_j^{\widehat{\alpha}_j}/\widehat{\beta}_j^{\,1/\alpha_k} \leq r_k \leq \infty$, we have to solve an immediate integral and another one of the same type as in (5.9), with $a = \pi\left(\lambda_k + \lambda_j\widehat{\beta}_j^{\,2/\alpha}\right)$, $b = -2\pi\lambda_j\widehat{\beta}_j^{\,1/\alpha}\Delta_j$, $c = \pi\lambda_j\Delta_j^2$, and $n = \Delta_j\widehat{\beta}_j^{\,-1/\alpha}$. Adding everything up completes the proof. ■

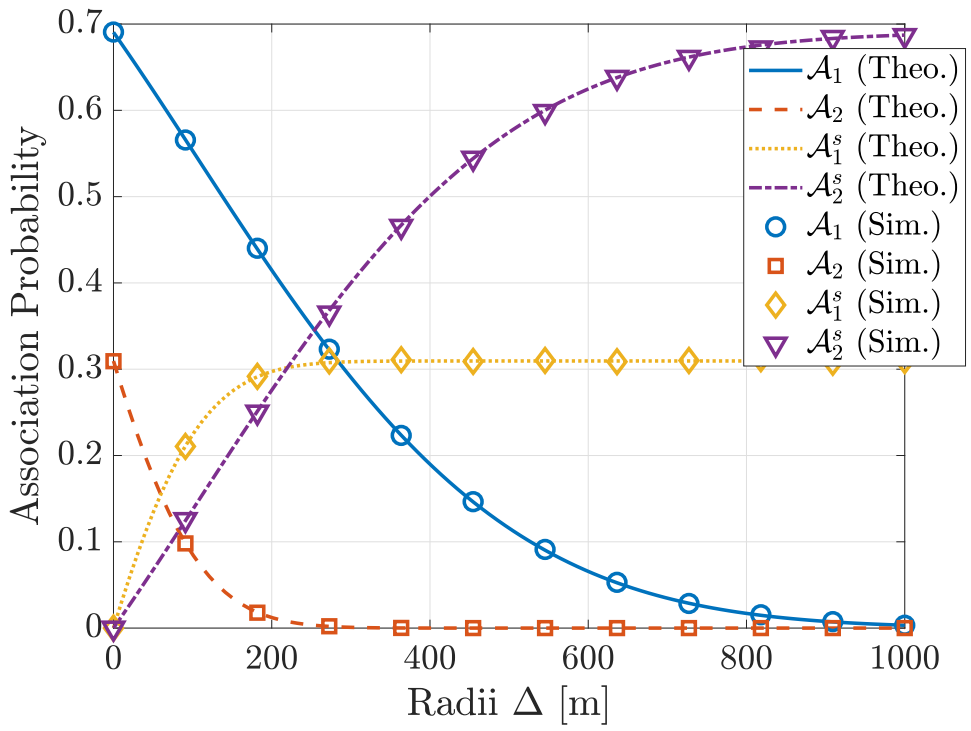

Figure 5.2: Association probability for different radii $\Delta = \Delta_1 = \Delta_2$ in a two-tier cellular network with $\{\lambda_1, \lambda_2\} = \left\{\frac{2}{\pi 500^2}, \frac{4}{\pi 500^2}\right\}$ m^{-2}, $\{\alpha_1, \alpha_2\} = \{3.76, 3.67\}$, $\{P_1, P_2\} = \{46, 30\}$ dBm, and $\{B_1, B_2\} = \{1, 1\}$.

Remark. *Similarly to the radius Δ_k, the radius Δ_j acts as a weighting function over the association probability given by (5.10) and (5.13). When $\Delta_j \to \infty$, $\mathcal{A}_k^s \to 1 - \kappa$, meaning, if we skip all the HOs in the j^{th} tier, users will connect to the k^{th} tier every time even when it is not the strongest one. On the contrary, when $\Delta_j \to 0$, users do not skip any HO to the j^{th} tier so that the skipping association probability tends to be zero.*

In Fig. 5.2, although, in general, $\Delta_1 \neq \Delta_2$, we show the association probability as a function of the search radii $\Delta = \Delta_1 = \Delta_2$ as an example. The Monte Carlo simulations present a high degree of agreement with the expressions derived in this subsection. Also, we can observe the trade-off between the association probability to one tier and the association probability after skipping. For instance, the sum of the probabilities $\mathcal{A}_1$ and $\mathcal{A}_2^s$ is always the same value, i.e. $\mathcal{A}_1$ when $\Delta = 0$ m. Note that our proposed technique can dynamically associate users to each tier through Δ.

5.2.2 Distance Distributions

The typical user can be associated to the k^{th} tier via two ways: the strongest tier or the skipped tier. Denote X_k as the distance between the typical user and its serving cell when the k^{th} tier is the strongest, and X_k^s likewise when the j^{th} tier has been skipped. Either way, the distance to the serving cell is a random variable whose probability density function (PDF) is given in Lemma 3.

Lemma 3. *The PDF of the distance X_k between a typical user and its serving cell when the k^{th} tier is the strongest (see Fig. 5.3) is:*

$$f_{X_k}(x) = \frac{2\pi\lambda_k}{\mathcal{A}_k} x \exp\left\{-\pi \sum_{j=1}^{2} \lambda_j \widehat{\beta}_j^{\,2/\alpha_j} \left(x + \delta_{jk}\right)^{2/\widehat{\alpha}_j}\right\}, \tag{5.14}$$

while the PDF of the distance X_k^s between a typical user and its serving cell when the j^{th} tier has been skipped (see Fig. 5.3) is:

$$f_{X_k^s}(x) = \frac{2\pi\lambda_k}{\mathcal{A}_k^s} x \exp\left(-\pi\lambda_k x^2\right) \theta_j(x). \tag{5.15}$$

Proof. The PDF of $f_{X_k}(x)$ is obtained by differentiating the cumulative distribution function (CDF) as

$$f_{X_k}(x) = \frac{\mathrm{d}F_{X_k}(x)}{\mathrm{d}x} = \frac{\mathrm{d}\left(1 - \mathbb{P}\left[X_k > x\right]\right)}{\mathrm{d}x} = -\frac{\mathrm{d}\mathbb{P}\left[X_k > x\right]}{\mathrm{d}x} \tag{5.16}$$

where $\mathbb{P}\left[X_k > x\right]$ is the void probability of a PPP weighted by the association probability $\mathcal{A}_k$. A similar approach applies to $f_{X_k^s}(x)$, exchanging $\mathcal{A}_k$ for $\mathcal{A}_k^s$. ■

Given a typical user associated to the k^{th} tier by the strongest cell criterion, the interference at distance $X_k = x$ from the k^{th} tier is the sum of all interfering BSs that are outside a disc of radius x. Also, the aggregate interference from the j^{th} tier is the sum of all BSs outside a disc of radius $\widehat{\beta}_j^{\,1/\alpha_j} \left(x + \Delta_k\right)^{1/\widehat{\alpha}_j}$. When the j^{th} tier has been skipped, the interference at distance $X_k^s = x$ from both tiers remains the same. However, the aggregate interference from the j^{th} tier is the sum of all BSs outside a disc of radius $\widehat{\beta}_j^{\,1/\alpha_j} x^{1/\widehat{\alpha}_j}$ plus the one from the skipped BS, which is inside an annulus with inner and outer radii $\widehat{\beta}_j^{\,1/\alpha_j} x^{1/\widehat{\alpha}_j} - \Delta_j$ and $\widehat{\beta}_j^{\,1/\alpha_j} x^{1/\widehat{\alpha}_j}$, respectively. Denote Y_j^s as the distance between the typical user and the skipped cell in the j^{th} tier, its conditional PDF is given in the following lemma.

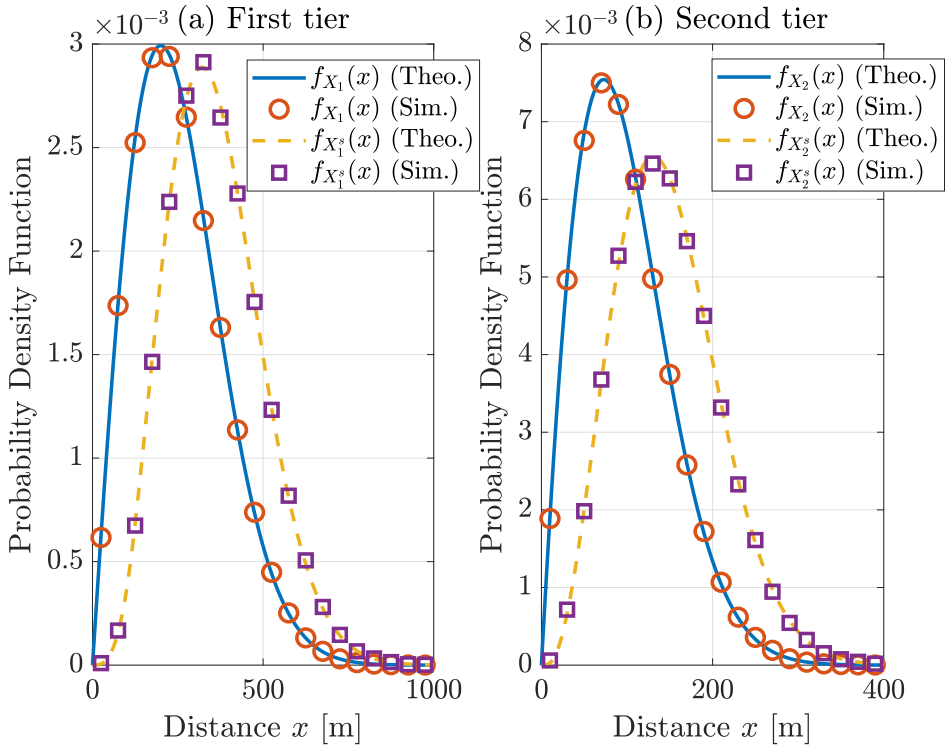

Figure 5.3: Serving cell distance distributions in a two-tier cellular network: (a) Serving cell in the first tier and, (b) Serving cell in the second tier.

Lemma 4. *The conditional PDF of the distance Y_k^s between the typical user and the skipped BS in the j^{th} tier, conditioned on the distance to the serving BS in the k^{th} tier (see Fig. 5.4) can be expressed as*

$$f_{Y_j^s}(y|X_k^s = x) = \frac{2\pi\lambda_j y \exp\left(-\pi\lambda_j y^2\right)}{\theta_j(x)}, \tag{5.17}$$

where $\widehat{\beta}_j^{\,1/\alpha_j} x^{1/\widehat{\alpha}_j} - \Delta_j \leq y \leq \widehat{\beta}_j^{\,1/\alpha_j} x^{1/\widehat{\alpha}_j} \leq \infty$.

Proof. The conditional PDF of the distance Y_k^s is obtained by first writing the joint distribution of the two independent HPPPs Φ_k, $k = \{1, 2\}$ given in (5.4), and then dividing it by the marginal PDF of the serving BS in the k^{th} tier. ■

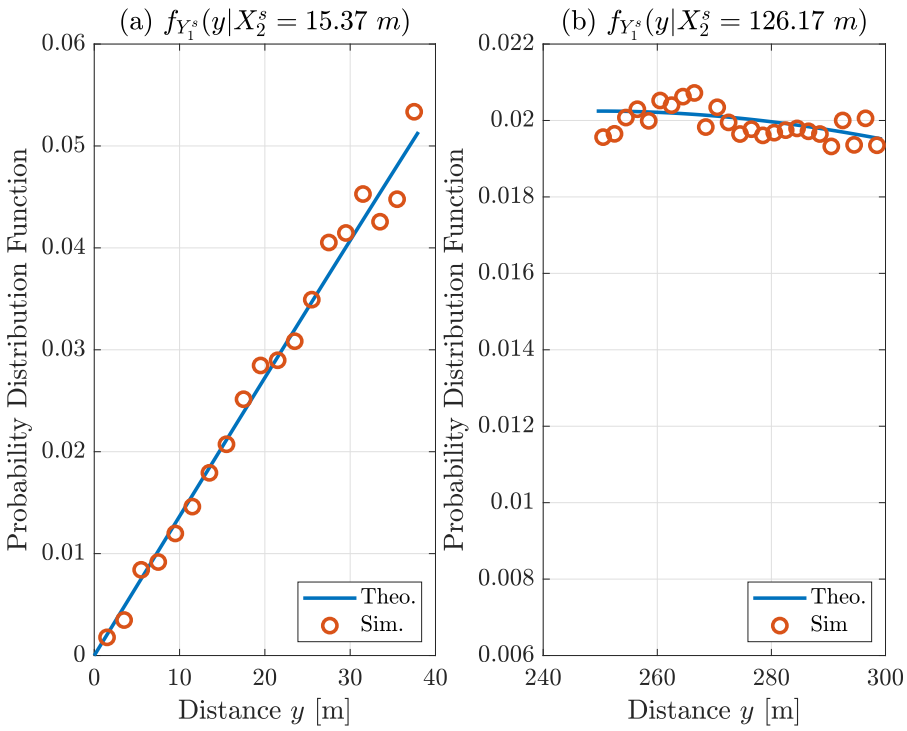

Figure 5.4: Skipped cell distance distribution in a two-tier cellular network: (a) when $\widehat{\beta}_j^{1/\alpha_j} x^{1/\widehat{\alpha}_j} - \Delta_j \leq 0$, and (b) $\widehat{\beta}_j^{1/\alpha_j} x^{1/\widehat{\alpha}_j} - \Delta_j > 0$.

5.3 Coverage Probability and Spectral Efficiency

5.3.1 Coverage Probability

The coverage probability $\mathcal{C}$ is defined as the probability that the SINR exceeds a given threshold τ. In the REM cell-association strategy, the typical user at the distance x connects to the BS in the k^{th} tier only if such BS will be the strongest within a circle of radius proportional to $x + \Delta_k$. If there is at least one cell belonging to the j^{th} tier, the user will connect to the strongest BS in the j^{th}. Then, from the law of total probability, the coverage probability under the REM cell selection scheme is:

$$\mathcal{C} = \sum_{k=1}^{2} \mathcal{A}_k^e \mathcal{C}_k + \mathcal{A}_k^s \mathcal{C}_k^s, \tag{5.18}$$

where $\mathcal{A}_k$ and $\mathcal{A}_k^s$ are the per-tier association probabilities derived in Lemma 1 and Lemma 2, and $\mathcal{C}_k$ and $\mathcal{C}_k^s$ are the coverage probabilities of a typical user associated with the k^{th} tier directly and after skipping, respectively. For a given threshold

τ and a typical user at the distance x from its serving cell without skipping, the coverage probability is:

$$\mathcal{C}_k \triangleq \mathbb{E}_x \left[\mathbb{P} \left[\mathrm{SINR}_k(x) > \tau \right] \right]. \tag{5.19}$$

In other words, the per-tier coverage probability is the expected value of the SINR when averaged across the network with $f_{X_k}(x)$ in (5.14). The SINR of a typical user at the distance x in this case is equal to

$$\mathrm{SINR}_k(x) = \frac{P_k h_{k0} x^{-\alpha_k}}{I_k + I_j + \frac{\sigma^2}{L_0}} \tag{5.20}$$

where $h_{k0} \sim \exp(1)$ is the fading coefficient from the serving cell b_{k0}, $I_k = \sum_{i \in \Phi_k \setminus b_{k0}} P_k h_{ki} r_{ki}^{-\alpha_k}$ is the interference power from the k^{th} tier excluding the serving cell b_{k0}, $I_j = \sum_{i \in \Phi_j} P_j h_{ji} r_{ji}^{-\alpha_j}$ is the interference from the j^{th} tier, and $h_{ki}, h_{ji} \overset{\text{i.i.d.}}{\sim} \exp(1)$ is the fading coefficient from the i^{th} interfering BS in the $\{k, j\}^{\text{th}}$ tier, respectively.

Analogously, for a given threshold τ and a typical user at the distance x from its serving cell after skipping, the coverage probability is:

$$\mathcal{C}_k^s \triangleq \mathbb{E}_{x,y} \left[\mathbb{P} \left[\mathrm{SINR}_k^s(x, y) > \tau \right] \right], \tag{5.21}$$

where the coverage probability does not only depend on the distance to the serving BS x through $f_{X_k^s}(x)$ defined in (5.15) but also on the distance to the skipped BS y in the other tier via $f_{Y_j^s}(y | X_k^s = x)$ as in (5.17). The SINR of a typical user at the distance x from its serving BS and at the distance y from the skipped BS follows

$$\mathrm{SINR}_k^s(x, y) = \frac{P_k h_{k0} x^{-\alpha_k}}{I_k^s + I_j^s + I_s(y) + \frac{\sigma^2}{L_0}}, \tag{5.22}$$

where $I_k^s = I_k = \sum_{i \in \Phi_k \setminus b_{k0}} P_k h_{ki} r_{ki}^{-\alpha_k}$ is the interference power from the k^{th} tier excluding the serving cell b_{k0}, $I_j^s = \sum_{i \in \Phi_j \setminus b_{j0}} P_j h_{ji} r_{ji}^{-\alpha_j}$ is the interference from the j^{th} tier excluding the skipped BS b_{j0}, and $I_s(y) = P_j h_{j0} y^{-\alpha_j}$ is precisely the interference caused by such BS.

We present our most general result hereafter for the per-tier coverage probability when associated directly or after skipping the other tier.

Theorem 1. *The coverage probability of a typical user associated to the k^{th} tier directly or after skipping the j^{th} tier with the REM cell-association strategy is given by (5.23) and (5.24):*

$$\mathcal{C}_k = \frac{2\pi\lambda_k}{\mathcal{A}_k} \int_0^\infty x \exp\Bigg\{ -\frac{\tau}{\mathrm{SNR}} - \pi \sum_{j=1}^{2} \lambda_j \Big(\widehat{\beta}_j^{\,2/\alpha_j} \left(x + \delta_{jk}\right)^{2/\widehat{\alpha}_j} + \widehat{P}_j^{2/\alpha_j} x^{2/\widehat{\alpha}_j} \Upsilon\left[\tau, \alpha_j, \widehat{B}_j, \chi_k(x)\right] \Big) \Bigg\} \mathrm{d}x, \tag{5.23}$$

$$\mathcal{C}_k^s = \frac{4\pi^2\lambda_k\lambda_j}{\mathcal{A}_k^s} \int_0^\infty x \exp\left\{ -\frac{\tau}{\mathrm{SNR}} - \pi \left(\lambda_k x^2 + \sum_{j=1}^{2} \lambda_j \widehat{P}_j^{2/\alpha_j} x^{2/\widehat{\alpha}_j} \Upsilon\left[\tau, \alpha_j, \widehat{B}_j, 1\right] \right) \right\} \times \int_{\widehat{\beta}_j^{1/\alpha_j} r_k^{1/\widehat{\alpha}_j} - \Delta_j}^{\widehat{\beta}_j^{1/\alpha_j} r_k^{1/\widehat{\alpha}_j}} \frac{y \exp\left(-\pi\lambda_j y^2\right)}{1 + \tau \widehat{P}_j x^{\alpha_k} y^{-\alpha_j}} \mathrm{d}y \, \mathrm{d}x. \tag{5.24}$$

Proof. The CCDF of the SINR of the typical user served directly by the closest BS in the k^{th} tier is given as

$$\begin{aligned} \mathbb{P}\left[\mathrm{SINR}_k(x) > \tau\right] &= \mathbb{P}\left[h_{k0} > \tau P_k^{-1} x^{\alpha_k} \left(I_k + I_j + \frac{\sigma^2}{L_0} \right) \right] \\ &\overset{(a)}{=} \mathbb{E}_{I_k, I_j} \left[\exp\left\{ -\tau P_k^{-1} x^{\alpha_k} \left(I_k + I_j + \frac{\sigma^2}{L_0} \right) \right\} \right] \\ &\overset{(b)}{=} \exp\left(-\frac{\tau}{\mathrm{SNR}} \right) \mathcal{L}_{I_k}(\tau P_k^{-1} x^{\alpha_k}) \mathcal{L}_{I_j}(\tau P_k^{-1} x^{\alpha_k}), \end{aligned} \tag{5.25}$$

where (a) is due to the distribution of h_{k0} being exponential, and (b) is because the interferences are independent. Moreover, we define $\mathrm{SNR} = \frac{P_k L_0 x^{-\alpha_k}}{\sigma^2}$, and $\mathcal{L}_X(s)$ denotes the Laplace transform (LT) of the random variable X evaluated at s. Their

expressions are given by

$$\begin{aligned}\mathcal{L}_{I_j}(s) &= \mathbb{E}_{I_j}\left[\exp\left(-sI_j\right)\right] \\ &\overset{(a)}{=} \mathbb{E}_{\Phi_j,\{h_{ji}\}}\left[\exp\left(-s\sum_{i\in\Phi_j\setminus b_{k0}} P_j h_{ji} r_{ji}^{-\alpha_j}\right)\right] \\ &= \mathbb{E}_{\Phi_j}\left[\prod_{i\in\Phi_j\setminus b_{k0}} \mathbb{E}_{h_j}\left[\exp\left(-sP_j h_j r_{ji}^{-\alpha_j}\right)\right]\right] \\ &= \mathbb{E}_{\Phi_j}\left[\prod_{i\in\Phi_j\setminus b_{k0}} \frac{1}{1+sP_j r_{ji}^{-\alpha_j}}\right] \\ &\overset{(b)}{=} \exp\left\{-2\pi\lambda_j \int_{l_j}^{\infty} \frac{v}{1+(sP_j)^{-1}v^{\alpha_j}}\,\mathrm{d}v\right\},\end{aligned} \tag{5.26}$$

where (a) comes from the i.i.d. character of h_{ji}, the last step (b) follows the probability generation functional (PGFL), and $l_j = \widehat{\beta}_j^{\,1/\alpha_j}\left(x+\delta_{jk}\right)^{1/\widehat{\alpha}_j}$ with $\delta_{jk} = \Delta_k \mathbb{1}_{j\neq k}$. Evaluating the function at $s = \tau P_k^{-1} x^{\alpha_k}$ and employing a change of variables $u = (\tau \widehat{P}_j x^{\alpha_k})^{-2/\alpha_j} v^2$ results in

$$\mathcal{L}_{I_j}(\tau P_k^{-1} x^{\alpha_k}) = \exp\left\{-\pi\lambda_j \widehat{P}_j^{2/\alpha_j} x^{2/\widehat{\alpha}_j} \Upsilon\left[\tau, \alpha_j, \widehat{B}_j, \chi_k(x)\right]\right\}, \tag{5.27}$$

where $\widehat{P}_j \triangleq \frac{P_j}{P_k}$, $\widehat{B}_j \triangleq \frac{B_j}{B_k}$, $\chi_k(x) = \left(\frac{x+\delta_{jk}}{x}\right)^{\alpha_k}$ and

$$\begin{aligned}\Upsilon\left[\tau, \alpha_j, \widehat{B}_j, \chi_k(x)\right] &= \tau^{2/\alpha_j} \int_{\left(\widehat{B}_j\chi_k(x)/\tau\right)^{2/\alpha_j}}^{\infty} \frac{1}{1+u^{\alpha_j/2}}\,\mathrm{d}u \\ &= \frac{2\tau\left[\widehat{B}_j\chi_k(x)\right]^{2/\alpha_j-1}}{\alpha_j-2} {}_2F_1\left[1, 1-\frac{2}{\alpha_j}, 2-\frac{2}{\alpha_j}, \frac{-\tau}{\widehat{B}_j\chi_k(x)}\right].\end{aligned} \tag{5.28}$$

The function ${}_2F_1(a,b,c,d)$ denotes the Gauss' hypergeometric function. Substituting (5.27) into (5.25), and unconditioning on (5.14) gives the result in (5.23).

Similarly, the CCDF of the SINR of the typical user served after skipping the j^{th} tier is given as

$$\mathbb{P}\left[\mathrm{SINR}_k^s(x) > \tau\right] = \exp\left(-\frac{\tau}{\mathrm{SNR}}\right) \mathcal{L}_{I_k^s}(\tau P_k^{-1} x^{\alpha_k}) \mathcal{L}_{I_j^s}(\tau P_k^{-1} x^{\alpha_k}) \mathcal{L}_{I_s(y)}(\tau P_k^{-1} x^{\alpha_k}), \tag{5.29}$$

where $\mathrm{SNR} = \frac{P_k L_0 x^{-\alpha_k}}{\sigma^2}$. Here, we can observe an extra term $\mathcal{L}_{I_s(y)}(\tau P_k^{-1} x^{\alpha_k})$ compared to when the user does not skip the cell association. Developing the LTs yields

$$\mathcal{L}_{I_j^s}(s) = \exp\left\{-2\pi\lambda_j \int_{l_j}^{\infty} \frac{v}{1+(sP_j)^{-1}v^{\alpha_j}}\,\mathrm{d}v\right\}, \tag{5.30}$$

where $l_j = \widehat{\beta}_j^{\,1/\alpha_j} x^{1/\widehat{\alpha}_j}$. In this case, the main interferer is closer, i.e. we do not have the δ_{jk} term. Similarly, employing the change of variables $u = (\tau \widehat{P}_j x^{\alpha_k})^{-2/\alpha_j} v^2$, the LTs turn into

$$\mathcal{L}_{I_j^s}(\tau P_k^{-1} x^{\alpha_k}) = \exp\left\{-\pi\lambda_j \widehat{P}_j^{2/\alpha_j} x^{2/\widehat{\alpha}_j} \Upsilon\left[\tau, \alpha_j, \widehat{B}_j, 1\right]\right\}. \tag{5.31}$$

For the skipped cell, unconditioning on the expression obtained in Lemma 4, we finally express the interference as

$$\mathcal{L}_{I_s(y)}(\tau P_k^{-1} x^{\alpha_k}) = \int_{\widehat{\beta}_j^{1/\alpha_j} r_k^{1/\widehat{\alpha}_j} - \Delta_j}^{\widehat{\beta}_j^{1/\alpha_j} r_k^{1/\widehat{\alpha}_j}} \frac{f_{Y_j^s}(y|x)}{1+\tau\widehat{P}_j x^{\alpha_k} y^{-\alpha_j}}\,\mathrm{d}y. \tag{5.32}$$

Combining (5.29) with (5.31) and (5.32) completes the proof of Theorem 1. ■

Given Theorem 1, it is difficult to find a closed-form expression for the coverage probability regardless of the skipping. The REM cell-association strategy associates users with the strongest cell in an extended radius $\propto x + \delta_{jk}$, and also imposes a restriction on the interferers. For example, in (5.23) the term $\chi_k(x)$ is a distance-dependent bias, reducing the amount of interference coming from other tiers since they are at least δ_{jk} from the serving cell. For small distances, δ_{jk} has a more prominent role that fades as the distance x increases as it can be observed in (5.27) and (5.28). Conversely, when a user is associated with the BS that gives you less RSS, the main interferer is within $\widehat{\beta}_j^{\,1/\alpha_j} x^{1/\widehat{\alpha}_j} - \Delta_j \leq y \leq \widehat{\beta}_j^{\,1/\alpha_j} x^{1/\widehat{\alpha}_j} \leq \infty$. Therefore, it ensures a lower interference than other methods that skip HOs without spatial awareness.

For the special case when $\{\alpha_j\} = \alpha = 4$, the LTs admit a simple expression that can be plugged into (5.23) and (5.24) given in the following corollary. These expressions will be use in Section 5.5 to compare our strategy with other approaches.

Corollary 3. *When $\{\alpha_j\} = \alpha = 4$, the LTs of the interference are*

$$\mathcal{L}_{I_j}(\tau P_k^{-1} x^4)\big|_{\alpha=4} = \exp\left\{-\pi\lambda_j \sqrt{\widehat{P}_j \tau} x^2 \arctan\left[\sqrt{\frac{\tau}{\widehat{B}_j \chi_k(x)}}\right]\right\}, \tag{5.33}$$

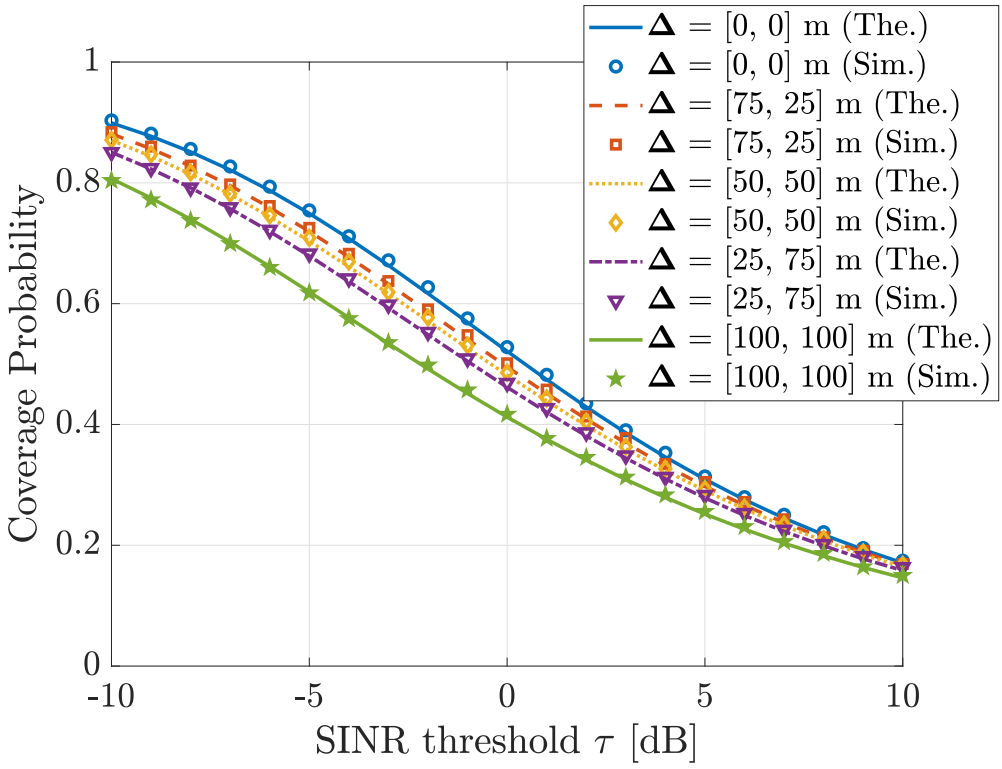

Figure 5.5: Coverage probability with respect to SINR threshold τ for different combinations of $\boldsymbol{\Delta} = \{\Delta_1, \Delta_2\}$ with $\{\lambda_1, \lambda_2\} = \left\{\frac{2}{\pi 500^2}, \frac{4}{\pi 500^2}\right\}$ m^{-2}, $\{\alpha_1, \alpha_2\} = \{3.76, 3.67\}$, $\{P_1, P_2\} = \{46, 30\}$ dBm, and $\{B_1, B_2\} = \{1, 1\}$.

where $\chi_k(x)|_{\alpha=4} = \left(\frac{x+\delta_{jk}}{x}\right)^4$, *and*

$$\mathcal{L}_{I_j^s}(\tau P_k^{-1} x^4)\Big|_{\alpha=4} = \exp\left\{-\pi\lambda_j \sqrt{\widehat{P}_j \tau} x^2 \arctan\left(\sqrt{\frac{\tau}{\widehat{B}_j}}\right)\right\}. \tag{5.34}$$

In Fig. 5.5, we compare the analytical results given from (5.18) with simulated results obtained through Monte Carlo simulations for different search radii Δ. We can see that they are remarkably close over the whole range of SINR thresholds considered, thus validating our analytical work.

5.3.2 Spectral Efficiency

In this subsection, we derive the average spectral efficiency as a function of the coverage probability. The average spectral efficiency of a typical user is given by the

law of total probability as

$$\mathcal{R} = \sum_{k=1}^{2} \mathcal{A}_k^e \mathcal{R}_k + \mathcal{A}_k^s \mathcal{R}_k^s, \tag{5.35}$$

where $\mathcal{A}_k$ and $\mathcal{A}_k^s$ are the same as in (5.18). The expression of the spectral efficiency per tier $\mathcal{R}_k$ and $\mathcal{R}_k^s$ can be found in the following theorem.

Theorem 2. *The average ergodic rate of a typical user associated to the k^{th} tier directly and after skipping the j^{th} tier in with the REM cell-association strategy is given by (5.36) and (5.37):*

$$\mathcal{R}_k = \frac{2\pi\lambda_k}{\mathcal{A}_k} \iint\limits_{\mathbb{R}_{\geq 0}} x \exp\Bigg\{ -\frac{2^t-1}{\mathrm{SNR}} - \pi \sum_{j=1}^{2} \lambda_j \Big(\widehat{\beta}_j^{\,2/\alpha_j} (x+\delta_{jk})^{2/\widehat{\alpha}_j} + \widehat{P}_j^{2/\alpha_j} x^{2/\widehat{\alpha}_j} \times \Upsilon\left[2^t-1, \alpha_j, \widehat{B}_j, \chi_k(x)\right] \Big) \Bigg\} \mathrm{d}x\, \mathrm{d}t, \tag{5.36}$$

$$\mathcal{R}_k^s = \frac{4\pi^2\lambda_k\lambda_j}{\mathcal{A}_k^s} \iint\limits_{\mathbb{R}_{\geq 0}} x \exp\Bigg\{ -\frac{2^t-1}{\mathrm{SNR}} - \pi \Bigg(\lambda_k x^2 + \sum_{j=1}^{2} \lambda_j \widehat{P}_j^{2/\alpha_j} x^{2/\widehat{\alpha}_j} \times \Upsilon\left[2^t-1, \alpha_j, \widehat{B}_j, 1\right] \Bigg) \Bigg\} \int\limits_{\widehat{\beta}_j^{1/\alpha_j} r_k^{1/\widehat{\alpha}_j} - \Delta_j}^{\widehat{\beta}_j^{1/\alpha_j} r_k^{1/\widehat{\alpha}_j}} \frac{y \exp\left(-\pi\lambda_j y^2\right)}{1+(2^t-1)\widehat{P}_j x^{\alpha_k} y^{-\alpha_j}} \mathrm{d}y\, \mathrm{d}x\, \mathrm{d}t. \tag{5.37}$$

Proof. The spectral efficiency is obtained averaging over twice: the first time over the fixed distance x from its serving cell, and the second over the distribution of x itself.

$$\begin{aligned}
\mathcal{R}_k &\triangleq \mathbb{E}_x \left[\mathbb{E}_{\mathrm{SINR}_k} \left[\log_2(1+\mathrm{SINR}_k(x)) \right] \right] \\
&= \int_0^\infty \mathbb{E}_{\mathrm{SINR}_k} \left[\log_2(1+\mathrm{SINR}_k(x)) \right] f_{X_k}(x)\, \mathrm{d}x \\
&\overset{(a)}{=} \int_0^\infty \int_0^\infty \mathbb{P}\left[\log_2(1+\mathrm{SINR}_k(x)) > t \right] f_{X_k}(x)\, \mathrm{d}t\, \mathrm{d}x \\
&\overset{(b)}{=} \int_0^\infty \int_0^\infty \mathbb{P}\left[\mathrm{SINR}_k(x) > 2^t - 1 \right] f_{X_k}(x)\, \mathrm{d}t\, \mathrm{d}x,
\end{aligned} \tag{5.38}$$

where (a) follows from $\mathbb{E}[X] = \int_0^\infty \mathbb{P}[X > x]\,\mathrm{d}x$ for $X > 0$, and (b) follows from rearranging the terms. The PDF $f_{X_k}(x)$ is given in Lemma 3 and $\mathbb{P}\left[\mathrm{SINR}_k(x) > 2^t - 1\right]$ can be obtained by plugging $\tau = 2^t - 1$ in Theorem 1. Putting everything together yields the expression presented in (5.36). The same applies to (5.37). ■

5.4 User Throughput and Backhaul Traffic

In this section, we present the performance metrics that will be discussed in Section 5.5.

5.4.1 User Throughput

The first metric is the average user throughput given by

$$\mathcal{T} = (1 - \mathcal{D})\mathcal{W}\mathcal{R}, \tag{5.39}$$

where $\mathcal{W}$ is the system bandwidth, $\mathcal{R}$ is the average ergodic rate derived in (5.35), and $\mathcal{D}$ is the handover cost defined as the normalised average time disconnected from the network [86]. The HO cost $\mathcal{D}$ for 2 tiers is described as

$$\mathcal{D} = \sum_{k=1}^{2}\sum_{j=1}^{2} H_{kj} d_{\max\{k,j\}}, \tag{5.40}$$

where H_{kj} represents the HO rate between tiers k and j, and $d_{\max\{k,j\}}$ denotes the delay associated with the type of HO. We assume that $d_1 < d_2$. For instance, the delay incurred by a macro-macro HO (co-tier HO) d_1 is shorter than a macro-pico HO (cross-tier) d_2 since the backhaul connection of macrocells is usually fibre optic, whereas picocells are not. The HO rate equals the number of intersections between the user trajectory and the cell boundaries of the Voronoi diagram. In [49], the HO rate for an arbitrary movement trajectory with speed v is expressed as

$$H_{kj} = \begin{cases} \frac{1}{\pi}\mu_1\left(\mathbf{T}_{kj}^{(1)}\right) v & \text{if } k \neq j, \\ \frac{2}{\pi}\mu_1\left(\mathbf{T}_{kj}^{(1)}\right) v & \text{if } k = j, \end{cases} \tag{5.41}$$

where $\mu_1\left(\mathbf{T}_{kj}^{(1)}\right)$ denotes the length intensity of a stationary and isotropic fibre process, whose expression is given by

$$\mu_1\left(\mathbf{T}_{kj}^{(1)}\right) = \begin{cases} \frac{\lambda_k \lambda_j \mathcal{F}(\beta_{kj})}{2\left(\sum_{i=1}^{K} \lambda_i \beta_{ik}^2\right)^{3/2}} + \frac{\lambda_j \lambda_k \mathcal{F}(\beta_{jk})}{2\left(\sum_{i=1}^{K} \lambda_i \beta_{ij}^2\right)^{3/2}} & \text{if } k \neq j, \\ \frac{\lambda_k^2 \mathcal{F}(1)}{2\left(\sum_{i=1}^{K} \lambda_i \beta_{ik}^2\right)^{3/2}} & \text{if } k = j, \end{cases} \tag{5.42}$$

where $\beta_{kj} = \left(\frac{P_k B_k}{P_j B_j}\right)^{1/\alpha}$, $\beta_{kj} = \frac{1}{\beta_{jk}}$, and

$$\mathcal{F}(\beta) \triangleq \frac{1}{\beta^2} \int_0^{\pi} \sqrt{(\beta^2 + 1) - 2\beta \cos(\theta)}\, \mathrm{d}\theta. \tag{5.43}$$

In the proposed REM cell-association strategy, users skip HO in both tiers with probabilities $\mathcal{A}_k^s$, $k = \{1, 2\}$. Thus we do not perform the totality of the HOs but a proportion of them as follows

$$\mathcal{D} = \frac{\mathcal{A}_1}{\mathcal{A}_1 + \mathcal{A}_2^s} H_{11} + \frac{\mathcal{A}_2}{\mathcal{A}_2 + \mathcal{A}_1^s} \left(H_{12} + H_{22} + H_{21}\right). \tag{5.44}$$

5.4.2 Backhaul Traffic

The second metric quantifies both upstream and downstream backhaul traffic in a Long-Term Evolution (LTE) network. LTE has two logical interfaces: S1 and X2 [118]. The S1 interface is a star network that links the advanced gateway with each cell and carries the average throughput of all user data $\mathcal{T}$ presented in (5.39), whereas the X2 interface is a mesh network that enables signalling exchange among cells, needed for HO or JT CoMP. The traffic on the X2 interface remains less than the S1 traffic unless cooperation is allowed because downlink data to one single user must be simultaneously transmitted over several links [8]. Also if the overhead, due to tunnelling protocols and HO events, is estimated at 14%, then X2 upstream traffic can be written as [119]

$$\mathcal{U}_{\text{pstream}} = \left[0.14\left(\mathcal{A}_1 + \mathcal{A}_2\right) + \bar{x}\right] \mathcal{T}, \tag{5.45}$$

where $\bar{x}$ represents the inter-site ratio, i.e., the X2 interface is only used when cells from different sites cooperate. For instance, if no cooperation is needed as in the

REM cell-association strategy $\bar{x} = 0$, in others, it will be the probability of collaboration. In the downstream, the backhaul carries data shared by all cooperating cells and is equal to [119]

$$\mathcal{D}_{\text{ownstream}} = [1 + 0.14\,(\mathcal{A}_1 + \mathcal{A}_2) + \bar{x}]\,\mathcal{T}. \tag{5.46}$$

5.4.3 Optimal Δ

We want to obtain the vector $\boldsymbol{\Delta}$ that maximises $\mathcal{T}$. Finding the optimal radii $\boldsymbol{\Delta}$ is crucial for the REM cell-association strategy to achieve a balance between the extra coverage provided by the small cells in opposition to the disconnection required to perform an HO. For example, if the search radii are too high, the REM cell-association strategy will skip too many HOs and the coverage would drop as was discussed in Subsection 5.2.1. Conversely, if the search radii are too low, our proposed strategy will not save much time by skipping HOs. Since the HO rate is directly proportional to the user speed, it is reasonable to assume that $\boldsymbol{\Delta}$ will be proportional to counteract the high number of disconnections. We formulate the following optimisation (maximisation) problem

$$\begin{aligned} &\underset{\boldsymbol{\Delta}}{\text{maximise}} \quad \mathcal{T}(\boldsymbol{\Delta}) \\ &\text{subject to} \quad \boldsymbol{\Delta} \succeq 0, \end{aligned} \tag{5.47}$$

where the vector $\boldsymbol{\Delta} = [\Delta_1, \Delta_2]^{\mathsf{T}}$ represents the different radii of each tier that influences the probability of skipping HOs from any tier, whose expressions were given in Lemma 1. Despite the existence of tractable expressions for the coverage probability, the optimisation problem in (5.47) is in nature quite challenging to tackle. It has been shown for similar optimisation problems that its convexity/concavity properties are difficult if not impossible to prove for general system setups [82]. In other cases, it is possible to reformulate the optimisation problem to a simpler one and use the solution back into the original problem [120]. Such an option is out of the scope of this chapter. From a practical standpoint, the optimal solution can be easily obtained numerically with any numerical optimisation package. In our case, we have used the function `fmincon` from the Optimization Toolbox in MATLAB.

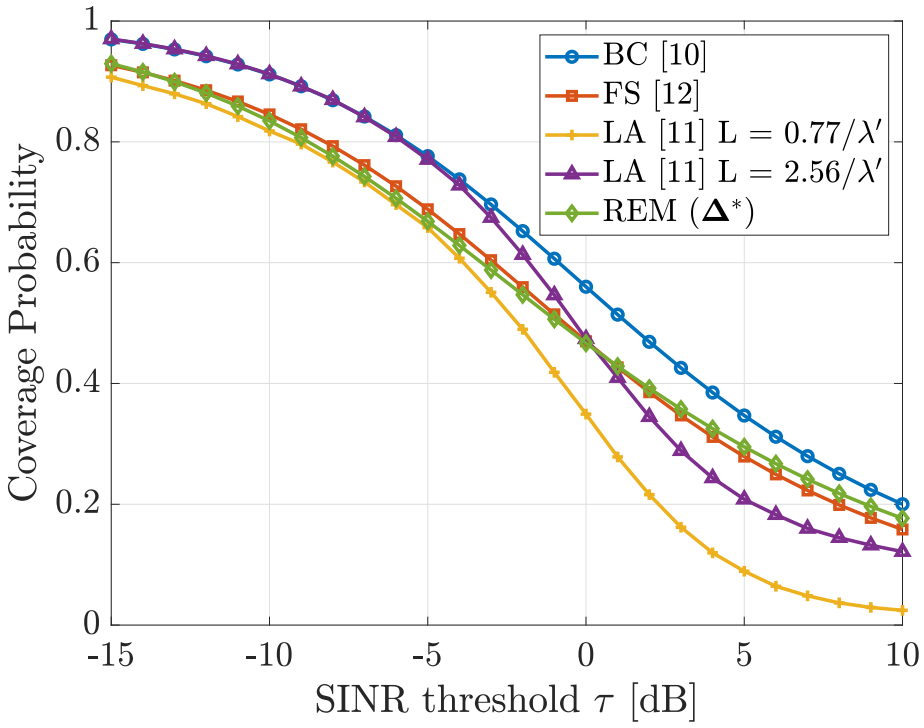

Figure 5.6: Coverage probability with respect to SINR threshold in dB with$\{\lambda_1, \lambda_2\} = \{30, 70\}$ km^{-2}, $\{\alpha_1, \alpha_2\} = \{4, 4\}$, $\{P_1, P_2\} = \{1, 0.1\}$ W, and $\{B_1, B_2\} = \{0, 0\}$ dB. The REM curve has been optimised for $v = 200$ km/h and $\{d_1, d_2\} = \{0.35, 0.70\}$ s.

5.5 Numerical Results

In this section, we show simulations results comparing different cell-association strategies: Best Connected (BC [80]), Femto Skipping (FS [86]), Location Aware (LA [42]), and our proposed technique REM-based cell-association strategy (REM). In FS and LA schemes, we have disregarded the interference cancellation capabilities because the expected gains would be the same for the rest of the methods. In LA, the authors propose two different distance threshold L = $\{0.77/\lambda', 2.56/\lambda'\}$ [42], where λ' is the total intensity of the BS in the network, i.e. $\lambda' = \lambda_1 + \lambda_2 = 100$ km^{-2}.

In Fig. 5.6, we present the coverage probability of all the considered methods against the SINR threshold τ. It can be seen that, without IC, none of the strategies outperforms the BC scheme. Our method depends on the search radii $\mathbf{\Delta}$ that are optimised to maximise throughput, not coverage probability. For illustrative purposes

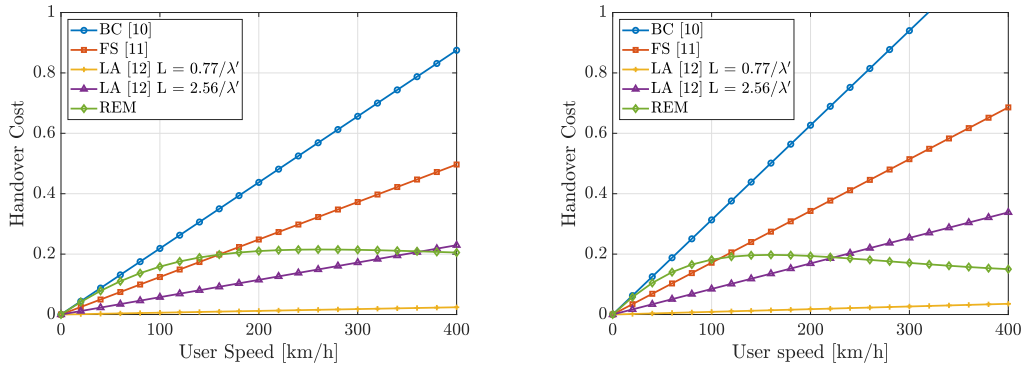

(a) $\{d_1, d_2\} = \{0.35, 0.70\}$ s. **(b)** $\{d_1, d_2\} = \{0.35, 1.05\}$ s

Figure 5.7: Handover cost with respect to user speed in km/h with $\{\lambda_1, \lambda_2\} = \{30, 70\}$ km^{-2}, $\{\alpha_1, \alpha_2\} = \{4, 4\}$, $\{P_1, P_2\} = \{1, 0.1\}$ W, $\{B_1, B_2\} = \{0, 0\}$ dB, and $B = 10$ MHz.

only, we have optimised our proposed technique for user speed $v = 200$ km/h and HO delays $\{d_1, d_2\} = \{0.35, 0.70\}$ s [86]. In this particular case, our performance is reasonably close to the FS approach. LA performs better for negative threshold because, when the SINR is already low, it means the user is far from its serving cell then skipping a HO and using CoMP will not affect the SINR significantly. On the contrary, when the SINR is positive, meaning the RSS from the serving cell is at least as high as the interference, skipping HOs based solely on distance might be counterproductive due to a strong interferer close to the user. Employing IC can improve this result, so will with the rest of the strategies.

Fig. 5.7 shows the handover cost for each strategy with different HO delays. The HO cost of all methods except ours increase linearly with the user speed because they do not adapt to the HO rate. For example, FS skips every other HO to the second tier alternatively, and LA skips HOs in both tiers based on a distance threshold. When this threshold is too small as L $= 0.77/\lambda'$, it avoids almost all disconnections at the expense of been served by CoMP. The REM-based cell-association strategy can restrain the number of disconnections depending on the HO rate. As the user speed grows, our proposed technique skips more HOs to improve the throughput as shown next. Fig. 5.8 depicts the average user throughput in the downlink assuming full buffer. In general, there is a linear decay of throughput as the HO rate increases due to the user speed. Fig. 5.8a and Fig. 5.8b show the results for unbiased and

biased cell association when the HO delay of the second tier is twice as much as the HO delay of the first tier. It can be seen that the throughput for the BC strategy degrades the quickest because it performs all the HOs, while the LA scheme with $L = 0.77/\lambda'$ skips almost all of them. Hence the throughput is almost flat because users are constantly served by the second and third strongest BS via CoMP.

However, with $L = 2.56/\lambda'$, the LA scheme outperforms BC after 100 km/h and 60 km/h for the unbiased and biased cases, respectively. Our method outperforms all of them for most of the cases of interest in urban areas (up to 140 km/h without bias and 120 km/h with bias). However, the REM-based cell-association strategy is optimised for each speed, so the degradation of the throughput is not linear. As a result, we provide almost the same user throughput as LA effectively with half the bandwidth, i.e. without CoMP. Similar observations can be made in Fig. 5.8c and Fig. 5.8d, where the HO delay of the second tier has been increased to three times. The gains of the REM-based cell-association strategy are higher in this case because performing a HO results in a higher delay. Our method provides better throughput for speeds up to 110 km/h and beyond 360 km/h in Fig. 5.8c, while the gap between our method and LA is less than 5% for the rest of the speeds.

Looking only at the throughput gives the false impression that LA outperforms REM for high-speed users. Nonetheless, LA employs CoMP to compensate for the degradation of throughput, doubling the amount of bandwidth needed for the cooperating BSs. CoMP has multiple benefits to improve spectral efficiency, but the LA technique fails to apply them properly. In Fig. 5.9, LA requires approximately 84 and 98% extra traffic per unit of data delivered to the user for $L = \{0.77/\lambda', 2.56/\lambda'\}$, respectively. Our proposed technique only needs 6–12% overhead per unit of data while still delivering the highest user throughput. This exemplifies one of the key advantages of using REMs for cell selection; instead of skipping HOs based on distance, REMs store far more information in them, for example, the location of BSs and the expected RSS per area. Furthermore, as we can locate users on the map and we know their current speed, we can dynamically decide whether to perform a HO with more available information.

The backhaul upstream is presented in Fig. 5.10, where our proposed scheme

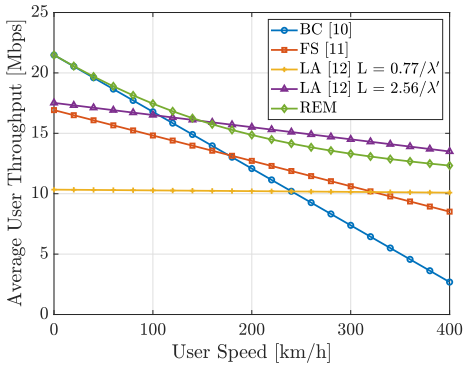

(a) $\{B_1, B_2\} = \{0, 0\}$ dB, $\{d_1, d_2\} = \{0.35, 0.70\}$ s.

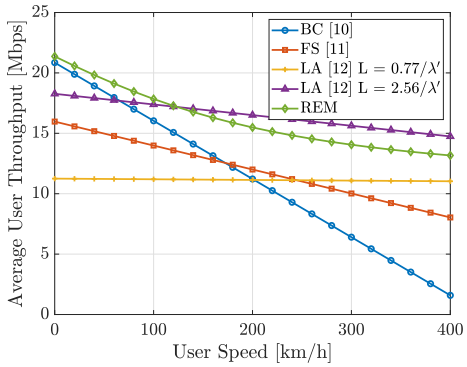

(b) $\{B_1, B_2\} = \{0, 6\}$ dB, $\{d_1, d_2\} = \{0.35, 0.70\}$ s

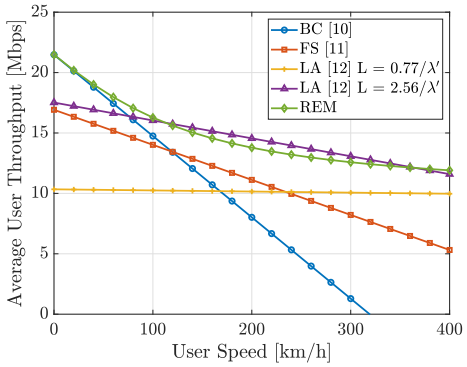

(c) $\{B_1, B_2\} = \{0, 0\}$ dB, $\{d_1, d_2\} = \{0.35, 1.05\}$ s.

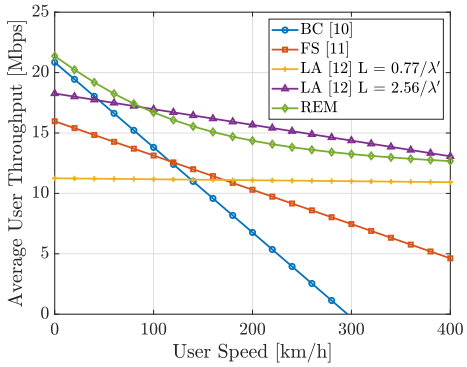

(d) $\{B_1, B_2\} = \{0, 6\}$ dB, $\{d_1, d_2\} = \{0.35, 1.05\}$ s

Figure 5.8: Average user throughput in Mbps with respect to user speed in km/h with $\{\lambda_1, \lambda_2\} = \{30, 70\}$ km^{-2}, $\{\alpha_1, \alpha_2\} = \{4, 4\}$, $\{P_1, P_2\} = \{1, 0.1\}$ W, and $B = 10$ MHz. BC and REM use half the bandwidth that FS and LA employ.

also excels. The REM-based cell-association strategy requires approximately 8–14% of the user throughput in the upstream whereas the BC strategy needs 14% throughout the whole range of speeds. The difference comes from the ability to skip user associations dynamically with REMs. FS incurs a 32% overhead in the upstream, lower than LA that can go up to 98% extra traffic in the downstream. Our technique achieves at least a reduction of 68% in the backhaul overhead as a result of not using CoMP and provides virtually the same performance on the user side when compared to LA and an average 65% gain over BC.

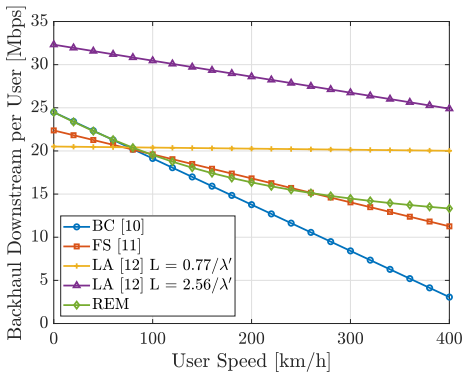

(a) $\{B_1, B_2\} = \{0, 0\}$ dB, $\{d_1, d_2\} = \{0.35, 0.70\}$ s.

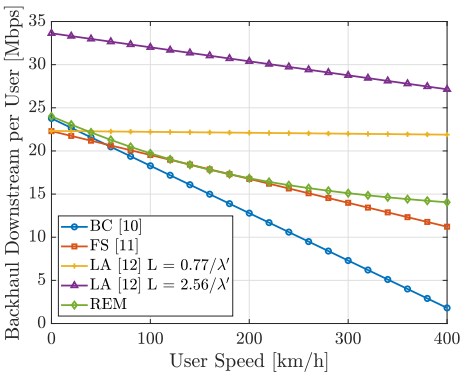

(b) $\{B_1, B_2\} = \{0, 6\}$ dB, $\{d_1, d_2\} = \{0.35, 0.70\}$ s

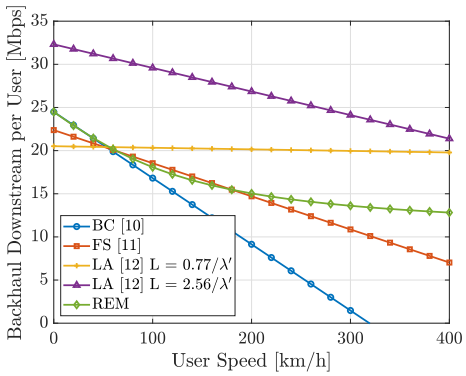

(c) $\{B_1, B_2\} = \{0, 0\}$ dB, $\{d_1, d_2\} = \{0.35, 1.05\}$ s.

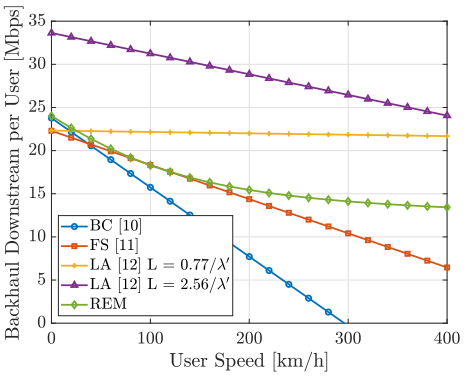

(d) $\{B_1, B_2\} = \{0, 6\}$ dB, $\{d_1, d_2\} = \{0.35, 1.05\}$ s

Figure 5.9: Backhaul downstream per user in Mbps with respect to user speed in km/h with $\{\lambda_1, \lambda_2\} = \{30, 70\}$ km^{-2}, $\{\alpha_1, \alpha_2\} = \{4, 4\}$, $\{P_1, P_2\} = \{1, 0.1\}$ W, and $B = 10$ MHz.

5.6 Summary

In this chapter, a novel REM-based cell-association strategy has been analysed for dense 5G networks. Based on distance distributions between the typical user and BSs, the association probability and the coverage probability have been derived for dense 5G networks, where the BSs' locations follow HPPPs. Moreover, user throughput and backhaul traffic have been presented to evaluate the mobility management performance in dense 5G networks. Numerical results indicate that the proposed method increases the average user throughput and reduces the overhead in the backhaul in dense 5G networks. Our scheme finds a balance between the coverage probability and the HO rate by numerical optimisation. Results show that

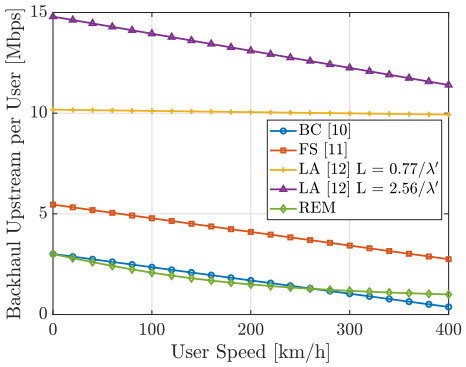

(a) $\{B_1, B_2\} = \{0, 0\}$ dB, $\{d_1, d_2\} = \{0.35, 0.70\}$ s.

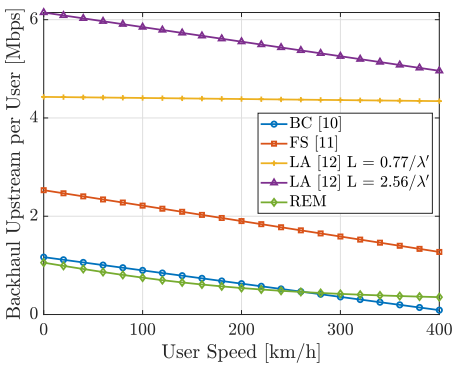

(b) $\{B_1, B_2\} = \{0, 6\}$ dB, $\{d_1, d_2\} = \{0.35, 0.70\}$ s

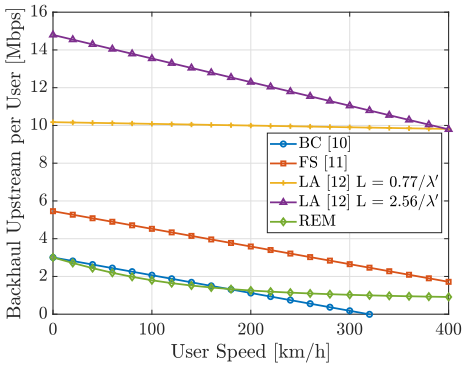

(c) $\{B_1, B_2\} = \{0, 0\}$ dB, $\{d_1, d_2\} = \{0.35, 1.05\}$ s.

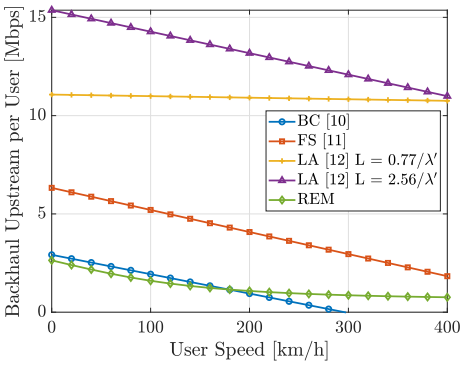

(d) $\{B_1, B_2\} = \{0, 6\}$ dB, $\{d_1, d_2\} = \{0.35, 1.05\}$ s

Figure 5.10: Backhaul upstream per user in Mbps with respect to user speed in km/h with $\{\lambda_1, \lambda_2\} = \{30, 70\}$ km^{-2}, $\{\alpha_1, \alpha_2\} = \{4, 4\}$, $\{P_1, P_2\} = \{1, 0.1\}$ W, and $B = 10$ MHz.

the REM-based cell-association strategy can increase the average user throughput 65% over the traditional approach on average. Furthermore, it reduces the amount of overhead needed up to 68% over other skipping strategies for dense 5G networks.

Chapter 6

Conclusion

6.1 Remarks

This thesis introduced research work on REMs for mobility management in 5G networks. In particular, handover in HetNets and cell selection in dense cellular networks were considered. In this context, the impact of our techniques in the backhaul and the expected average user throughput were also investigated. Our work resonates with the 3GPP specifications first and evolves into more broad networks as 5G networks are expected to become a conglomeration of different access technologies. The techniques presented in previous chapters led to location awareness in cellular networks beyond the legacy time-frequency-space resource allocation. Our main findings are:

Evaluation of Radio Environment Maps in 4G and 5G

We adopted a simulation-driven approach to explore the opportunities REM would bring in HetNets in terms of mobility management. As the complexity of cellular networks increases, analytical-based studies become quite challenging, and most of them tend to lose track of reality due to oversimplification. We implemented a network-level simulator following industry-grade guidelines and employed a publicly available dataset of mobility traces and radio environment data to evaluate our ideas. We found out that REMs can be effortlessly incorporated in LTE and 5G NR standards for handover decision-making algorithms. We tested a simple yet

effective handover scheme based on a predicted location that firstly was meant to reduce the number of unnecessary handovers, and secondly, we modified it to adapt for real-world traffic flows. Despite the lack of tractability at this stage, we showed that the capacity was not sacrificed in both the downstream and the upstream. At the same time, our original aim was fulfilled by reducing the number of handovers in general. It was a keystone for the rest of the thesis to benchmark our proposals against state-of-the-art counterparts so we could settle down to one version.

Analysis of REM-Based Handover Algorithm for Heterogeneous Networks

We developed an analytical framework for the handover algorithm we presented in the previous chapter. We demonstrated that, in a scenario where base stations with different transmit powers coexist such as HetNets, the coverage and failure areas could be characterised geometrically. We also included positioning errors in our formulation, so our algorithm could handle imperfect conditions. We described the probabilities for different events during a handover procedure, namely no handover, handover failure, and ping-pong handover. A numerical optimisation problem ensued, targeted to lower the number of ping-pong handovers while using the handover failures as a constraint. We compared this optimised version not only with the current LTE-HO algorithm but also with other schemes found in the literature. While no algorithm is perfect, our proposed one struck a balance between handover failures and ping-pong handovers. Results showed that even in the presence of imperfect location, our algorithm successfully accommodated a wide range of user speeds.

Network Optimisation in 5G Networks: A Radio Environment Approach

We studied the applicability of REMs in a global set-up, beyond handovers that are local. As heterogeneity becomes the rule in cellular networks and densification escalates, proper cell association becomes crucial to achieve uninterrupted service. Through stochastic geometry, we presented a cell-association strategy that exploits REMs to achieve a compromise between better coverage or disconnection time. We proposed per-tier search radii, the purpose of which is twofold: on the one hand, they

disregard associations that do not increase the user capacity in the long-term; and, on the other hand, they establish a guard zone around users where the main interferer is sure to be further than the radii. We obtained the per-tier association probabilities under this policy as well as the distance distributions to the serving cell and the interferers. Furthermore, the capacity and spectral efficiency of users are studied and included in a numerical optimisation problem to maximise the user throughput, where handovers incurred disconnection time penalising the overall result. Finally, we contrasted our policy to other skipping methods, showing that advanced signal-processing techniques overload the backhaul whereas REMs represent a lightweight alternative for future cellular networks.

6.2 Future Research

In this thesis, we have investigated the inclusion of REMs in cellular networks for mobility purposes. The work presented shows the importance of REM as an enabling technology for 4G and 5G to enhance the performance of both. However, there are potential problems that would benefit from geolocation awareness too. Some of them correspond with future use cases that current cellular networks cannot accommodate adequately, i.e. drone communications. Hereafter, we list potential prospective work:

Adding complexity to the geometric model

In a real-life REM, large-scale fading is inherently present since it is created from either measurements or realistic 3D propagation models. From a theoretical point of view, it will be useful to include shadowing in the geometric model to get a more accurate framework. However, the HO regions are expected not to be circles any more. Instead, a collection of HO regions will stem from the probabilistic nature of the random process. Some works in the literature deal with it by transferring this random process from the radio environment to another relevant parameter, for example, speed or TTT.

There is no need for measurement reports

As REMs become more widespread and more accurate, we can predict long-term radio parameters within tight bounds. Hence the necessity of continuously measuring pilot signals for cell discovery, handover, or quality of service vanishes. Moreover, as REMs are databases, we could extract other readily available advanced parameters such as the load factor of each BS and perform HOs in a more proactive way (network-triggered) rather than the user-triggered network-assisted approach.

Resource allocation wherever you go

Also, in real-world scenarios, user mobility is not random but rather direction oriented, based on its origin and destination. For example, we follow very recognisable mobility patterns during working days. Knowledge of these patterns would enable efficient resource management algorithms, making the quality of service "follow" the user. Another possibility would be using REMs to suggest best routes regarding QoS demands. Imagine that a user requires delay to be under a certain threshold, combining REMs with real-traffic data we could find the best route for such a user to fulfil this constraint.

The sky is the limit

Finally, expand the current REM framework to different scenarios where vertical positioning is needed, for example, multi-story buildings or unmanned aerial vehicles (UAVs). While this thesis has been exploring REMs in outdoor scenarios, radio environment mapping in indoor scenarios like offices, where cellular networks are surrounded by other radio access technologies in unlicensed bands, could also be of interest. Furthermore, UAVs have recently drawn a lot of attention from researchers. Extending REMs from longitude-latitude to longitude-latitude-height coordinates imposes a massive amount of data that needs to be collected from drones hovering in the area of interest. Two ideas to cut down the number of samples needed would be creating sliced REMs for a reduced series of heights and interpolate the rest, as if it were a building, or using a hybrid method combining measurements and

simulations.

Abbreviations

3G	Third Generation
4G	Fourth Generation
5G	Fifth Generation
3GPP	3rd Generation Partnership Project
AHFL	Adaptive HMM based on Fuzzy Logic
ASE	Area Spectral Efficiency
BC	Best Connected
BS	Base Station
CHO	Conditional HandOver
CP	Cyclic Prefix
CSI	Channel State Information
D2D	Device-to-Device
eMBB	Enhanced Mobile BroadBand
eNB	Evolved Node B
fREM	REM-HO with fixed prediction time
FRK	Fixed Rank Kriging

FS	Femto Skipping
FS-IC	Femto Skipping with Interference Cancellation
GIDS	Gradient plus Inverse Distance Squared (GIDS)
GNSS	Global Navigation Satellite System
GPS	Global Positioning System
HeNB	Home evolved Node B
HetNet	Heterogeneous Networks
HF	Handover Failure
HHM	Handover Hysteresis Margin
HO	HandOver
HST	High-Speed Train
IC	Interference Cancellation
IDW	Inverse Distance Weighting
IEEE	Institute of Electrical and Electronics Engineers
IMT-2020	International Mobile Telecommunications-2020
ISD	Inter-Site Distance
ITS	Intelligent Transportation Systems
JT CoMP	Joint Transmission Coordinated MultiPoint
KPI	Key Performance Indicators
L1	Layer 1
L3	Layer 3
LA	Location Aware

LA-GPS	Location Aware with geolocation errors
LOS	Line-Of-Sight
LSA	Licensed Shared Access
LTE	Long-Term Evolution
MCD	Measurement Capable Device
MDT	Minimization of Drive Test
METIS	Mobile and wireless communications Enablers for the Twenty-twenty Information Society 5G
MM	Mobility Management
MNO	Mobile Network Operator
MSE	Mobility State Estimation
MSM	Modified Shepard's Method
mMIMO	Massive Multiple-Input Multiple-Output
mMTC	Massive Machine-Type Communications
mmWave	Millimetre Wave
NCL	Neighbour Cell Lists
NLOS	Non-Line-Of-Sight
NOMA	Non-Orthogonal Multiple Access
NR	New Radio
OFDM	Orthogonal Frequency-Division Multiplexing
OTDOA	Observed Time-Difference Of Arrival
PDF	Probability Density Function

PP Ping-Pong

PPP Poisson Point Process

QoE Quality of Experience

QoS Quality of Service

REM Radio Environment Map

RF Radio Frequency

RLF Radio Link Failure

RMSE Root-Mean-Square Error

RRC Radio Resource Control

RRM Radio Resource Management

RSRP Reference Signal Received Power

RSRQ Reference Signal Received Quality

RSS Received Signal Strength

RWP Random WayPoint

SFR Soft Frequency Reuse

SIC Successive Interference Cancellation

SINR Signal-to-Interference-plus-Noise Ratio

SIR Signal-to-Interference Ratio

SON Self-Organising Network

SUMO Simulation of Urban MObility

TETRA TErrestrial Trunked RAdio

TOPSIS Technique for Order Preferences by Similarity to Ideal Solution

ToS Time of Stay

TTT Time-To-Trigger

TVWS TV White Spaces

UAV Unmanned Aerial Vehicle

UE User Equipment

URLLC Ultra-Reliable and Low-Latency Communications

V2X Vehicle-To-Everything

Bibliography

[1] International Mobile Telecommunications-2020, "IMT Vision - "Framework and overall objectives of the future development of IMT for 2020 and beyond"," IMT-2020 M.2083 (09/2015), Tech. Rep., 2015.

[2] D. Lopez-Perez, I. Guvenc, and X. Chu, "Mobility management challenges in 3GPP heterogeneous networks," *IEEE Communications Magazine*, vol. 50, no. 12, pp. 70–78, 2012.

[3] J. Perez-Romero, A. Zalonis, L. Boukhatem, A. Kliks, K. Koutlia, N. Dimitriou, and R. Kurda, "On the use of radio environment maps for interference management in heterogeneous networks," *IEEE Communications Magazine*, vol. 53, no. 8, pp. 184–191, 2015.

[4] 3rd Generation Partnership Project, "Evolved Universal Terrestrial Radio Access (E-UTRA); Mobility enhancements in heterogeneous networks," 3GPP TR 36.839 V11.1.0, Tech. Rep., 2012.

[5] W. Webb, *Wireless Communications: The Future*. John Wiley & Sons, Inc., 2007.

[6] Cisco Systems, Inc., "Cisco Visual Networking Index: Global Mobile Data Traffic Forecast Update, 2017–2022 White Paper," 2019. [Online]. Available: https://www.cisco.com/c/en/us/solutions/collateral/service-provider/visual-networking-index-vni/white-paper-c11-738429.html

[7] J. G. Andrews, S. Buzzi, W. Choi, S. V. Hanly, A. Lozano, A. C. K. Soong, and J. C. Zhang, "What Will 5G Be?" *IEEE Journal on Selected Areas in Communications*, vol. 32, no. 6, pp. 1065–1082, 2014.

[8] V. Jungnickel, K. Manolakis, W. Zirwas, B. Panzner, V. Braun, M. Lossow, M. Sternad, R. Apelfrojd, and T. Svensson, "The role of small cells, coordinated multipoint, and massive MIMO in 5G," *IEEE Communications Magazine*, vol. 52, no. 5, pp. 44–51, 2014.

[9] M. Shafi, A. F. Molisch, P. J. Smith, T. Haustein, P. Zhu, P. De Silva, F. Tufvesson, A. Benjebbour, and G. Wunder, "5G: A Tutorial Overview of Standards, Trials, Challenges, Deployment, and Practice," *IEEE Journal on Selected Areas in Communications*, vol. 35, no. 6, pp. 1201–1221, 2017.

[10] D. Lopez-Perez, M. Ding, H. Claussen, and A. H. Jafari, "Towards 1 Gbps/UE in Cellular Systems: Understanding Ultra-Dense Small Cell Deployments," *IEEE Communications Surveys & Tutorials*, vol. 17, no. 4, pp. 2078–2101, 2015.

[11] A. Gupta and R. K. Jha, "A Survey of 5G Network: Architecture and Emerging Technologies," *IEEE Access*, vol. 3, pp. 1206–1232, 2015.

[12] E. G. Larsson, O. Edfors, F. Tufvesson, and T. L. Marzetta, "Massive MIMO for next generation wireless systems," *IEEE Communications Magazine*, vol. 52, no. 2, pp. 186–195, 2014.

[13] A. Osseiran, F. Boccardi, V. Braun, K. Kusume, P. Marsch, M. Maternia, O. Queseth, M. Schellmann, H. Schotten, H. Taoka, H. Tullberg, M. A. Uusitalo, B. Timus, and M. Fallgren, "Scenarios for 5G mobile and wireless communications: the vision of the METIS project," *IEEE Communications Magazine*, vol. 52, no. 5, pp. 26–35, 2014.

[14] X. Hong, J. Wang, C. Wang, and J. Shi, "Cognitive radio in 5G: a perspective on energy-spectral efficiency trade-off," *IEEE Communications Magazine*, vol. 52, no. 7, pp. 46–53, 2014.

[15] M. Lauridsen, L. C. Gimenez, I. Rodriguez, T. B. Sorensen, and P. Mogensen, "From LTE to 5G for Connected Mobility," *IEEE Communications Magazine*, vol. 55, no. 3, pp. 156–162, 2017.

[16] M. Polese, M. Giordani, M. Mezzavilla, S. Rangan, and M. Zorzi, "Improved Handover Through Dual Connectivity in 5G mmWave Mobile Networks," *IEEE Journal on Selected Areas in Communications*, vol. 35, no. 9, pp. 2069–2084, 2017.

[17] 3rd Generation Partnership Project, "Study on New Radio Access Technology; Radio Interface Protocol Aspects," 3GPP TR 38.804 V14.0.0, Tech. Rep., 2017.

[18] H. Park, Y. Lee, T. Kim, B. Kim, and J. Lee, "Handover Mechanism in NR for Ultra-Reliable Low-Latency Communications," *IEEE Network*, vol. 32, no. 2, pp. 41–47, 2018.

[19] H. Martikainen, I. Viering, A. Lobinger, and T. Jokela, "On the Basics of Conditional Handover for 5G Mobility," in *2018 IEEE 29th Annual International Symposium on Personal, Indoor and Mobile Radio Communications (PIMRC)*, 2018, Conference Proceedings, pp. 1–7.

[20] M. Ding and D. López-Pérez, "Performance Impact of Base Station Antenna Heights in Dense Cellular Networks," *IEEE Transactions on Wireless Communications*, vol. 16, no. 12, pp. 8147–8161, 2017.

[21] J. An, K. Yang, J. Wu, N. Ye, S. Guo, and Z. Liao, "Achieving Sustainable Ultra-Dense Heterogeneous Networks for 5G," *IEEE Communications Magazine*, vol. 55, no. 12, pp. 84–90, 2017.

[22] X. Ge, S. Tu, G. Mao, C. Wang, and T. Han, "5G Ultra-Dense Cellular Networks," *IEEE Wireless Communications*, vol. 23, no. 1, pp. 72–79, 2016.

[23] Y. Zhao, J. H. Reed, S. Mao, and K. K. Bae, "Overhead Analysis for Radio Environment Mapenabled Cognitive Radio Networks," in *2006 1st IEEE Workshop on Networking Technologies for Software Defined Radio Networks*, 2006, Conference Proceedings, pp. 18–25.

[24] Y. Corre and Y. Lostanlen, "Three-Dimensional Urban EM Wave Propagation Model for Radio Network Planning and Optimization Over Large Areas,"

IEEE Transactions on Vehicular Technology, vol. 58, no. 7, pp. 3112–3123, 2009.

[25] M. Angjelicinoski, V. Atanasovski, and L. Gavrilovska, "Comparative analysis of spatial interpolation methods for creating radio environment maps," in *2011 19thTelecommunications Forum (TELFOR) Proceedings of Papers*, 2011, Conference Proceedings, pp. 334–337.

[26] C. Phillips, M. Ton, D. Sicker, and D. Grunwald, "Practical radio environment mapping with geostatistics," in *2012 IEEE International Symposium on Dynamic Spectrum Access Networks*, 2012, Conference Proceedings, pp. 422–433.

[27] A. Palaios, S. Jagadeesan, N. Perpinias, J. Riihijärvi, and P. Mähönen, "Studying and mitigating the impact of GPS localization error on radio environment map construction," in *2014 IEEE 25th Annual International Symposium on Personal, Indoor, and Mobile Radio Communication (PIMRC)*, 2014, Conference Proceedings, pp. 258–263.

[28] T. Farnham, "Radio environment map techniques and performance in the presence of errors," in *2016 IEEE 27th Annual International Symposium on Personal, Indoor, and Mobile Radio Communications (PIMRC)*, 2016, Conference Proceedings, pp. 1–6.

[29] H. B. Yilmaz, T. Tugcu, F. Alagöz, and S. Bayhan, "Radio environment map as enabler for practical cognitive radio networks," *IEEE Communications Magazine*, vol. 51, no. 12, pp. 162–169, 2013.

[30] J. V. D. Beek, T. Cai, S. Grimoud, B. Sayrac, P. Mahonen, J. Nasreddine, and J. Riihijarvi, "How a layered rem architecture brings cognition to today's mobile networks," *IEEE Wireless Communications*, vol. 19, no. 4, pp. 17–24, 2012.

[31] B. A. Jayawickrama, E. Dutkiewicz, M. Mueck, and Y. He, "On the Usage of Geolocation-Aware Spectrum Measurements for Incumbent Location

and Transmit Power Detection," *IEEE Transactions on Vehicular Technology*, vol. 65, no. 10, pp. 8177–8189, Oct. 2016.

[32] A. Haniz, G. K. Tran, K. Sakaguchi, J. Takada, T. Yamaguchi, T. Mitsui, and S. Arata, "Construction and Interpolation of a Multi-frequency Radio Map," in *2019 International Conference on Robotics,Electrical and Signal Processing Techniques (ICREST)*, 2019, Conference Proceedings, pp. 632–637.

[33] J. Zhang, Q. Zhao, and J. Zou, "The IEEE802.22 WRAN System Based on Radio Environment Map (REM)," in *2009 First International Workshop on Education Technology and Computer Science*, vol. 1, 2009, Conference Proceedings, pp. 98–101.

[34] European Comission, "Flexible and spectrum-Aware Radio Access through Measurements and modelling In cognitive Radio systems," 2019. [Online]. Available: https://cordis.europa.eu/project/rcn/93764/factsheet/en

[35] S. Grimoud, B. Sayrac, S. B. Jemaa, and E. Moulines, "Best Sensor Selection for an Iterative REM Construction," in *2011 IEEE Vehicular Technology Conference (VTC Fall)*, 2011, Conference Proceedings, pp. 1–5.

[36] H. Braham, S. B. Jemaa, G. Fort, E. Moulines, and B. Sayrac, "Fixed Rank Kriging for Cellular Coverage Analysis," *IEEE Transactions on Vehicular Technology*, vol. 66, no. 5, pp. 4212–4222, 2017.

[37] E. Meshkova, J. Ansari, D. Denkovski, J. Riihijarvi, J. Nasreddine, M. Pavloski, L. Gavrilovska, and P. Mähönen, "Experimental spectrum sensor testbed for constructing indoor Radio Environmental Maps," in *2011 IEEE International Symposium on Dynamic Spectrum Access Networks (DySPAN)*, 2011, Conference Proceedings, pp. 603–607.

[38] F. Casadevall and A. Umbert, "REM-based real time testbed: A proof of concept on the benefits of using REM for improving radio resource management capabilities," in *Telecommunications (ICT), 2013 20th International Conference on*, 2013, Conference Proceedings, pp. 1–5.

[39] A. Palaios, J. Riihijärvi, O. Holland, and P. Mähönen, "Detailed Measurement Study of Spatial Similarity in Spectrum Use in Dense Urban Environments," *IEEE Transactions on Vehicular Technology*, vol. 66, no. 10, pp. 8951–8963, 2017.

[40] K. I. Pedersen, P. H. Michaelsen, C. Rosa, and S. Barbera, "Mobility enhancements for lte-advanced multilayer networks with inter-site carrier aggregation," *IEEE Communications Magazine*, vol. 51, no. 5, pp. 64–71, 2013.

[41] D. Lopez-Perez, X. Chu, and I. Guvenc, "On the Expanded Region of Picocells in Heterogeneous Networks," *IEEE Journal of Selected Topics in Signal Processing*, vol. 6, no. 3, pp. 281–294, June 2012.

[42] R. Arshad, H. Elsawy, S. Sorour, T. Y. Al-Naffouri, and M.-S. Alouini, "Handover Management in 5G and Beyond: A Topology Aware Skipping Approach," *IEEE Access*, vol. 4, pp. 9073–9081, 2016.

[43] E. Demarchou, C. Psomas, and I. Krikidis, "Mobility Management in Ultra-Dense Networks: Handover Skipping Techniques," *IEEE Access*, vol. 6, pp. 11 921–11 930, 2018.

[44] D. Lopez-Perez, I. Guvenc, and X. Chu, "Theoretical analysis of handover failure and ping-pong rates for heterogeneous networks," in *2012 IEEE International Conference on Communications (ICC)*, 2012, Conference Proceedings, pp. 6774–6779.

[45] K. Vasudeva, M. Simsek, D. Lopez-Perez, and I. Guvenc, "Analysis of Handover Failures in Heterogeneous Networks With Fading," *IEEE Transactions on Vehicular Technology*, vol. 66, no. 7, pp. 6060–6074, July 2017.

[46] C. H. M. d. Lima, M. Bennis, and M. Latva-aho, "Modeling and analysis of handover failure probability in small cell networks," in *2014 IEEE Conference on Computer Communications Workshops (INFOCOM WKSHPS)*, 2014, Conference Proceedings, pp. 736–741.

[47] X. Xu, Z. Sun, X. Dai, T. Svensson, and X. Tao, "Modeling and Analyzing the Cross-Tier Handover in Heterogeneous Networks," *IEEE Transactions on Wireless Communications*, vol. 16, no. 12, pp. 7859–7869, Dec 2017.

[48] W. Bao and B. Liang, "Handoff Rate Analysis in Heterogeneous Wireless Networks with Poisson and Poisson Cluster Patterns," in *Proceedings of the 16th ACM International Symposium on Mobile Ad Hoc Networking and Computing*, ser. MobiHoc '15. New York, NY, USA: ACM, 2015, pp. 77–86.

[49] ——, "Stochastic Geometric Analysis of User Mobility in Heterogeneous Wireless Networks," *IEEE Journal on Selected Areas in Communications*, vol. 33, no. 10, pp. 2212–2225, Oct 2015.

[50] Q. Kuang, J. Belschner, Z. Bleicher, H. Droste, and J. Speidel, "A measurement-based study of handover improvement through range expansion and interference coordination," *Wireless Communications and Mobile Computing*, vol. 15, no. 14, pp. 1784–1798, 2015.

[51] D. Xenakis, N. Passas, L. Merakos, and C. Verikoukis, "Mobility Management for Femtocells in LTE-Advanced: Key Aspects and Survey of Handover Decision Algorithms," *IEEE Communications Surveys & Tutorials*, vol. 16, no. 1, pp. 64–91, 2014.

[52] M. Jung-Min and C. Dong-Ho, "Efficient handoff algorithm for inbound mobility in hierarchical macro/femto cell networks," *IEEE Communications Letters*, vol. 13, no. 10, pp. 755–757, 2009.

[53] L. Tian, J. Li, Y. Huang, J. Shi, and J. Zhou, "Seamless Dual-Link Handover Scheme in Broadband Wireless Communication Systems for High-Speed Rail," *IEEE Journal on Selected Areas in Communications*, vol. 30, no. 4, pp. 708–718, 2012.

[54] H. Zhang, W. Ma, W. Li, W. Zheng, X. Wen, and C. Jiang, "Signalling Cost Evaluation of Handover Management Schemes in LTE-Advanced Femtocell,"

in *Vehicular Technology Conference (VTC Spring), 2011 IEEE 73rd*, 2011, Conference Proceedings, pp. 1–5.

[55] S. Barbera, P. H. Michaelsen, M. Säily, and K. Pedersen, "Improved mobility performance in LTE co-channel hetnets through speed differentiated enhancements," in *2012 IEEE Globecom Workshops*, 2012, Conference Proceedings, pp. 426–430.

[56] D. Xenakis, N. Passas, L. Merakos, and C. Verikoukis, "Handover decision for small cells: Algorithms, lessons learned and simulation study," *Computer Networks*, vol. 100, pp. 64–74, 2016.

[57] Z. Becvar and P. Mach, "Adaptive Hysteresis Margin for Handover in Femtocell Networks," in *Wireless and Mobile Communications (ICWMC), 2010 6th International Conference on*, 2010, Conference Proceedings, pp. 256–261.

[58] D. Xenakis, N. Passas, and C. Verikoukis, "An energy-centric handover decision algorithm for the integrated LTE macrocell–femtocell network," *Computer Communications*, vol. 35, no. 14, pp. 1684–1694, 2012.

[59] D.-W. Lee, G.-T. Gil, and D.-H. Kim, "A Cost-Based Adaptive Handover Hysteresis Scheme to Minimize the Handover Failure Rate in 3GPP LTE System," *EURASIP Journal on Wireless Communications and Networking*, vol. 2010, no. 1, pp. 1–7, 2010.

[60] E. Bjornson, E. A. Jorswieck, M. Debbah, and B. Ottersten, "Multiobjective Signal Processing Optimization: The way to balance conflicting metrics in 5G systems," *IEEE Signal Processing Magazine*, vol. 31, no. 6, pp. 14–23, 2014.

[61] M. Alhabo and L. Zhang, "Multi-Criteria Handover Using Modified Weighted TOPSIS Methods for Heterogeneous Networks," *IEEE Access*, vol. 6, pp. 40 547–40 558, 2018.

[62] F. Guidolin, I. Pappalardo, A. Zanella, and M. Zorzi, "Context-Aware Handover Policies in HetNets," *IEEE Transactions on Wireless Communications*, vol. 15, no. 3, pp. 1895–1906, March 2016.

[63] N. P. Kuruvatti, W. Zhou, and H. D. Schotten, "Mobility Prediction of Diurnal Users for Enabling Context Aware Resource Allocation," in *2016 IEEE 83rd Vehicular Technology Conference (VTC Spring)*, 2016, Conference Proceedings, pp. 1–5.

[64] D. Calabuig, S. Barmpounakis, S. Gimenez, A. Kousaridas, T. R. Lakshmana, J. Lorca, P. Lunden, Z. Ren, P. Sroka, E. Ternon, V. Venkatasubramanian, and M. Maternia, "Resource and Mobility Management in the Network Layer of 5G Cellular Ultra-Dense Networks," *IEEE Communications Magazine*, vol. 55, no. 6, pp. 162–169, 2017.

[65] Y. S. Hussein, B. M. Ali, M. F. A. Rasid, A. Sali, and A. M. Mansoor, "A novel cell-selection optimization handover for long-term evolution (LTE) macrocellusing fuzzy TOPSIS," *Computer Communications*, vol. 73, pp. 22–33, 2016.

[66] K. Da Costa Silva, Z. Becvar, and C. R. L. Frances, "Adaptive Hysteresis Margin Based on Fuzzy Logic for Handover in Mobile Networks With Dense Small Cells," *IEEE Access*, vol. 6, pp. 17 178–17 189, 2018.

[67] 3rd Generation Partnership Project, "Radio Resource Control (RRC); Protocol specification," 3GPP TR 36.331 V15.5.1, Tech. Rep., 2019.

[68] C. Jiang, H. Zhang, Y. Ren, Z. Han, K. Chen, and L. Hanzo, "Machine Learning Paradigms for Next-Generation Wireless Networks," *IEEE Wireless Communications*, vol. 24, no. 2, pp. 98–105, 2017.

[69] N. Sinclair, D. Harle, I. A. Glover, J. Irvine, and R. C. Atkinson, "An Advanced SOM Algorithm Applied to Handover Management Within LTE," *IEEE Transactions on Vehicular Technology*, vol. 62, no. 5, pp. 1883–1894, 2013.

[70] S. Chaudhuri, I. Baig, and D. Das, "Self organizing method for handover performance optimization in LTE-advanced network," *Computer Communications*, vol. 110, pp. 151–163, 2017. [Online]. Available: http://www.sciencedirect.com/science/article/pii/S0140366417300464

[71] M. Simsek, M. Bennis, and I. Guvenc, "Mobility management in HetNets: a learning-based perspective," *EURASIP Journal on Wireless Communications and Networking*, vol. 2015, no. 1, pp. 1–13, 2015.

[72] M. M. Hasan, S. Kwon, and J. Na, "Adaptive Mobility Load Balancing Algorithm for LTE Small-Cell Networks," *IEEE Transactions on Wireless Communications*, vol. 17, no. 4, pp. 2205–2217, 2018.

[73] T. Po-Hsuan and F. Kai-Ten, "Location tracking assisted handover algorithms for broadband wireless networks," in *2008 IEEE 19th International Symposium on Personal, Indoor and Mobile Radio Communications*, 2008, Conference Proceedings, pp. 1–5.

[74] M. Chen, Y. Yang, and Z. Zhong, "Location-Based Handover Decision Algorithm in LTE Networks under High-Speed Mobility Scenario," in *2014 IEEE 79th Vehicular Technology Conference (VTC Spring)*, 2014, Conference Proceedings, pp. 1–5.

[75] J. Zhao, Y. Liu, C. Wang, L. Xiong, and L. Fan, "High-speed based adaptive beamforming handover scheme in LTE-R," *IET Communications*, vol. 12, no. 10, pp. 1215–1222, 2018.

[76] Y. Xiaohuan, Y. A. Sekercioglu, and N. Mani, "A method for minimizing unnecessary handovers in heterogeneous wireless networks," in *2008 International Symposium on a World of Wireless, Mobile and Multimedia Networks*, 2008, Conference Proceedings, pp. 1–5.

[77] Z. Becvar and P. Mach, "Mitigation of Redundant Handovers to Femtocells by Estimation of throughput Gain," *Mobile Information Systems*, vol. 9, no. 4, 2013.

[78] J. G. Andrews, F. Baccelli, and R. K. Ganti, "A Tractable Approach to Coverage and Rate in Cellular Networks," *IEEE Transactions on Communications*, vol. 59, no. 11, pp. 3122–3134, 2011.

[79] H. S. Dhillon, R. K. Ganti, F. Baccelli, and J. G. Andrews, "Modeling and Analysis of K-Tier Downlink Heterogeneous Cellular Networks," *IEEE Journal on Selected Areas in Communications*, vol. 30, no. 3, pp. 550–560, 2012.

[80] H.-S. Jo, Y. J. Sang, P. Xia, and J. G. Andrews, "Heterogeneous Cellular Networks with Flexible Cell Association: A Comprehensive Downlink SINR Analysis," *IEEE Transactions on Wireless Communications*, vol. 11, no. 10, pp. 3484–3495, 2012.

[81] S. Singh, H. S. Dhillon, and J. G. Andrews, "Offloading in Heterogeneous Networks: Modeling, Analysis, and Design Insights," *IEEE Transactions on Wireless Communications*, vol. 12, no. 5, pp. 2484–2497, 2013.

[82] W. Lu and M. Di Renzo, "Stochastic Geometry Modeling and System-Level Analysis & Optimization of Relay-Aided Downlink Cellular Networks," *IEEE Transactions on Communications*, vol. 63, no. 11, pp. 4063–4085, 2015.

[83] X. Zhang, Y. Xie, Y. Cui, Q. Cui, and X. Tao, "Multi-Slot Coverage Probability and SINR-Based Handover Rate Analysis for Mobile User in Hetnet," *IEEE Access*, vol. 6, pp. 17 868–17 879, 2018.

[84] B. Yang, X. Yang, X. Ge, and Q. Li, "Coverage and Handover Analysis of Ultra-Dense Millimeter-Wave Networks With Control and User Plane Separation Architecture," *IEEE Access*, vol. 6, pp. 54 739–54 750, 2018.

[85] X. Lin, R. K. Ganti, P. J. Fleming, and J. G. Andrews, "Towards Understanding the Fundamentals of Mobility in Cellular Networks," *IEEE Transactions on Wireless Communications*, vol. 12, no. 4, pp. 1686–1698, 2013.

[86] R. Arshad, H. ElSawy, S. Sorour, T. Y. Al-Naffouri, and M. S. Alouini, "Velocity-Aware Handover Management in Two-Tier Cellular Networks," *IEEE Transactions on Wireless Communications*, vol. 16, no. 3, pp. 1851–1867, March 2017.

[87] M. Wildemeersch, T. Q. S. Quek, M. Kountouris, A. Rabbachin, and C. H. Slump, "Successive Interference Cancellation in Heterogeneous Networks," *IEEE Transactions on Communications*, vol. 62, no. 12, pp. 4440–4453, 2014.

[88] S. Grimoud, S. B. Jemaa, B. Sayrac, and E. Moulines, "A REM enabled soft frequency reuse scheme," in *2010 IEEE Globecom Workshops*, 2010, Conference Proceedings, pp. 819–823.

[89] R. C. Dwarakanath, J. D. Naranjo, and A. Ravanshid, "Modeling of interference maps for Licensed Shared Access in LTE-advanced networks supporting Carrier Aggregation," in *2013 IFIP Wireless Days (WD)*, 2013, Conference Proceedings, pp. 1–6.

[90] O. Holland and M. Dohler, "Geolocation-Based Architecture for Heterogeneous Spectrum Usage in 5G," in *2015 IEEE Globecom Workshops (GC Wkshps)*, 2015, Conference Proceedings, pp. 1–6.

[91] L. Gavrilovska, J. van de Beek, Y. Xie, E. Lidström, J. Riihijärvi, P. Mähönen, V. Atanasovski, D. Denkovski, and V. Rakovic, "Enabling LTE in TVWS with radio environment maps: From an architecture design towards a system level prototype," *Computer Communications*, vol. 53, pp. 62–72, 2014.

[92] Z. Xue and L. Wang, "Geolocation database based resource sharing among multiple device-to-device links in TV white space," in *Wireless Communications & Signal Processing (WCSP), 2015 International Conference on*, 2015, Conference Proceedings, pp. 1–6.

[93] H. Zaaraoui, Z. Altman, E. Altman, and T. Jimenez, "Forecast scheduling for mobile users," in *2016 IEEE 27th Annual International Symposium on Personal, Indoor, and Mobile Radio Communications (PIMRC)*, 2016, Conference Proceedings, pp. 1–6.

[94] Z. Hou, Y. Zhou, L. Tian, J. Shi, Y. Li, and B. Vucetic, "Radio Environment Map-Aided Doppler Shift Estimation in LTE Railway," *IEEE Transactions on Vehicular Technology*, vol. 66, no. 5, pp. 4462–4467, 2017.

[95] F. Letourneux, Y. Corre, E. Suteau, and Y. Lostanlen, "3D coverage analysis of LTE urban heterogeneous networks with dense femtocell deployments," *EURASIP Journal on Wireless Communications and Networking*, vol. 2012, no. 1, p. 319, 2012.

[96] A. Galindo-Serrano, B. Sayrac, S. B. Jemaa, J. Riihijärvi, and P. Mähönen, "Harvesting MDT data: Radio environment maps for coverage analysis in cellular networks," in *8th International Conference on Cognitive Radio Oriented Wireless Networks*, 2013, Conference Proceedings, pp. 37–42.

[97] A. Prasad, P. Lunden, O. Tirkkonen, and C. Wijting, "Energy Efficient Small-Cell Discovery Using Received Signal Strength Based Radio Maps," in *Vehicular Technology Conference (VTC Spring), 2013 IEEE 77th*, 2013, Conference Proceedings, pp. 1–5.

[98] 3rd Generation Partnership Project, "Evolved Universal Terrestrial Radio Access (E-UTRA); Requirements for support of radio resource management," 3GPP TR 36.133 V16.2.0, Tech. Rep., 2019.

[99] J. Johansson, W. A. Hapsari, S. Kelley, and G. Bodog, "Minimization of drive tests in 3GPP release 11," *IEEE Communications Magazine*, vol. 50, no. 11, pp. 36–43, 2012.

[100] H. Holma, A. Toskala, and J. Reunanen, *LTE Small Cell Optimization: 3GPP Evolution to Release 13*. ISBN: 9781118912577: John Wiley & Sons, 2015.

[101] A. Patel, "Hexagonal Grids," 2019. [Online]. Available: https://www.redblobgames.com/grids/hexagons/

[102] 3rd Generation Partnership Project, "Study on 3D channel model for LTE," 3GPP TR 36.133 V12.7.0, Tech. Rep., 2018.

[103] Mobile and wireless communications Enablers for Twenty-twenty (2020) Information Society, "Performance evaluation framework," METIS-II Deliverable D2.1, Tech. Rep., 2016.

[104] 3rd Generation Partnership Project, "Discussions on Wrapping Methodology," 3GPP TSG RAN WG1 Meeting #76 R1-140842, Tech. Rep., 2014.

[105] M. S. Alouini and A. J. Goldsmith, "Area spectral efficiency of cellular mobile radio systems," *IEEE Transactions on Vehicular Technology*, vol. 48, no. 4, pp. 1047–1066, 1999.

[106] S. Sesia, I. Toufik, and M. Baker, *LTE - The UMTS Long Term Evolution: From Theory to Practice, 2nd Edition.* ISBN: 978-0-470-66025-6: John Wiley & Sons, 2011.

[107] D. Krajzewicz, J. Erdmann, M. Behrisch, and L. Bieker, "Recent development and applications of SUMO-Simulation of Urban MObility," *International Journal On Advances in Systems and Measurements*, vol. 5, no. 3&4, 2012.

[108] K. Sato, "Measurement-based Spectrum Database for Spatial Spectrum Sharing," PhD, 2017.

[109] C. Suarez-Rodriguez, B. A. Jayawickrama, F. Bader, E. Dutkiewicz, and M. Heimlich, "REM-based handover algorithm for next-generation multi-tier cellular networks," in *2018 IEEE Wireless Communications and Networking Conference (WCNC)*, 2018, Conference Proceedings, pp. 1–6.

[110] V. Jungnickel, S. Jaeckel, K. Börner, M. Schlosser, and L. Thiele, "Estimating the mobile backhaul traffic in distributed coordinated multi-point systems," in *2012 IEEE Wireless Communications and Networking Conference (WCNC)*, 2012, Conference Proceedings, pp. 3763–3768.

[111] US Government, "GPS Standard Positioning Service (SPS) Performance Standard 4th Edition," GPS SPS PS, Tech. Rep., 2008.

[112] P. Ranacher, R. Brunauer, W. Trutschnig, S. Van der Spek, and S. Reich, "Why GPS makes distances bigger than they are," *International Journal of Geographical Information Science*, vol. 30, no. 2, pp. 316–333, 2016.

[113] R. Irmer, H. Droste, P. Marsch, M. Grieger, G. Fettweis, S. Brueck, H.-P. Mayer, L. Thiele, and V. Jungnickel, "Coordinated multipoint: concepts, performance, and field trial results," *IEEE Communications Magazine*, vol. 49, no. 2, pp. 102–111, 2011.

[114] J. G. Proakis and M. Salehi, *Digital Communications*. ISBN: 9780072957167: McGraw Hill, 2007.

[115] 3rd Generation Partnership Project, "Further advancements for E-UTRA physical layer aspects," 3GPP TR 38.814 V9.2.0, Tech. Rep., 2017.

[116] K. Sato and T. Fujii, "Kriging-Based Interference Power Constraint: Integrated Design of the Radio Environment Map and Transmission Power," *IEEE Transactions on Cognitive Communications and Networking*, vol. 3, no. 1, pp. 13–25, 2017.

[117] H. S. Dhillon and J. G. Andrews, "Downlink Rate Distribution in Heterogeneous Cellular Networks under Generalized Cell Selection," *IEEE Wireless Communications Letters*, vol. 3, no. 1, pp. 42–45, 2014.

[118] 3GPP, "Evolved Universal Terrestrial Radio Access (E-UTRA) and Evolved Universal Terrestrial Radio Access Network (E-UTRAN); Overall description; Stage 2," 3rd Generation Partnership Project (3GPP), Technical Specification (TS) 36.330, 01 2019, version 15.4.0.

[119] V. Jungnickel, K. Manolakis, S. Jaeckel, M. Lossow, P. Farkas, M. Schlosser, and V. Braun, "Backhaul requirements for inter-site cooperation in heterogeneous LTE-Advanced networks," in *2013 IEEE International Conference on Communications Workshops (ICC)*, 2013, Conference Proceedings, pp. 905–910.

[120] Y. Lin, W. Bao, W. Yu, and B. Liang, "Optimizing User Association and Spectrum Allocation in HetNets: A Utility Perspective," *IEEE Journal on Selected Areas in Communications*, vol. 33, no. 6, pp. 1025–1039, 2015.